1 OF 2
AD
A059920

FINAL TECHNICAL REPORT

Contract No. N00014-75-C-0909

LEVEL (9)

STUDIES OF SOLID STATE REACTIONS
ON ELEMENTAL AND COMPOUND
SEMICONDUCTOR SURFACES

by

E. J. Scheibner

Applied Sciences Laboratory

DDC

OCT 12 1978

F
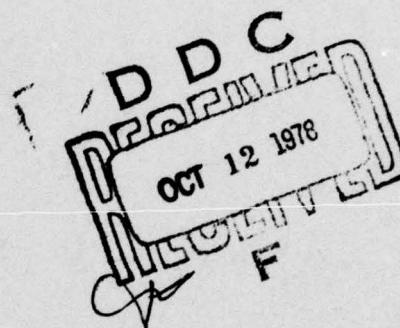
Prepared for

OFFICE OF NAVAL RESEARCH

Department of the Navy

Arlington, Virginia 22217

31 July 1978

GEORGIA INSTITUTE OF TECHNOLOGY

Engineering Experiment Station
Atlanta, Georgia 30332

GT EES

1978

410604 78 10 02 068

SECURITY CLASSIFICATION OF THIS PAGE *(When Data Entered)*

REPORT DOCUMENTATION PAGE		READ INSTRUCTIONS BEFORE COMPLETING FORM
1. REPORT NUMBER	2. GOVT ACCESSION NO.	3. RECIPIENT'S CATALOG NUMBER
4. TITLE *(and Subtitle)* Studies of Solid State Reactions on Elemental and Compound Semiconductor Surfaces		5. TYPE OF REPORT & PERIOD COVERED Final rept. 1 May 1975 to 30 April 1978
		6. PERFORMING ORG. REPORT NUMBER
7. AUTHOR(s) Edwin J. Scheibner		8. CONTRACT OR GRANT NUMBER(s) N00014-75-C-0909
9. PERFORMING ORGANIZATION NAME AND ADDRESS Applied Sciences Laboratory Engineering Experiment Station 30332 Georgia Institute of Technology, Atlanta, Ga.		10. PROGRAM ELEMENT, PROJECT, TASK AREA & WORK UNIT NUMBERS
11. CONTROLLING OFFICE NAME AND ADDRESS Office of Naval Research, Department of the Navy, 800 N. Quincy Street, Arlington, Virginia 22217		12. REPORT DATE 31 July 1978
		13. NUMBER OF PAGES 134
14. MONITORING AGENCY NAME & ADDRESS *(if different from Controlling Office)*		15. SECURITY CLASS. *(of this report)* Unclassified
		15a. DECLASSIFICATION/DOWNGRADING SCHEDULE

16. DISTRIBUTION STATEMENT *(of this Report)*

Distribution unlimited

This document has been approved for public release and sale; its distribution is unlimited.

17. DISTRIBUTION STATEMENT *(of the abstract entered in Block 20, if different from Report)*

18. SUPPLEMENTARY NOTES

19. KEY WORDS *(Continue on reverse side if necessary and identify by block number)*

SEMICONDUCTORS, SILICON, GALLIUM ARSENIDE, SURFACES, INTERFACES, AUGER ELECTRON SPECTROSCOPY, X-RAY PHOTOELECTRON SPECTROSCOPY, MOS DEVICES, SCHOTTKY DIODES, ELECTRON SCATTERING, PASSIVATION, ELECTRONIC STATES

20. ABSTRACT *(Continue on reverse side if necessary and identify by block number)*

The results of investigations on the solid state reactions which occur at the various interfaces in thin composite structures on the elemental and compound semiconductors, silicon and gallium arsenide, are reported. Free energies derived from bulk thermodynamic data predict the direction of oxidation-reduction reactions at interfaces. The identification of the resulting solid state phases used high energy resolution Auger electron spectroscopy (AES) and X-ray photoelectron spectroscopy (XPS) techniques

DD FORM
1 JAN 73 1473   EDITION OF 1 NOV 65 IS OBSOLETE
S/N 0102-014-6601 |

SECURITY CLASSIFICATION OF THIS PAGE *(When Data Entered)*

410 604

and the chemical shifts in energy associated with Auger or photoelectron peaks when an element is oxidized. Experimental MOS and Schottky barrier test structures were fabricated to correlate the chemical data and other interface characteristics with electrical measurements. Theoretical interpretation of data from high energy resolution AES and XPS studies of thin films on aluminum gave a value for the attenuation length of ~1400 eV electrons in Al_2O_3 and information on various electron scattering mechanisms. A review of GaAs passivation is made and a method based upon interface reactions is suggested. Finally, localized models for predicting surface/ interface states on the elemental and compound semiconductors for application to the interface problem are developed and photoemission, energy loss spectroscopy and LEED studies are examined for consistency with the predictions of the theoretical studies.

ACCESSION for

NTIS	White Section	✓
DDC	Buff Section	
UNANNOUNCED		
JUSTIFICATION		

BY
DISTRIBUTION/AVAILABILITY CODES

Dist	SPECIAL
A	

STUDIES OF SOLID STATE REACTIONS

ON ELEMENTAL AND COMPOUND SEMICONDUCTOR SURFACES

by

E. J. Scheibner

Applied Sciences Laboratory
Engineering Experiment Station
Georgia Institute of Technology
Atlanta, Georgia 30332

Technical Monitor

Dr. Larry R. Cooper

Electronic and Solid State Sciences Program
Office of Naval Research

31 July 1978

FINAL TECHNICAL REPORT
Contract No. N00014-75-C-0909

ABSTRACT

Under a three year program investigations were conducted on the solid
state reactions which occur at the various interfaces in thin composite
structures on the elemental and compound semiconductors, silicon and gal-
lium arsenide. This report summarizes the results of these investigations.
Free energies derived from bulk thermodynamic data are used to predict the
direction of oxidation-reduction reactions at interfaces. The identifica-
tion of the resulting solid state phases is accomplished by using high
energy resolution Auger electron spectroscopy (AES) and X-ray photoelectron
spectroscopy (XPS) techniques and observing the chemical shifts in energy
associated with Auger or photoelectron peaks when an element is oxidized.
Experimental MOS and Schottky barrier test structures were fabricated in
order to correlate the chemical data and other interface characteristics
with electrical measurements made on these devices. Theoretical interpre-
tation of the results of high energy resolution AES and XPS studies of thin
films on aluminum gave a value for the attenuation length of ~1400 eV elec-
trons in Al_2O_3 and information on various electron scattering mechanisms.
A review of GaAs passivation is made and a method based upon the solid state
reactions occurring at interfaces is suggested. Finally, localized models
for predicting surface/interface states on the elemental and compound semi-
conductors for application to the interface problem are developed and photo-
emission, energy loss spectroscopy and LEED studies are examined for con-
sistency with the predictions of the theoretical studies.

ii

FOREWORD

TABLE OF CONTENTS

LIST OF FIGURES

I. INTRODUCTION:

The solid state device requirements for advanced, reliable electronic systems provide a considerable need for the development of new device concepts and fabrication techniques and an understanding of materials interactions on a fundamental level. The purpose of the research program described in this report was to meet this need in part by investigating the solid state reactions which occur at the various interfaces in device-type structures on the elemental and compound semiconductors, silicon and gallium arsenide.

In our initial proposal of February 18, 1975 we presented the results of calculations of the standard free energy change on the formation of various inorganic oxides as a function of temperature. On the basis of these calculations, that is, from the sign of the free energy change of a solid state reaction between two solid phases, it was predicted that certain metals on silicon dioxide, for example, would reduce SiO_2 and form a metal oxide phase at the interface. In order to identify the intermediate oxide phase it was proposed to use the techniques of Auger electron spectroscopy (AES) and X-ray photoelectron spectroscopy (XPS) taking advantage of the fact that there is a chemical shift in energy between the peak representing the metal and that representing the oxide. During the first year preliminary studies which comprised Auger concentration profiles through an Al-SiO_2-Si structure and XPS data at the Al/SiO_2 interface demonstrated the feasibility of identifying the intermediate metal oxide phase by AES and XPS techniques. High energy resolution AES and XPS studies were also initiated on thin oxide films on aluminum. The intensities of the separate peaks for Al in Al_2O_3 and elemental Al were determined as a function of oxide thickness and the

1

direction in which theoretical interpretation of the data would proceed was outlined. In the same year improvements in the UHV/Auger system were made and an evaporator for fabricating MOS or Schottky barrier test structures within the UHV system was designed.

During the second year the theoretical analysis of the high resolution Auger and XPS data for the thin oxide films on aluminum was completed and an attenuation length for ~ 1400 eV electrons in Al_2O_3 was derived. High resolution Auger and XPS data for oxidized GaAs surfaces and for Al/GaAs interfaces were also obtained. In addition, MOS and Schottky barrier planar test structures on GaAs were prepared in a controlled manner in the Auger system and I-V and C-V measurements were made on diodes fabricated from the planar structures by photoresist and masking techniques.

During the third year further studies were pursued on the preparation and characterization of GaAs surfaces, particularly on molecular beam epitaxial (MBE) material, and additional Schottky barrier devices were evaluated. The problem of the passivation and stabilization of GaAs surfaces was then considered as an application of the fundamental knowledge of solid state reactions at interfaces. The final effort during this year included the beginning of a study of localized theoretical models for determining surface/interface states and the evaluation of existing photoemission, electron energy loss and LEED data for silicon and gallium arsenide surfaces.

A discussion of the thermodynamics of interface reactions is presented in Chapter II. The basic concepts are then applied in studies of various interfaces on silicon and gallium arsenide (Chapters III and IV). The high energy resolution AES and XPS studies of Al_2O_3 on Al and GaAs, and related optical studies, are summarized in Chapters V and VI, respectively. GaAs

2

surface passivation is covered in Chapter VII and the theoretical study of surface/interface states is detailed in Chapter VIII. Recommendations are made in Chapter XII for further extensions of the research described herein.

II. THERMODYNAMICS OF INTERFACE REACTIONS:

The research under the program was directed towards the achievement of a fundamental understanding of the physics and chemistry of interfaces on elemental and compound semiconductors. One important problem area that was particularly singled out was the nature of solid state reactions occurring at metal-oxide, insulator-insulator, oxide-semiconductor and metal-semiconductor interfaces. Thermodynamically one can determine the likelihood of the chemical reaction that might occur at an interface between two solid phases by examining the standard free energy change of the process.

The Gibbs free energy change of a reaction, ΔG, is expressed in terms of the enthalpy, ΔH, and the entropy, ΔS, according to the relation

$$\Delta G = \Delta H - T\Delta S.$$

The coefficients in the free energy equations for ΔG and ΔS are tabulated in the CRC Handbook for Physics and Chemistry. If one were to assume that ΔG and ΔS were independent of temperature, then the temperature dependence of ΔG could be obtained readily from the above equation. The standard free energy change, ΔG°, refers to a reaction for which all reactants and products are in their standard states at the given temperature and 1 atm pressure. Standard free energy changes, ΔG°, for the formation of inorganic oxides including those that were of possible interest in our program were calculated from tabulated data for each compound for a range of temperatures. The results are shown in Figure 1.

A graph of this type is useful in evaluating relative reducing or oxidizing tendencies of materials. For example, at all temperatures Al will reduce Cr_2O_3 to Cr. The driving force for this oxidation-reduction reaction

4
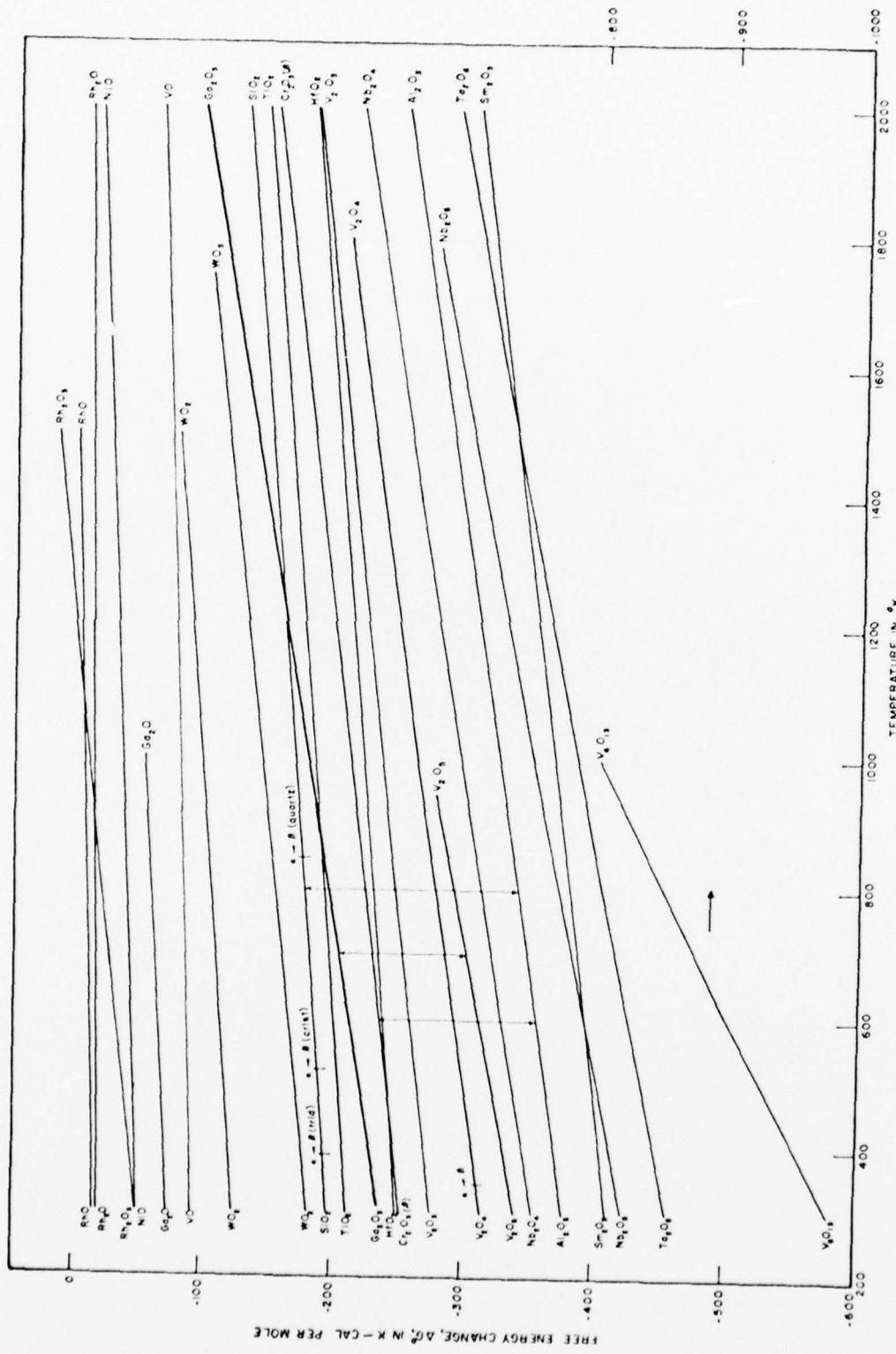
Figure 1. Free Energy Change in the Formation of Various Oxides as a Function of Temperature.

5

may be readily obtained from consideration of $\Delta G°$ for the two compounds. At 600 °C

$$2Al(s) + 3/2 \; O_2(g) \rightarrow Al_2O_3(s) \quad \Delta G° = -355 \text{ kcal/mole}$$

$$2Cr(s) + 3/2 \; O_2(g) \rightarrow Cr_2O_3(s) \quad \Delta G° = -234 \text{ kcal/mole}$$
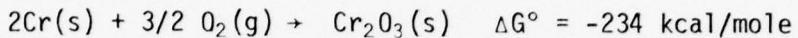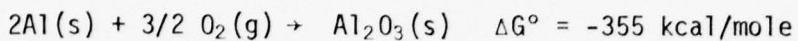
Subtracting the second reaction from the first yields

$$2Al(s) + Cr_2O_3(s) \rightarrow Al_2O_3(s) + 2Cr(s) \quad \Delta G° = -121 \text{ kcal/mole}$$

The negative value of $\Delta G°$ indicates the driving force for the reaction reducing the Cr_2O_3 to Cr and oxidizing the Al to form Al_2O_3.

Also illustrated in Figure 1 are differences in the free energy change on formation for V_2O_5 and Ga_2O_3, at 700 °K, and for Al_2O_3 and SiO_2 at 800 °K. Consideration of the $\Delta G°$ for the first pair of compounds indicates that heat treatment at 700 °K of vanadium on Ga_2O_3 will result in the formation of V_2O_5 (or other vanadium compounds except VO) and the reduction of Ga_2O_3 to Ga at the metal-oxide interface. Similar arguments apply for the reduction of SiO_2 by aluminum at 800 °K. Note also that according to the bulk data, Ti is expected to reduce Ga_2O_3 at high temperatures but not below 850 °K. A list of the standard heats of formation ($\Delta H°$) and standard free energies of formation ($\Delta G°$) of various oxides is given in Table 1. Note that Al is expected to reduce Ga_2O_3 or As_2O_3 to form Al_2O_3 and free Ga or As, and to reduce SiO_2 to form Al_2O_3 and free Si. There are other metals which are also thermodynamically favorable for reducing these oxides, e.g., Zr, Cr, Nb and Ta.

The sign of the free energy change of a solid state reaction between two solid phases, for example, the metal and the oxide, of course governs only the feasibility of the reaction. Thus, a ΔG which is negative will indicate that the reaction might proceed. The kinetics of the reaction,

6

TABLE I.

Standard Heat of Formation ($\Delta H°$) and Standard Free Energy of Formation ($\Delta G°$) of Various Oxides at 25°C (in kilo-calories per gram mole)*

	$\Delta H°$	$\Delta G°$
Ag_2O_2	-6.62	
Ag_2O	-7.74	-2.59
RhO	-22.65	
Rh_2O	-23.74	
Cu_2O	-39.84	-34.98
SeO_2	-53.77	
RuO_2	-57.29	
CdO	-60.86	-53.79
GeO	-60.9	
SnO	-68.4	-61.5
Rh_2O_3	-70.06	
TeO	-77.69	-64.6
Rb_2O	-78.9	
Ga_2O	-81.0	
ZnO	-83.17	-76.05
Rb_2O_2	-101.7	
TcO_2	-103.4	
TiO	-125.0	
GeO_2	-128.3	
TcO_3	-129.0	
MoO_2	-130,0	
SnO_2	-138.8	-124.2
CrO_3	-141.0	
SrO	-141.1	-133.8
CrO_2	-142.0	
MgO	-143.84	-136.13
As_2O_3(Monoclinic)	-150.76	
SrO_2	-153.6	
As_2O_3(orthorhombic)	-154.87	
As_2O_4	-173.69	

7

TABLE I.

Standard Heat of Formation (ΔH°) and Standard Free Energy of Formation (ΔG°) of Various Oxides at 25°C (in kilo-calories per gram mole)*

(Continued)

	$\Delta H°$	$\Delta G°$
MoO_3	-180.33	-161.95
As_2O_5	-218.6	-184.6
Sb_2O_4	-214.0	-188
SiO_2 (quartz)	-205.4	-192.4
$Mg(OH)_2$	-221.0	-199.27
In_2O_3	-222.5	
TiO_2	-228.0	
$Sr(OH)_2$	-229.3	
Sb_2O_5	-234.4	-200.5
Ga_2O_3	-258.0	
ZrO_2	-258.2	-244.4
Tc_2O_7	-266.0	
Cr_2O_3	-278.0	
Sb_2O_6	-336.8	-298.0
$Y(OH)_3$	-337.6	-308.3
Ti_2O_3	-360.0	
Nb_2O_4	-387.8	
Al_2O_3 (corundum)	-399.09	-376.77
Y_2O_3	-419.6	
Nb_2O_5	-463.2	
$Al_2O_3 \cdot H_2O$	-471.0	-435
Ta_2O_5	-493.0	
Ti_3O_5	-588.0	
$Al_2O_3 \cdot 3H_2O$	-613.7	-547.9

---

*from Handbook of Chemistry and Physics, 47th Edition, Chemical Rubber Co., (1966).

8

that is, the reaction rates as a function of temperature need to be deter-
mined by other means. There are, however, other factors which need to be
considered before applying these thermodynamic concepts directly to the
interface reactions on the elemental and compound semiconductors. The first
is that the thin film situation is likely to be somewhat different from the
bulk so that the free energy changes might not be accurate. Secondly, one
should be concerned about the distribution of the elements Ga, As or Si
after the reduction reaction has occurred. For example, it is expected
that these elements will diffuse from the interface into both the metal and
the oxide phases. In fact, recent Auger studies[1,2] on the interdiffusion
between aluminum thin films and GaAs indicate that Ga does migrate readily
through a 2000 Å film of Al at 250 °C.

The thermodynamic concepts presented here are basic to the studies pre-
sented in later chapters and, therefore, reference will be made frequently
to this chapter and the expected free energy change of a solid state reaction.

III. INTERFACE EFFECTS ON SCHOTTKY BARRIERS:

3.1 Introduction

Several experiments were performed to determine the effect of interface modifications on the electrical properties of Schottky barriers formed on GaAs. Surface cleanliness, stoichiometry, lattice damage and oxidation were some of the interface conditions investigated. In all cases the Schottky barrier structures were prepared within the UHV/Auger system. This procedure enabled the characterization of the initial GaAs surface and the evaluation of cleaning procedures by AES, the controlled growth of an oxide film as desired with monitoring of the oxygen (510 eV) Auger peak, and deposition of metal (Au or Al) using a specially designed in situ evaporator. Both (100) GaAs substrate material and (100) GaAs MBE material were used. Subsequent to this fabrication procedure, the specimens were removed from the vacuum system and actual devices were formed using standard photoresist and masking techniques. Typically, patterns of 20 mil dots were prepared on the metal plating.

The evaluation of the experimental devices involves the determination of the height of the potential barrier formed at the metal-semiconductor interface[3]. There are several techniques that can be used to determine the barrier height[4]. The instrumentation we used enabled measurements of the barrier height from the current-voltage characteristics and the capacitance-voltage characteristics of the Schottky diodes.

Current-voltage characteristics were obtained by using a Tektronics Type 575 transistor curve tracer in conjunction with an external picoammeter and digital voltmeter. To obtain the experimental data, the current through the diode was measured as the forward bias voltage was increased. The ideal

forward I-V characteristics can be written as[4]

$$J = A^{**}T^2 \exp\left(\frac{-q\phi_{Bo}}{kT}\right) \exp\left(\frac{q(\Delta\phi + V)}{kT}\right)$$

where ϕ_{Bo} is the zero field barrier height, A^{**} is the effective Richardson constant, $\Delta\phi$ is the Schottky barrier lowering, V is the applied voltage, T is the temperature and k is the Boltzmann constant. If the saturation current density is J_s at zero applied bias, then the barrier height can be obtained from

$$\phi_{Bn} = \frac{kT}{q} \ln\left(\frac{A^{**}T^2}{J_s}\right) .$$

By plotting J versus V on semi-log paper, the saturation current may be determined by extrapolation of the current density at zero voltage.

Capacitance-voltage characteristics were measured either with a Boonton Model 750 Direct Capacitance Bridge or the Boonton 1 MHz impedance bridge which is an integral component of an automatic depth profiler. The profiler measures the impurity concentration profiles of semiconductors by the differential capacitance method. It also operates in the C-V mode, whereby it automatically plots the capacitance of the device as a function of applied bias. The C-V characteristics are given by[4]

$$C = \left[\frac{q\epsilon_s N_D}{2(V_{bi} - V - \frac{kT}{q})}\right]^{1/2}$$

where q is the unit charge, N_D is the doping concentration, ϵ_s is the semiconductor permitivity and V_{bi} the built-in voltage. Thus, from the voltage intercept of a plot of $1/C^2$ versus V, the barrier height can be determined from

11

$$\phi_{Bn} = V_i + V_n + \frac{kT}{q} - \Delta\phi$$

where V_i is the voltage intercept and V_n is the depth of the Fermi-level below the conduction band.

3.2 Low Pressure Oxidation of GaAs

The formation of a natural oxide on GaAs under low oxygen gas pressure was studied in one series of experiments. A small wafer of (100) oriented n-type GaAs substrate material was obtained. It was cut into two pieces and loaded into the Auger system. The system was pumped overnight with a 10 hour bakeout to obtain a pressure of 1×10^{-9} Torr. The samples had been exposed to air for a long time and therefore initial Auger analysis showed a great deal of surface carbon and oxygen. One specimen was then cleaned by argon ion sputtering for 30 minutes with 500 eV ions at an argon pressure of 5×10^{-5} Torr. The specimen was then examined using AES and then plated with 500 Å of pure gold, using the _in situ_ evaporator. The Auger spectrum of the initial surface condition before Au deposition showed very little carbon and oxygen remaining on the surface and the fine structure in the low energy Ga and As peaks became quite apparent. Since the low and high energy peaks of Ga and As have different escape depths,[5] the low energy peaks will give information about the surface composition whereas the high energy peaks can be used to study bulk composition. The high energy peaks of Ga (1070 eV) and As (1228 eV) have escape depths of 19.0 and 20.5 Å, respectively. The escape depth is 5.0 Å for the As (31 eV) peak.[5] No annealing was done after sputtering so that lattice damage may be a contributing factor to the results obtained.

The second specimen was cleaned in exactly the same manner and showed almost identical surface conditions after cleaning. It was then exposed to

research grade oxygen at a pressure of 1×10^{-5} Torr by backfilling the Auger system using the automatic pressure controller. The low energy range (20 to 550 eV) of the Auger spectrum was monitored as a function of exposure time. Particular attention was paid to the growth of the oxygen (510 eV) peak. The oxygen peak-to-peak height grew at a constant rate of .067 cm/min. up to 120 minutes exposure time. As the exposure was increased, the oxidation rate tapered off. After 180 minutes of exposure, the oxygen peak had increased from .3 cm to 12.8 cm. At this point, the oxygen was pumped out and 500 $\overset{o}{A}$ of gold was deposited on the sample.

Afterwards, both specimens were removed from the vacuum system and 20 mil diameter dots were formed on the plated side. Ni-Au ohmic contacts were formed on the reverse side of each. I-V and C-V measurements were made as described earlier and barrier heights were calculated. From the I-V measurements, barrier heights of .85 volts and .93 volts were obtained for the clean and oxidized specimen, respectively. C-V measurements gave .84 and .93 volts, respectively. Thus, the barrier height does appear to depend upon the interfacial oxide layer, confirming the results of other investigators, Pruniaux and Adams,[6] for example. The growth rate of the oxide layer in our case was probably influenced by the operating hot filament ionization gauge[7] as well as by the existence of lattice damage in the sputtered GaAs surface.

3.3 Oxidation of GaAs in Air

The oxidation of GaAs in air at room temperature was studied and the dependence of the barrier height of Schottky diodes with interfacial layers on the layer thickness was determined. High resolution Auger and XPS data were used to determine the nature of the surface oxide.

A wafer of GaAs was obtained and cut into eight pieces. Ni-Au ohmic contacts were formed on the back side of each and then each sample was

13

chemically cleaned in a sequence of methanol, trichlorethylene and acetone baths. Each piece was then etched in 36% HCl for 20 seconds and kept under methanol until loading into the vacuum. This procedure has been shown to leave consistently clean surfaces with only about 10 Å of oxide on the surface.[6] The system was pumped down overnight to a pressure of 1×10^{-9} Torr. Initial AES examination showed the presence of a great deal of carbon and a small Cl peak.

Three of the specimens were ion cleaned to give surface conditions very similar to those described in Section 3.2. About 500 Å of gold was deposited on one sample as is. The others were then exposed to air at room temperature for one and two hours, respectively. After exposure each was examined by AES and then plated with 500 Å of gold. The fourth sample was ion cleaned also, but much more thoroughly. It was exposed for three hours and then plated in the same manner.

The remaining samples were ion cleaned to give conditions similar to the first three specimens. Two were oxidized for three hours in air and then plated with Al instead of Au. The remaining sample was also exposed for three hours, but no metal film was deposited on it. All the samples except for one of the Al coated specimens and the unplated specimen went through the photoresist process to form diodes for the barrier height measurements.

Figure 2 shows a plot of the barrier height versus exposure time and the oxygen (510 eV) peak-to-peak amplitude versus exposure time, for the first four samples. Both show a linear behavior with time for the first three specimens. However, the fourth sample that was more thoroughly cleaned showed a much lower oxidation rate. The small difference in the initial surface conditions seems to have quite an effect on the oxidation

14
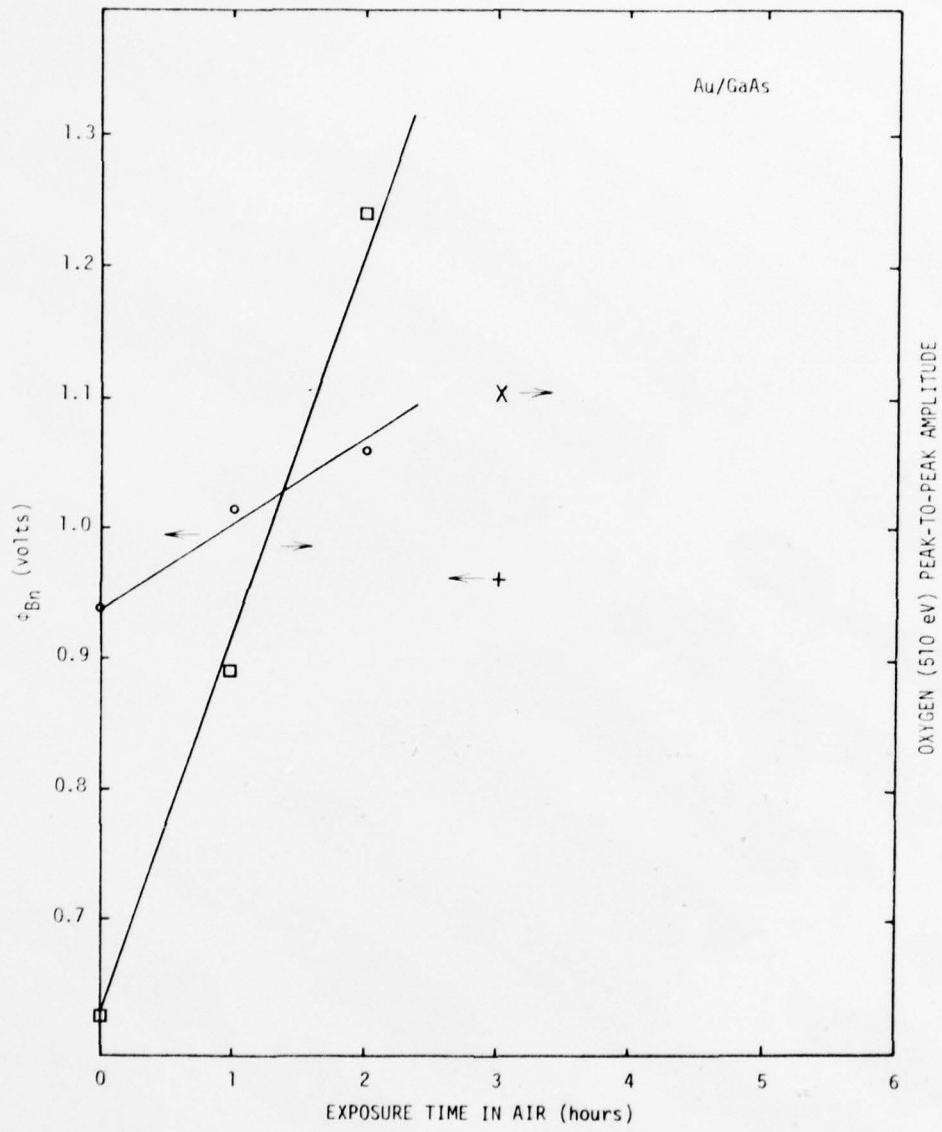
Figure 2. Barrier Height, ϕ_{Bn}, of Au/GaAs Diodes and Oxygen (510 eV) Peak-to-Peak Amplitudes versus Exposure Time in Air at Room Temperature of GaAs Substrates prior to Deposition of Au _in_ _situ_.

rate and the barrier height. Pruniaux and Adams[6] also found two different oxidation rates and barrier height dependencies, which they supposed was caused by different initial surface conditions, although they had no way of determining the surface conditions in their experiments.

The sample which was oxidized, but not plated, was used to obtain high resolution Auger and X-ray photoelectron spectra (see Section 5.2). The oxide on the GaAs was analyzed before and after sputter removal of approximately 15 Å. There is presently some disagreement as to whether the oxygen on the surface bonds to Ga or As atoms or possibly bridges both.[8-10] Our high resolution data indicate the presence of gallium oxide on the surface initially and no arsenic oxide. See, however, the results of photoemission studies discussed in Chapter VIII which indicate that oxygen bonds to the As atoms on a (110) cleaved surface.

Barrier height measurements were made on the Al/GaAs diode from its C-V characteristics. The plot of $1/C^2$ versus V was linear over the voltage range used. Compared to the reported values on vacuum cleaved Al/GaAs diodes[4,11] the barrier height was somewhat larger. The high resolution Auger data taken on the other sample, which was prepared in exactly the same manner, showed no evidence of either gallium oxide or an arsenic oxide. There was, however, an aluminum oxide at the interface, extending through a region of greater than 55 Å in thickness (see Section 5.2). These results are believed to be direct evidence for the reduction of Ga_2O_3 by Al to form Al_2O_3, as predicted by the thermodynamic considerations discussed in the previous chapter.

3.4 Experiments with MBE Material

A series of experiments were performed using (100) GaAs MBE material

as the starting material for Schottky diodes. A program in the Solid State Sciences Division, "Molecular Beam Epitaxial Materials Study for Microwave and Millimeter Wave Devices," (Contract No. N00173-76-C-0372), provided a ready source of MBE material.

Following the MBE run the GaAs specimen was cut in half and both pieces mounted in the Auger system, one on a heated stage. The system was then pumped and baked for approximately 16 hours attaining an ultimate pressure of ~2 x 10^{-9} Torr. Approximately 500 Å of Au was deposited on one specimen after surface characterization by AES. The other specimen was cleaned by argon ion sputtering to remove the carbon followed by heating to 600 °C to decompose the oxide. Then a 500 Å film was deposited on the cleaned surface.

Low energy (10-650 eV) and high energy (650-1300 eV) Auger spectra for the specimens showing the initial surface conditions are plotted in Figures 3A and 3B, respectively. Note, particularly, the presence of carbon at 271 eV and oxygen at 508 eV. The ratio of peak-to-peak amplitudes for the surface sensitive 50 eV (Ga) and 30 eV (As) peaks is 1.6 while the ratio for the bulk 1066 eV (Ga) and 1227 eV (As) peaks is 1.5.

After sputtering in argon (0.5 keV, 25 ma, 5 x 10^{-5} Torr) for 20 minutes the low and high energy Auger spectra of Figures 4A and 4B were obtained. A considerable reduction in the carbon peak and a marked increase in the 50 eV (Ga) and 30 eV (As) peaks compared to the same peaks in Figure 3A is noted. The ratio for the 50 eV (Ga) and 30 eV (As) peaks is 0.8 while that for the 1066 eV (Ga) and 1227 eV (As) peaks is 1.48, approximately the same as that before sputtering.

Heating to 600 °C for approximately 4 minutes resulted in the complete
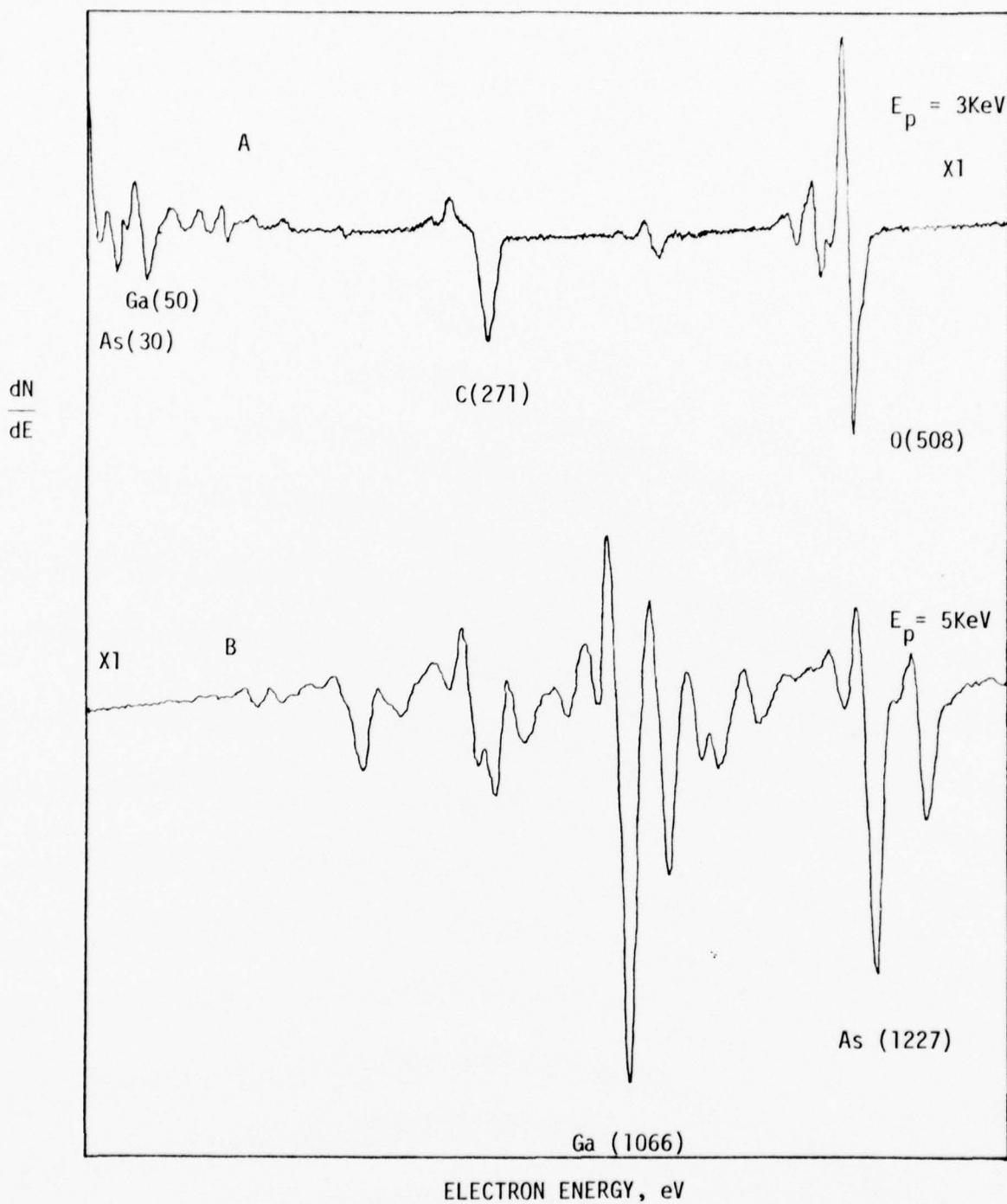
Figure 3. Auger Spectra for MBE GaAs Specimens
with Initial Surface Conditions. A(10-650eV);
B (650-1300eV).
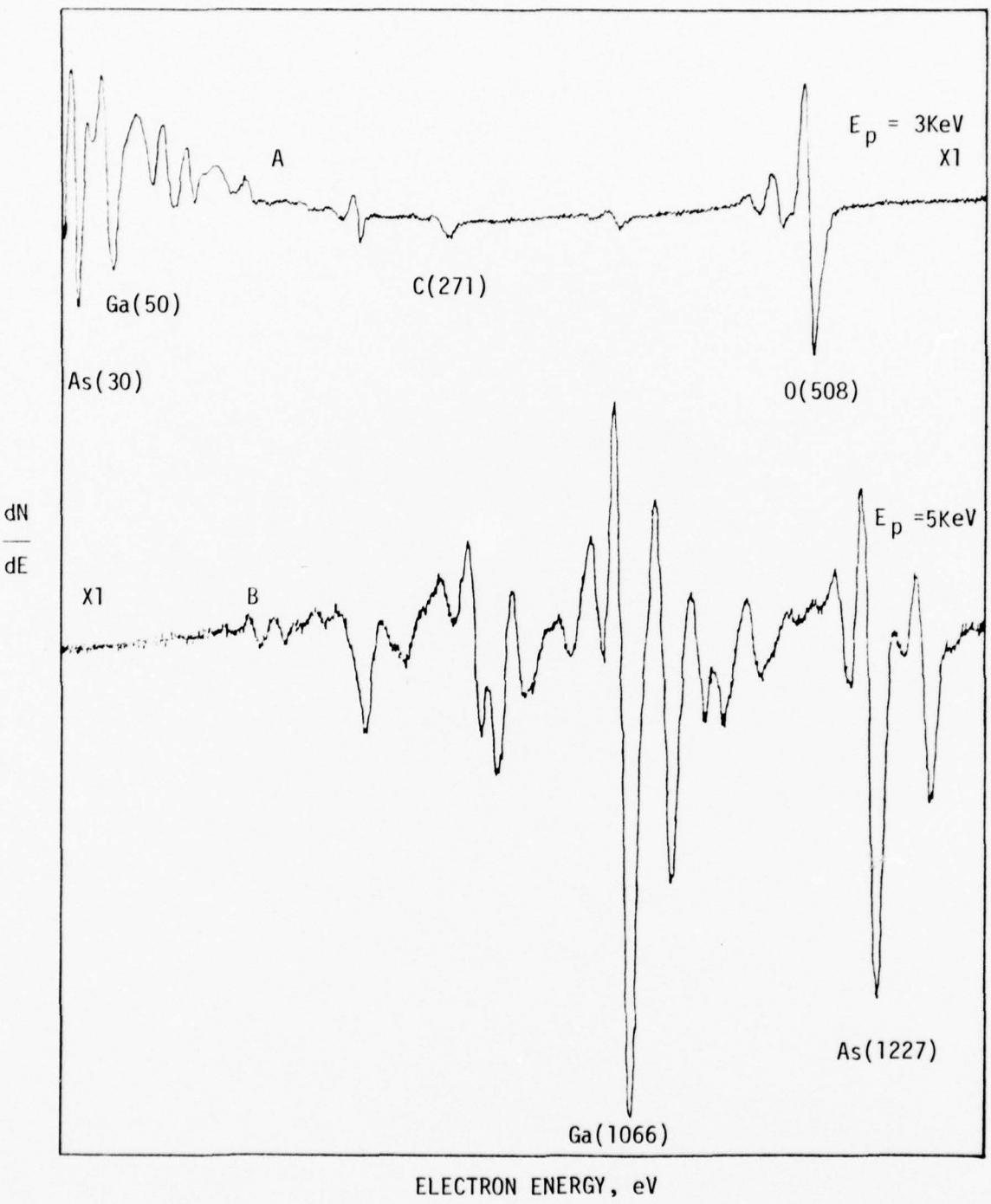
Figure 4. Auger Spectra for MBE GaAs Specimens
after Argon Ion Sputtering. A(10-650eV);
B (650-1300eV).

disappearance of the oxygen peak as shown in Figure 5A, however, a depletion of As is indicated in Figure 5B by the change in the ratio of the peak-to-peak amplitudes for the 1066 eV (Ga) and the 1227 eV (As) peaks, that is, 2.72 compared to the previous value of 1.5.

Measurements were made of $1/C^2$ versus V for several of the diodes on the wafer which had gold plated over the existing oxide. Consistent results were obtained showing a linear plot and an intercept in the neighborhood of 1.1 eV. The $1/C^2$ vs V curves for the cleaned GaAs, however, showed a nonlinearity at higher voltages and a range of intercept values from 0.8 to 1.2 eV. This nonreproducibility is possibly associated with the nonuniformity of cleaning and the nonlinearity with the As depletion. Further studies of this type are indicated to define more clearly the relation between the particular surface conditions and the capacitance-voltage characteristics.
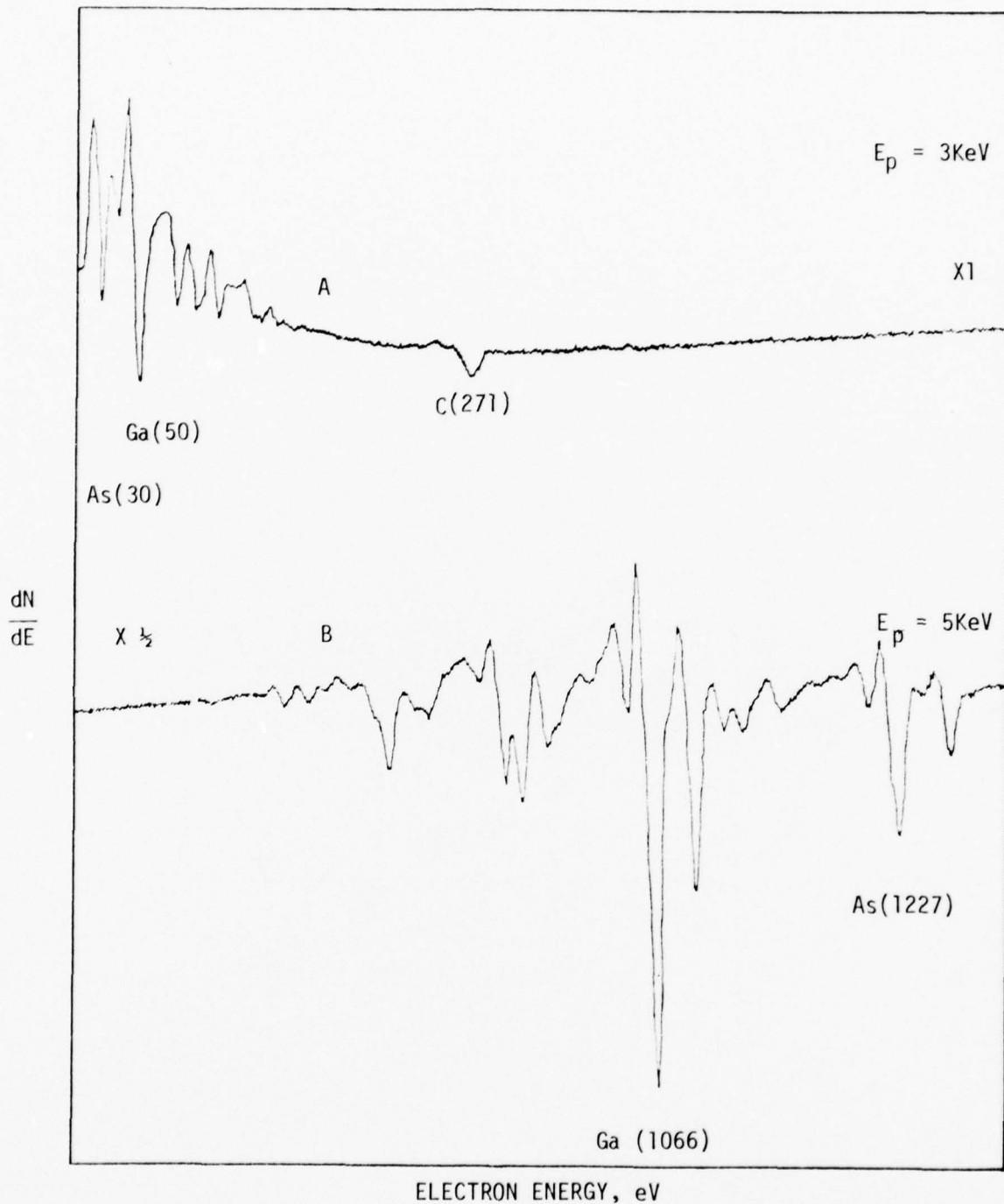
Figure 5. Auger Spectra for MBE GaAs Specimens
after Heating to 600°C. A(10-650eV);
B(650-1300eV).

21

IV. INTERFACE STUDIES OF Al-SiO$_2$-Si STRUCTURES:

In preliminary work on MOS structures fabricated by depositing Al on thermally oxidized silicon wafers, as reported in our Interim Technical Report of 21 January 1976, it was shown that the chemical shift in energy between the Al-2p photoelectron peak due to Al and that due to Al in Al$_2$O$_3$ was sufficient to identify the two separate solid state phases as one sputtered through the Al/SiO$_2$ interface of an Al-SiO$_2$-Si structure. The spectra obtained indicated that an Al$_2$O$_3$ layer was formed at the Al/SiO$_2$ interface according to the predictions of bulk thermodynamics, as discussed in Chapter II. The Si peaks were not monitored at that time so that the results were inconclusive with respect to the reduction of SiO$_2$ by the Al to form free silicon.

Subsequently, similar specimens were examined more thoroughly in a Varian Auger electron spectrometer which incorporated a cylindrical mirror analyzer with a 0.25% energy resolution. Auger derivative data were taken using four channels of a multiplexer to obtain an Auger profile thorugh the Al-SiO$_2$-Si structure. The lower channel included both the Al-LVV peaks due to the Al and Al$_2$O$_3$ and the Si-LVV peaks due to Si and SiO$_2$; the second channel included only the O-KLL peak; the third channel included the KLL peaks due to Al and Al$_2$O$_3$; and the fourth channel included the KLL peaks due to Si and SiO$_2$. Since the Auger profile is a point plot of the largest peak in each channel as a function of sputtering time it is not possible to distinguish between Al and Al$_2$O$_3$ or Si and SiO$_2$ peaks from such a profile. However, we have simultaneously plotted the data within each channel on a strip chart recorder. From the strip chart records one can, therefore, obtain information on the concentrations of the different phases through the

22

Al/SiO_2 interface.

The striking results of these studies show the presence of free Al, Al_2O_3, free Si and SiO_2 at the Al/SiO_2 interface; an Al_2O_3 distribution extending from the interface approximately 150 $\overset{o}{A}$ into the Al and approximately 150 $\overset{o}{A}$ into the SiO_2; and a distribution of free Si extending partly into the Al (< 150 $\overset{o}{A}$) and to a greater extent into the SiO_2 (> 200 $\overset{o}{A}$). The broad reaction zone was not expected in that the sample was maintained at a relatively low temperature ($\approx$ 70 °C or less) during the Al deposition. However, the energy released in the solid state reaction involving the reduction of SiO_2 and the formation of Al_2O_3 could be sufficient to cause considerable intermixing of the several components. A consequence of these studies is that further annealing of the Al films as is ordinarily done in the production of MOS devices (typically, 470 °C in dry N_2 for 20 min.) will probably not appreciably extend the chemical reduction of SiO_2 by Al. Further studies of the phenomena involving different deposition methods and conditions, different metals and thinner oxide films are indicated.

A paper covering the details of these experiments by Y. E. Strausser (Varian), E. J. Scheibner and J. S. Johannessen (Stanford) has been accepted for publication in Thin Solid Films.

V. HIGH RESOLUTION AUGER AND X-RAY PHOTOELECTRON SPECTROSCOPY OF ALUMINUM AND GALLIUM ARSENIDE SURFACES:

In this phase of the research a double-pass cylindrical mirror analyzer with retarding grids[12] was used to obtain high energy resolution electron-excited Auger and X-ray photoelectron spectra from thin oxide films on aluminum and from different oxidized gallium arsenide surfaces. With the double-pass CMA the incident Auger electrons (or photoelectrons) are decelerated in the retarding field of spherically-shaped grids in such a manner that a constant pass energy through the CMA is obtained. The result is that the absolute resolution, as indicated by the FWHM of the elastic peak, is a function only of the pass energy and the size apertures used in the analyzer and is not dependent upon the incident electron energy, as it is for the single-pass CMA. For the conditions we used, that is, pass energies of the order of 50 eV and small apertures, the absolute resolution was about 0.7 eV. This made it possible, for example, to distinguish easily between the Auger KLL peaks due to Al in Al_2O_3 and those due to Al metal, which are separated in energy by about 6.7 eV. In fact, both Auger and X-ray photoelectron spectra exhibit such chemical shifts for quite a number of metal-metal oxide pairs.[13] In general, the Auger chemical shifts are considerably larger than the photoelectron shifts when the transitions involve only core-level electrons.

The analysis of the Auger KLL spectra and the Al-2p photoelectron spectra for different oxide film thicknesses on aluminum films was presented in a paper submitted to the Journal of Electron Spectroscopy and Related Phenomena. A copy of that paper is also included in the Interim Technical Report dated 28 January 1977.[14] Studies of the gallium arsenide surfaces are also included in the same report. The principal results of both studies will be summarized

24

here.

5.1 Aluminum/Aluminum Oxide

Specimens used in this investigation were aluminum films sputtered in a Sloan DC Sputtergun system onto thermally oxidized silicon wafers. The aluminum oxide films were the natural oxide of aluminum formed in air during 24 hours in the sputtering system. Sputter etching of the Al_2O_3 films to obtain different oxide film thicknesses was accomplished by argon ion bombardment in the Auger/XPS system at a rate of approximately 30 Å/min. Auger and XPS spectra were recorded initially and after each stage of argon ion sputtering.

Figure 6 is a high resolution Auger spectrum obtained from the surface of an oxidized aluminum specimen showing the major peaks in the Al KLL spectrum. These include the most intense KLL peaks, the $KL_2L_3(^1D_2)$ and the $KL_1L_2(^1P_1)$ peaks, and the weaker $KL_2L_2(^1S_0)$ and $KL_1L_{23}(^3P_{0,1,2})$ peaks. Additional KLL peaks should occur at approximately 1301 eV for the $KL_1L_1(^1S_0)$ transition, which is outside the range of our data, and at 1392 eV for the $KL_3L_3(^3P_{0,2})$ transitions, which, however, is below the limit of detection of our instrument. Bulk plasmon loss peaks associated with the $KL_2L_3(^1D)$ and the $KL_1L_2(^1P)$ Auger electrons as well as surface plasmon peaks associated with the $KL_2L_3(^1D)$ Auger electrons are indicated. The lower curves in the figure which are energy loss data for a primary electron energy corresponding to the $KL_2L_3(^1D_2)$ Auger energy show the bulk plasmon loss peaks in multiples of 15.6 eV from the primary energy. The surface plasmon loss peaks in the Auger spectrum occur at a $E_p/\sqrt{2} = 11.0$ eV and at $E_p/\sqrt{3} = 9.0$ eV from the $KL_2L_3(^1D_2)$ Auger energy. These values are related to the metal-vacuum interface topography, a planar interface giving an energy difference,
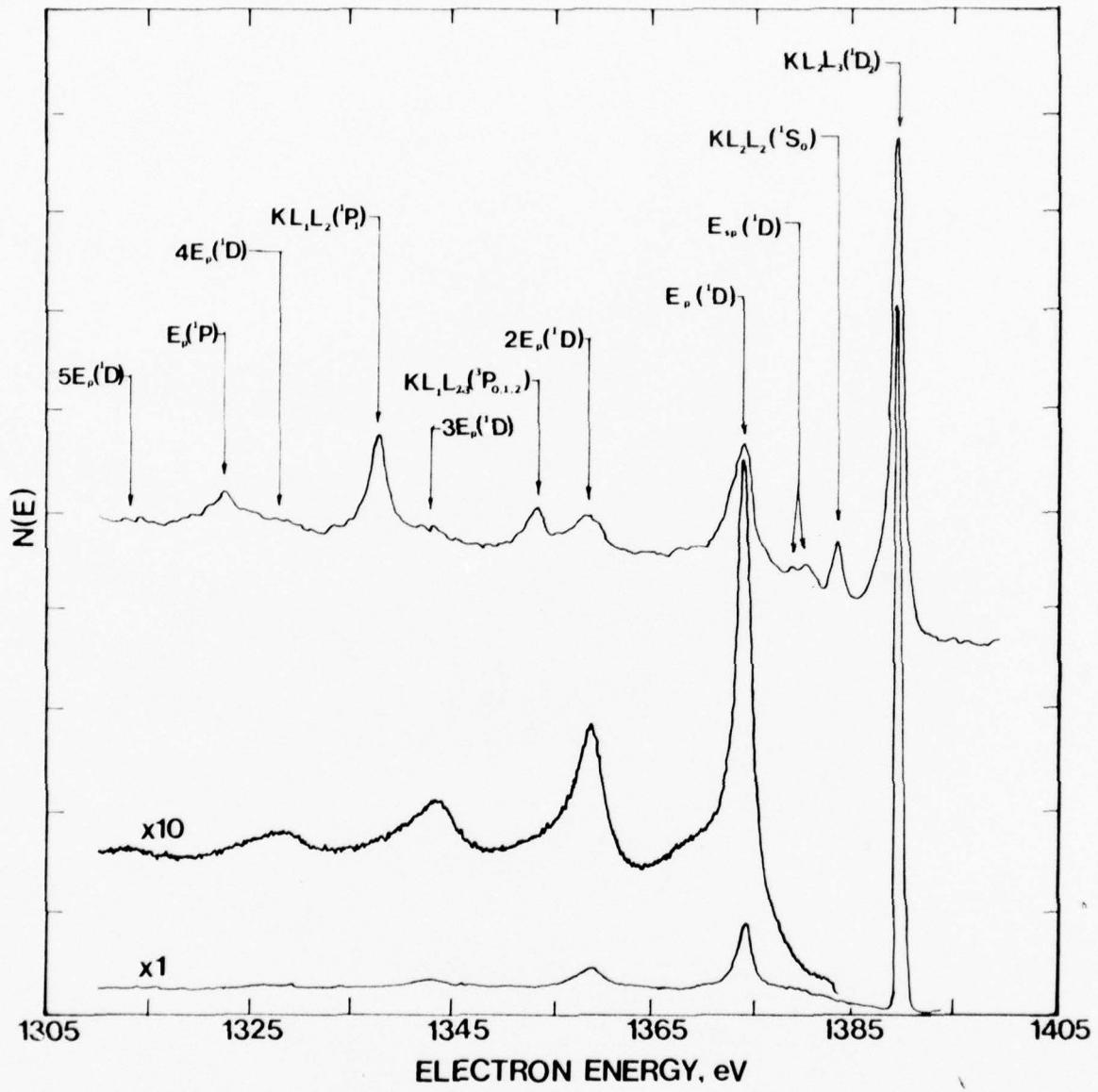
Figure 6. High Resolution Auger Spectrum from Aluminum Showing KLL Transitions and Bulk and Surface Plasmon Loss Peaks. The lower curves are electron energy loss data for primary electrons of the $KL_2L_3(^1D_2)$ Auger energy.

ΔE, equal to $E_p/\sqrt{2}$ and a rough or spherical interface giving a ΔE of $E_p/\sqrt{3}$.

Figure 7 shows high resolution Auger spectra, $N(E)$ vs E, for the KL_2L_3 transitions before argon ion sputtering (curve A), after 15 $\overset{\circ}{A}$ removal (curve B), after 30 $\overset{\circ}{A}$ removal (curve C) and for the aluminum at 75 $\overset{\circ}{A}$ removal (curve D). The total thickness of the oxide film was of the order of 40 $\overset{\circ}{A}$. Large Auger chemical shifts of over 7 eV between the metal and oxide peaks are shown in curves A and B. The slight differences may be due to compositional variations in the oxide or to surface charging. The aluminum curve (curve D) shows weak peaks at 1378.8 eV and at 1382.1 eV. By comparison with Figure 6 the 1382.1 eV peak is identified as the $KL_2L_2(^1S_0)$ Auger peak and the 1378.8 eV peak is associated with the excitation of surface plasmons by Auger electrons from the $KL_2L_3(^1D_2)$ peak. The increasing intensity at the left of each curve results from the bulk plasmon loss peak. Curve C includes contributions from the $KL_2L_2(^1S_0)$ Auger peak and from the surface plasmon peak. In our analysis we find that the surface plasmon peak shifts to a lower ΔE value in the presence of a thin oxide layer as suggested in the figure. For a thick oxide the appropriate relation for the surface plasmon energy would be $E_p/\sqrt{1+\varepsilon}$ where ε is the dielectric constant of the oxide.[15]

High resolution photoelectron spectra of the Al-2p photoelectron peak are shown in Figure 8 for an oxidized aluminum specimen before sputtering (curve A), after 30 $\overset{\circ}{A}$ removal (curve B) and for the aluminum (curve C). The smaller chemical shift between the Al-2p aluminum peak at 71.7 eV of 2.5 eV is in agreement with Wagner's data.[13]

The different Auger and X-ray photoelectron spectra were analyzed as follows. The experimental shape of a single peak is usually a Voigt function, a convolution of Lorentzian (L) and Gaussian (G) functions. We

27
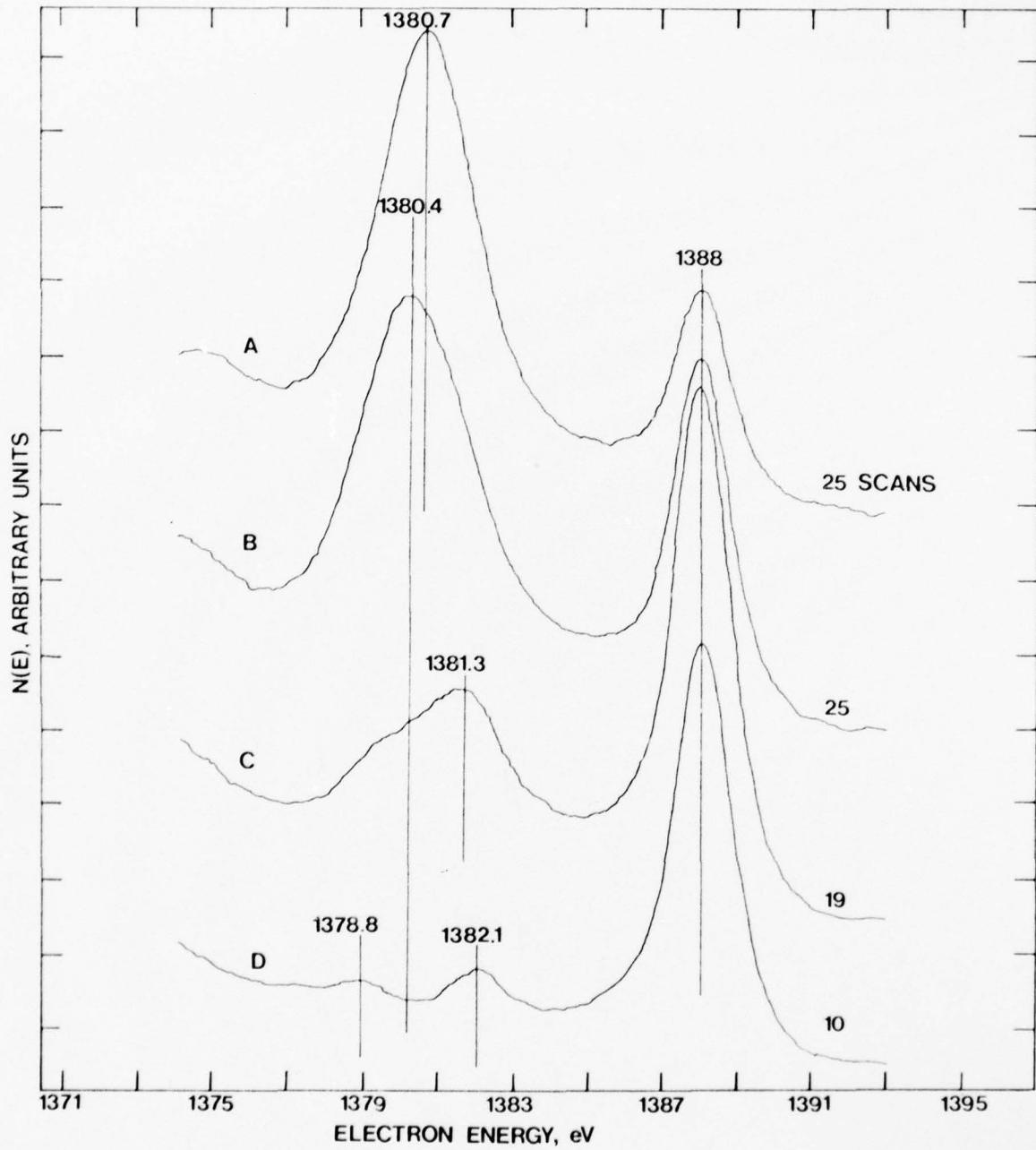
Figure 7. Auger Spectra for the KL_2L_3 Transition Showing Metal and Oxide Peaks for Different Thicknesses of Al_2O_3 on Aluminum. Oxide thickness is of the order of 40 Å. Curve A is for the specimen before argon ion sputtering, curve B is after 15 Å removal, curve C is after 30 Å removal and curve D is for the aluminum without an oxide.
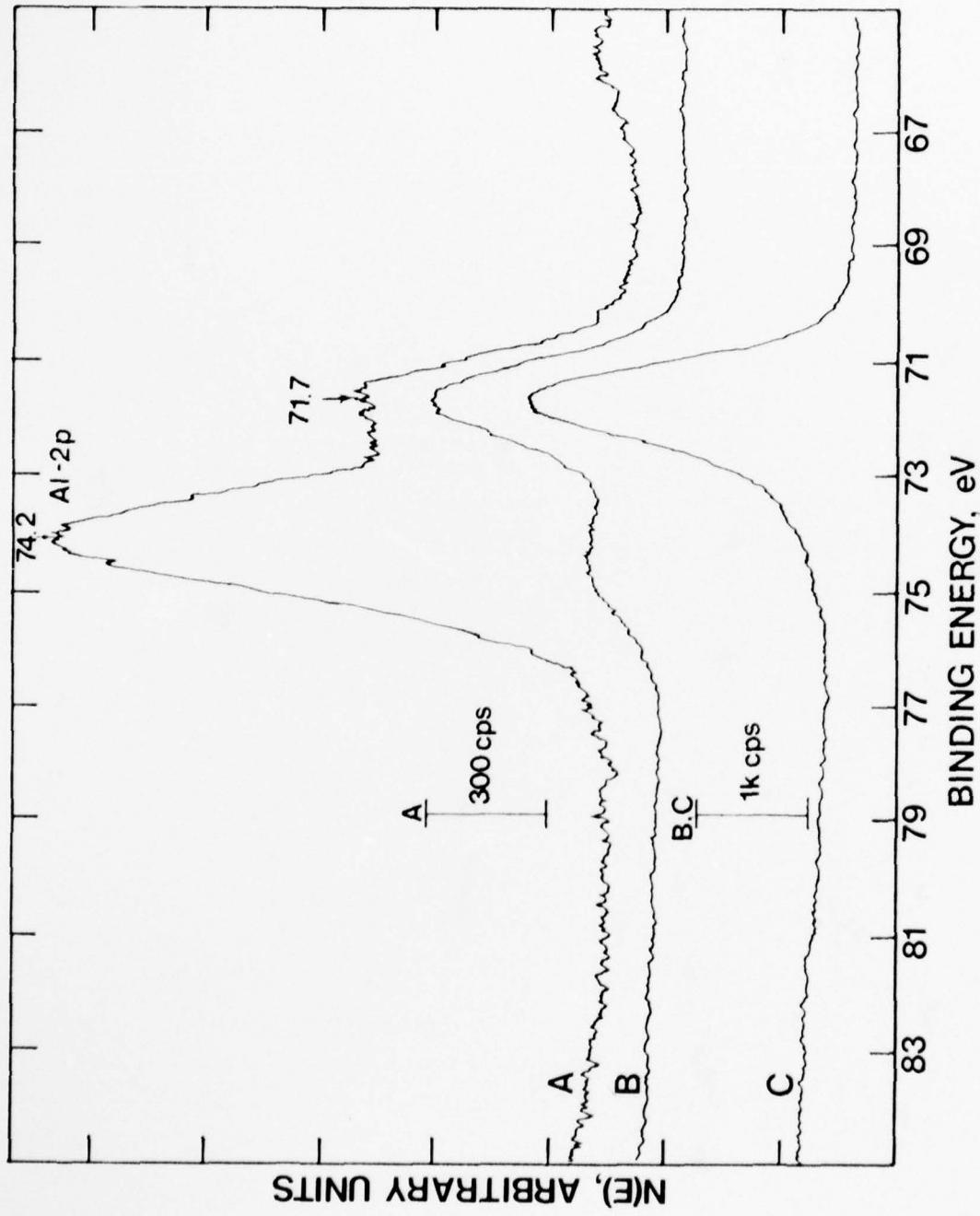
Figure 8. High Resolution XPS Spectra Showing Al-2p Peaks due to the Metal and the Oxide for Different Thicknesses of Al₂O₃ on Aluminum. Oxide thickness is of the order of 40 Å. Curve A is for the specimen before argon ion sputtering, curve B is after 30 Å removal and curve C is for the aluminum without an oxide.

approximated the Voigt function by a linear combination of L and G components involving the height, position and FWHM of the peak and a L-G mixing coefficient.[16] We then fitted all the peaks, one peak at a time, using a non-linear least squares fitting procedure. A background subtraction which includes the characteristic loss spectrum is made and an iteration procedure is followed until the best fit is obtained. The results of the fitting procedure for the Auger data are shown in Figure 9 where the solid lines are the experimental data. For the XPS data, it should be noted that each peak is an unresolved doublet involving the $2p_{3/2}$ and $2p_{1/2}$ states. With the theoretical $2p_{3/2}/2p_{1/2}$ intensity ratio of 2 and a splitting of 0.4 eV,[17] the peaks in curves A and B were successfully fitted. A "relaxed" fit was obtained for curve C by allowing the 2p doublet to relax for the best fit without imposing restrictions on the splitting or the intensity ratio. The results of the fitting procedure for the XPS data are shown in Figure 10.

After the fitting was completed for both Auger and XPS peaks and the contribution from the background and neighboring peaks removed, the area under each metal and oxide peak was found by integrating under the experimental curve. The attenuation length λ, in Al_2O_3, for electrons of approximately 1400 eV was then found by computing the effect of geometry and the oxide layer thickness on the Auger and XPS intensities and including appropriate emission functions for the oxide and the metal as described by Shelton.[18] An average value of $\lambda = 31 \pm 3$ Å was obtained by taking the mean of all the attenuations for the metal and oxide peaks in both the AES and XPS spectra. The oxide and metal normalized integrated intensities plotted versus t/λ are shown in Figure 11.

30
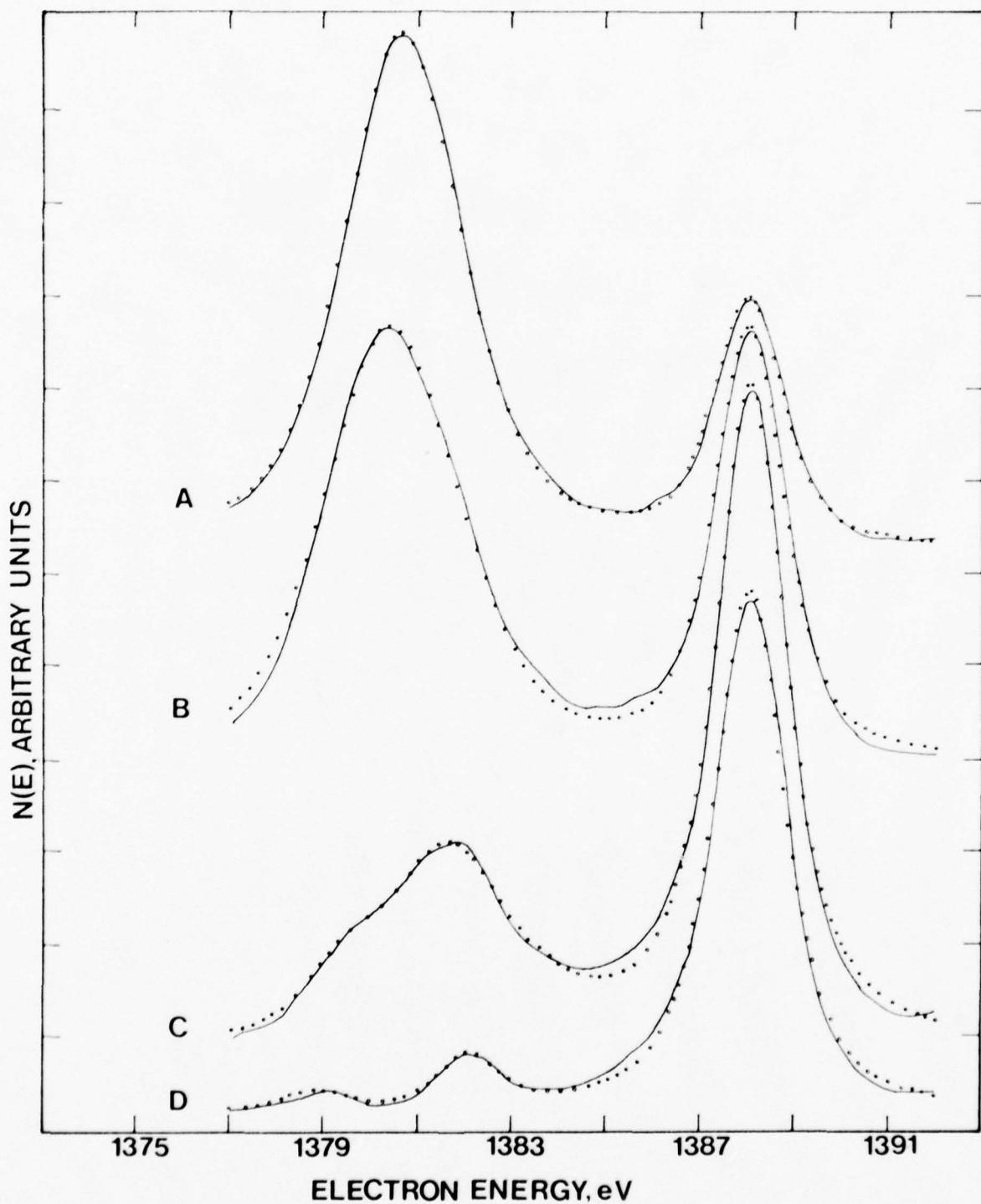
Figure 9. Computer Results of Fitting the Voigt Function to Experimental Auger Spectra. Solid lines are smoothed experimental data; dots are computed points. The designated curves correspond to those of Figure 7.
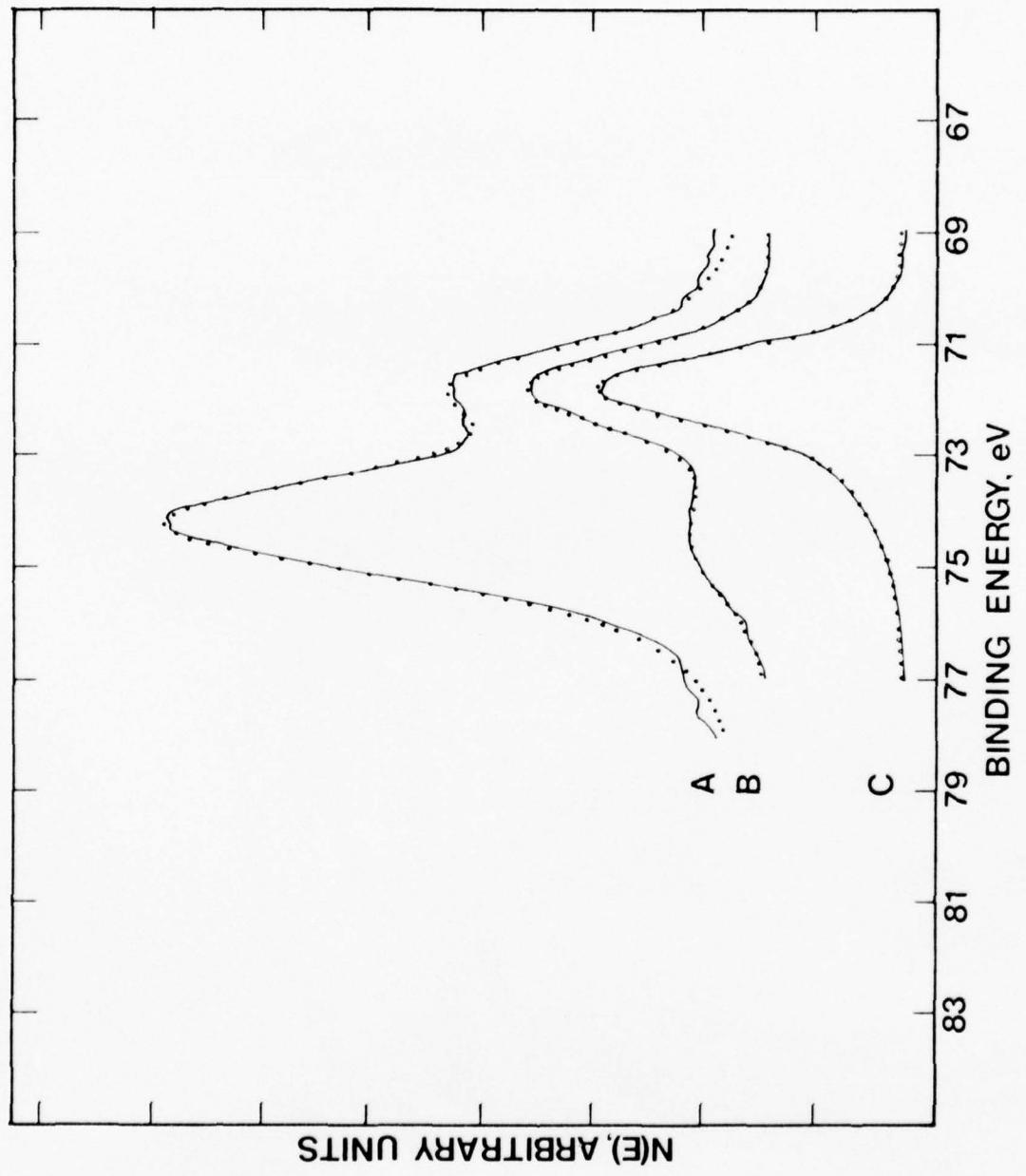
Figure 10. Computer Results of Fitting Theoretical Functions to Experimental XPS Spectra. Solid lines are smoothed experimental data; dots are computed points. The designated curves correspond to those of Figure 8.
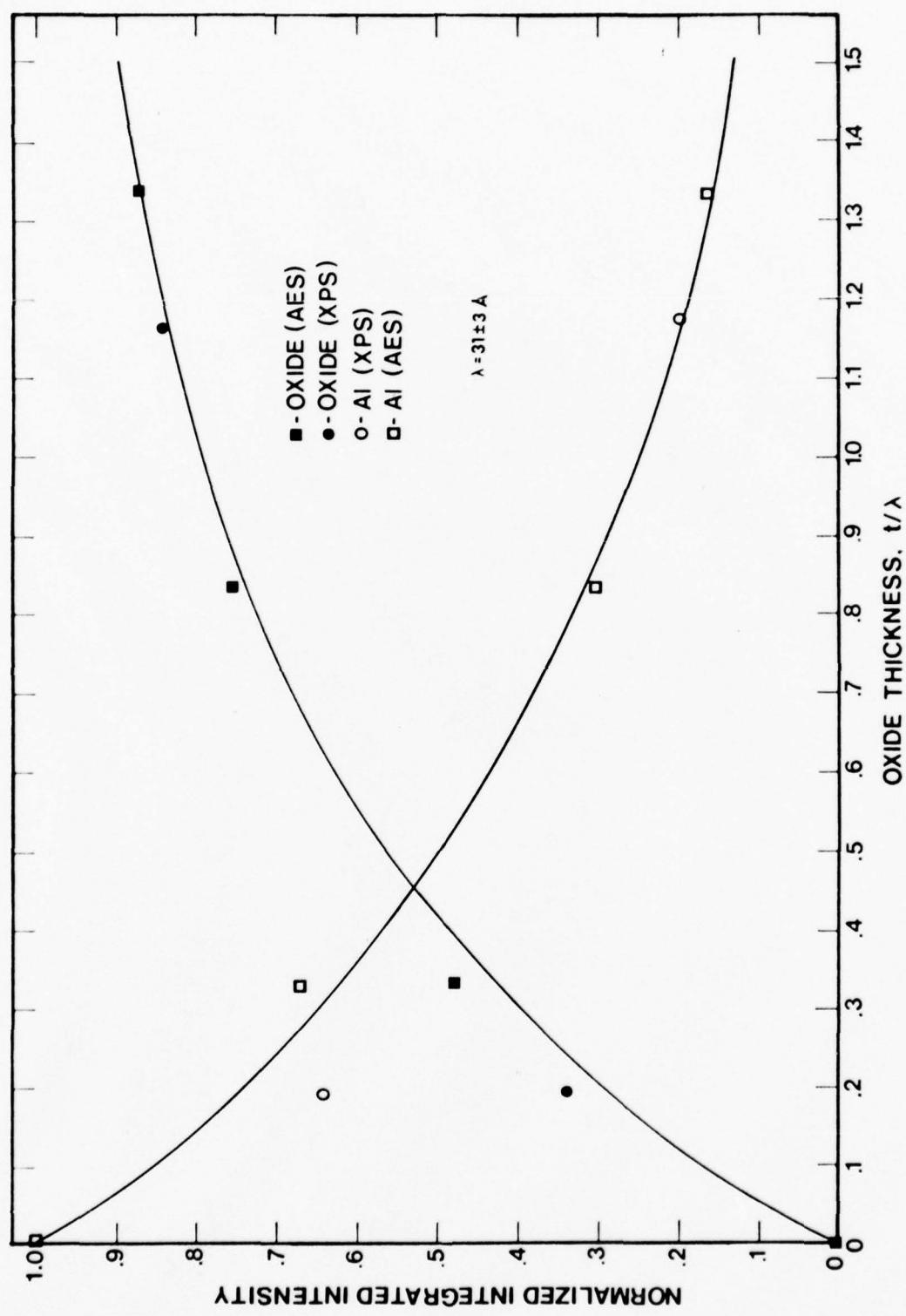
Figure 11. Attenuation Plots Showing Normalized Integrated Intensities versus Oxide Thickness for the Metal and Oxide Peaks from AES and XPS Spectra.

33

The value of the attenuation length may be in error due to the difference in sputtering rate for the calibration film used, Ta_2O_5, and Al_2O_3. Further experiments during the course of the program were directed toward the preparation of thin oxide films on tantalum and aluminum by anodization and reactive sputtering, and an independent measurement of the film thickness by ellipsometry. Using such specimens with known film thicknesses in each Auger or XPS run would enable a more precise determination of the sputtering rates. When these experiments are completed a reevaluation of the attenuation data is anticipated. A summary discussion of the optical methods used in the program is included in the next chapter of this report.

The results of the computer analysis also yield information on lifetime and phonon broadening. These topics are discussed fully in the complete paper

5.2 Gallium Arsenide

Three types of GaAs samples were prepared and examined by high resolution Auger and XPS techniques: (1) a (100) GaAs specimen oxidized in air at room temperature; (2) an Al/GaAs junction formed by depositing Al in situ on a (100) GaAs specimen oxidized in air for 3 hours at room temperature; and (3) a (100) GaAs specimen thermally oxidized in O_2 at 600 °C for 20 minutes.

Figure 12 shows the Ga $2p_{3/2}$ photoelectron peaks for a gallium arsenide sample oxidized in air at room temperature. Curve A is for the oxidized specimen; curve B is for the same specimen after removing approximately 15 Å by argon ion sputtering. A chemical shift in energy between the peak due to gallium and the peak due to gallium in the oxide is about 1.2 eV. It should be noted also that because of the high binding energies (1117 and 1118.2 eV)

34
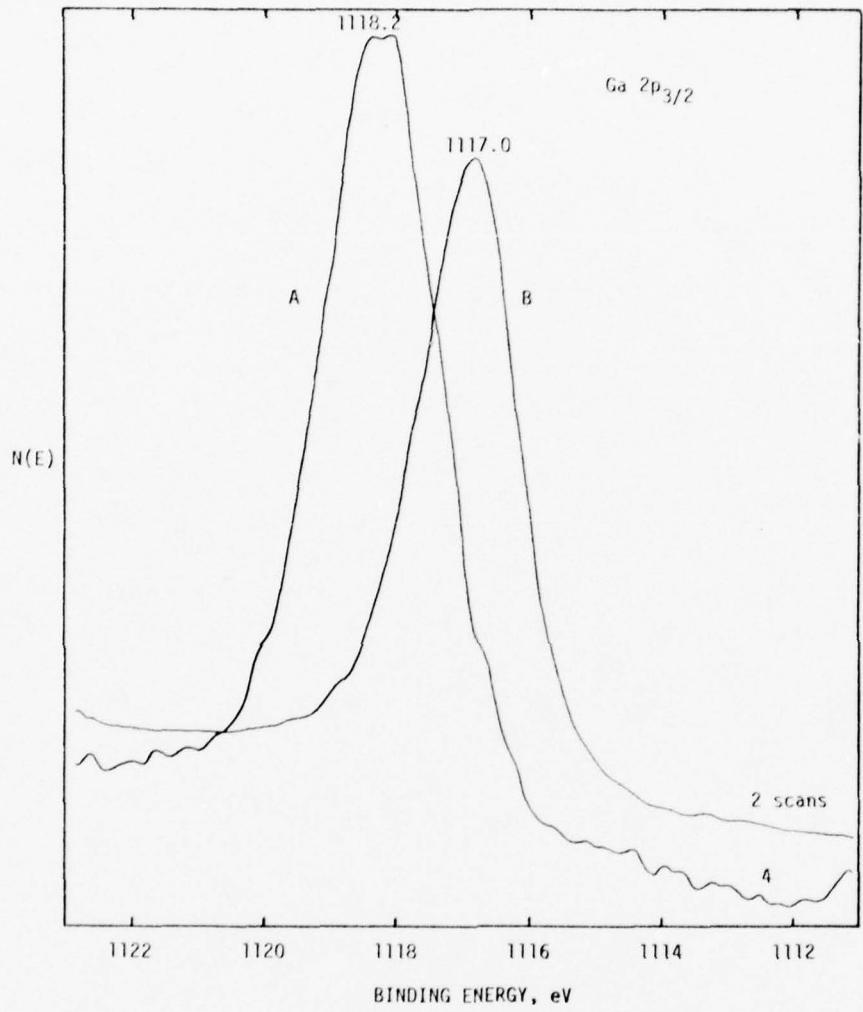
Figure 12. Ga 2p$_{3/2}$ Photoelectron Peaks for Gallium Arsenide Oxidized in Air at Room Temperature. Curve A, showing a chemical shift of about 1.2 eV, is for the oxidized specimen; curve B is for the same specimen after removing approximately 15 Å by argon ion sputtering. The number of scans in the signal averager is indicated on each curve.

and the MgKα photon energy of 1253.6 eV the kinetic energies of the photo-electrons are only of the order of 130 eV. The escape depth for electrons of this energy is small enough that there is practically no contribution to the oxide peak due to photoelectrons from the Ga in the substrate.

Figure 13 shows the X-ray excited Auger peaks for the same gallium arsenide specimen which was oxidized in air at room temperature. Curve A is for the oxidized specimen; curve B is for the same specimen after sputter removal of 15 Å. The Auger peaks occur in the XPS spectrum at apparent binding energies equal to the photon energy less the sum of the Auger energy and the spectrometer work function. For these peaks the Auger energies are about 1060 eV and there will be an appreciable contribution to the Auger peaks due to the oxide from the Auger electrons of the Ga in the substrate because of the greater escape depth at the higher energy. The spectra in Figure 12 and 13 show that room temperature oxidation produces a gallium oxide; no evidence for an arsenic oxide was found in either Auger or XPS data for the specimens examined. However, a different pre-oxidation surface treatment and/or a different crystallographic orientation may show the growth of arsenic oxide at room temperature. Detailed oxidation studies would be required to establish the conditions for the growth of either or both type oxide films.

In order to determine the effect of an Al layer deposited on the room temperature oxide a GaAs specimen was oxidized in air for 3 hours at room temperature and then an Al layer was deposited in the ultra-high vacuum Auger system using an in situ evaporator. A similar specimen was prepared for the Schottky diode measurements reported in chapter III. Figure 14 shows the Al-KLL Auger spectra for different thicknesses through the Al/GaAs
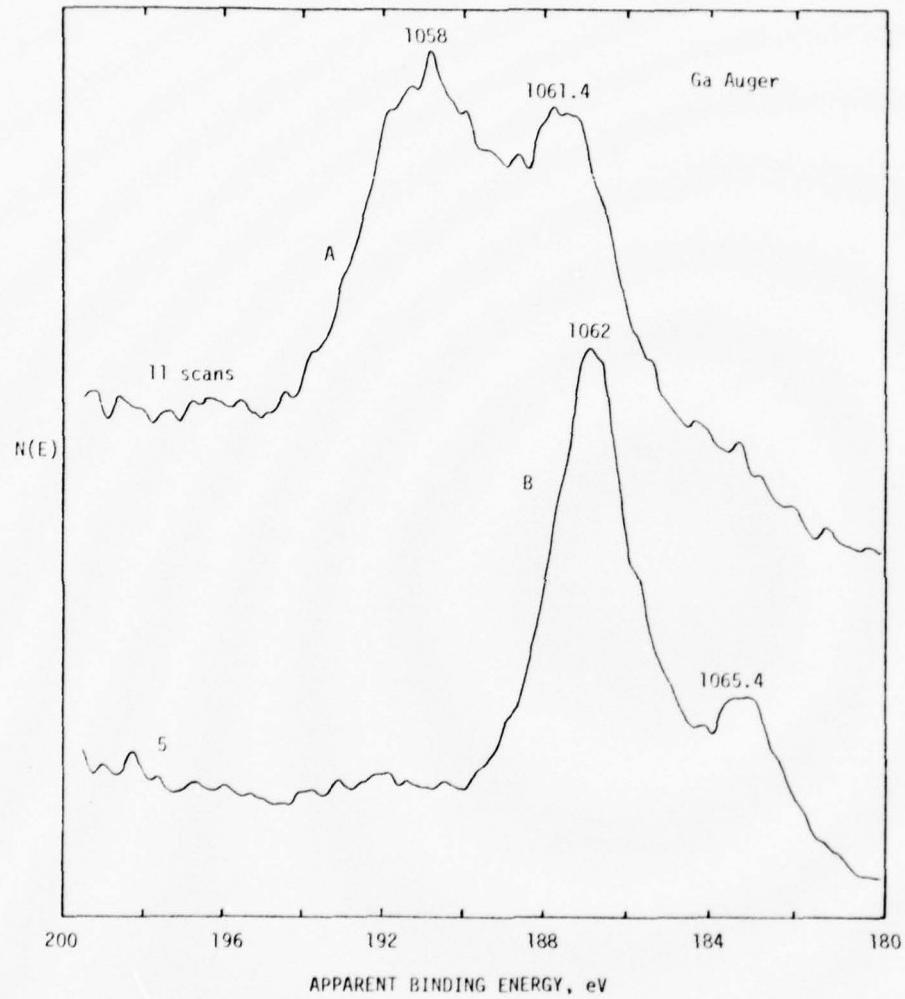
Figure 13. X-ray Excited Ga Auger Peaks for Gallium Arsenide Oxidized in Air at Room Temperature. Curve A is for the oxidized specimen, curve B is for the same specimen after sputter removal of 15 Å. The number of scans is indicated on each curve. Auger peaks occur in the XPS spectrum at apparent binding energies equal to the photon energy (for MgKα radiation, the photon energy is 1253.6 eV) less the sum of the Auger energy and the spectrometer work function. For example, B.E. = 1253.6 - (1058 + 4) = 191.6 eV.
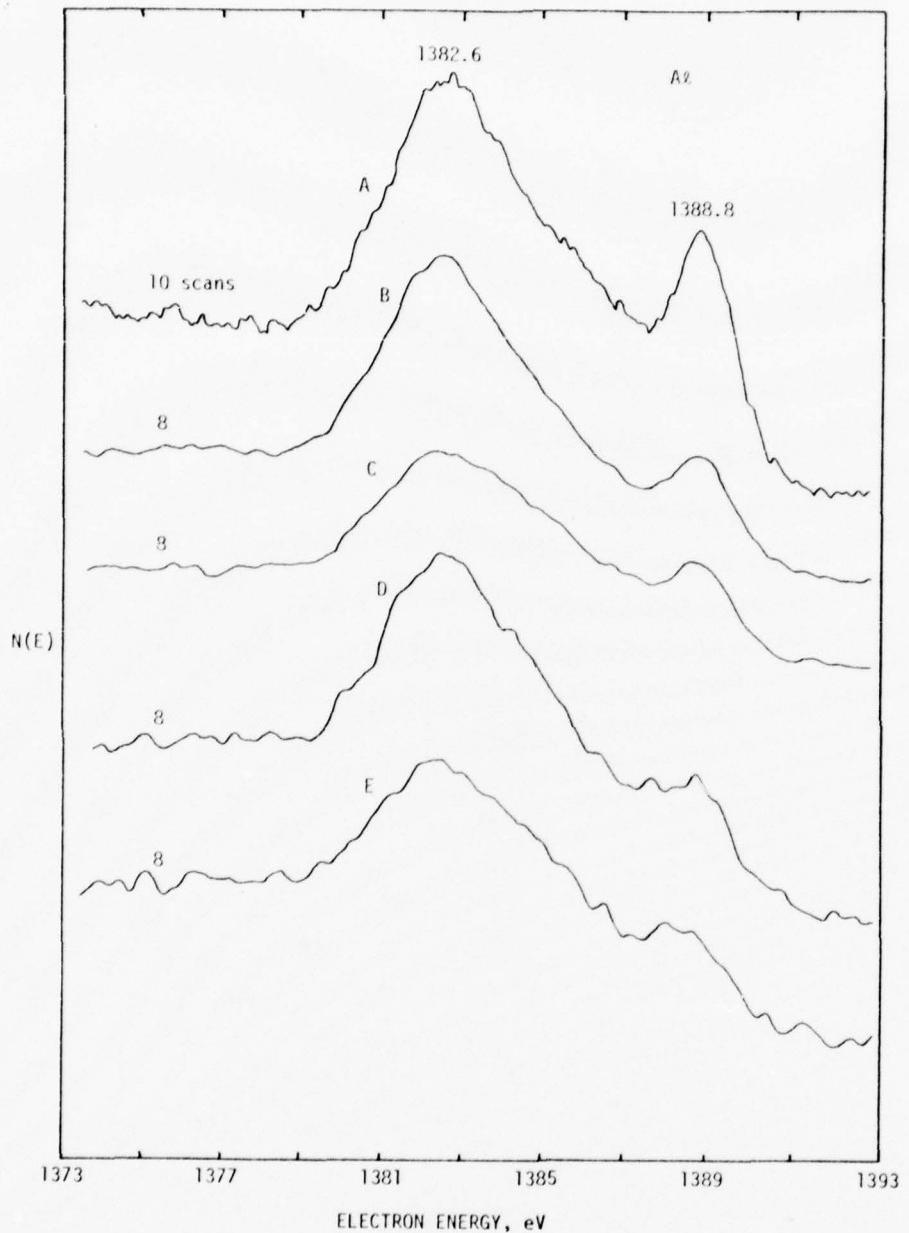
Figure 14. Aℓ-KLL Auger Spectra for Different Thicknesses through the
Interface of an Aℓ/GaAs Junction formed by Depositing Aℓ
in situ on a GaAs Specimen Oxidized in Air for 3 Hours at
Room Temperature. Curve A is after removal of approximately
130 Å of Aℓ; curve B is after 10 Å removed from curve A depth;
curve D is after 40 Å removed from curve A depth; and curve E
is after 55 Å removed from curve A depth. The number of scans
is indicated on each curve.

38

interface. Curve A is after removal of approximately 130 $\overset{o}{A}$ of Al; curve B

is after 10 $\overset{o}{A}$ removed from the curve A depth; curve C is after 20 $\overset{o}{A}$ removed

from the curve A depth; curve D is after 40 $\overset{o}{A}$ removed from the curve A

depth; and curve E is after 55 $\overset{o}{A}$ removed from the curve A depth. The pre-

sence of Al and Al_2O_3 in a broad interface region is similar to the result

obtained for the Al/SiO_2 interface (Chapter IV). Arsenic and gallium LMM

Auger spectra showed only elemental As and Ga, and no residual Ga_2O_3 or As_2O_3.

The third sample examined was thermally oxidized GaAs specimen. The

purpose was to determine the composition of the oxide, mainly near the outer

oxide surface. Figure 15 shows Ga $2p_{3/2}$ photoelectron peaks for the oxide

surface (curve A); after 30 $\overset{o}{A}$ removed (curve B); and after 60 $\overset{o}{A}$ removed

(curve C). The interpretation is that the oxide is Ga_2O_3. The peak posi-

tion agrees with the oxide peak position in Figure 12. Note that the peak

intensity increases then remains relatively constant through the oxide film.

Figure 16 shows As 3d photoelectron peaks for the oxide surface (curve

A); after 30 $\overset{o}{A}$ removed (curve B); after 60 $\overset{o}{A}$ removed (curve C); and after

120 $\overset{o}{A}$ removed (curve D). The As peak at 41.5 eV builds up to a constant

value after removing approximately 120 $\overset{o}{A}$ while the peak due to As in As_2O_3

decreases rapidly from a high value at the surface. The interpretation is

that there is an As_2O_3 layer at the surface which decreases exponentially

into the Ga_2O_3, and that there is free As distributed through the Ga_2O_3

thickness. The lower Ga_2O_3 peak intensity for curve A of Figure 15 is con-

sistent with this picture since the Auger electrons from the Ga in Ga_2O_3

would be attenuated by the As_2O_3 layer.

The significant result of this section is the apparent reduction of

Ga_2O_3 by Al to form Al_2O_3 at the interface. The stability of Schottky diodes
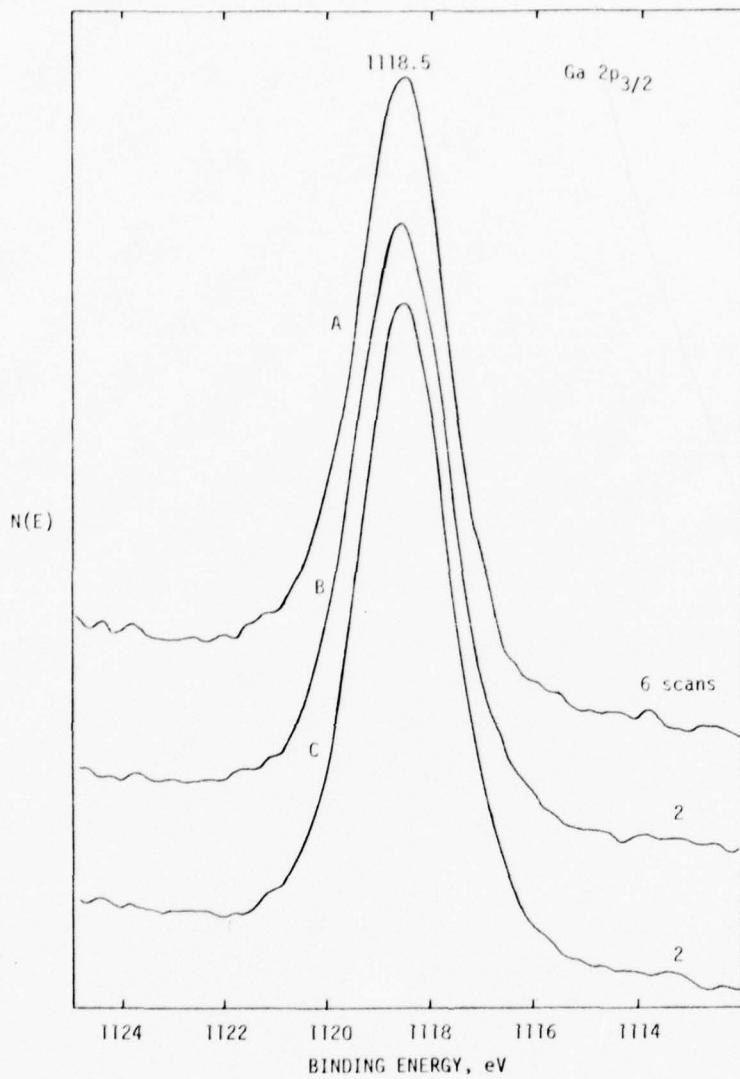
Figure 15. Ga $2p_{3/2}$ Photoelectron Peaks for a Thermally Oxidized GaAs Specimen (heated in O_2 at 600°C for 20 min.). Curve A is for the oxide surface; curve B is after 30 Å removed; and curve C is after 60 Å removed. The number of scans is indicated on each curve.
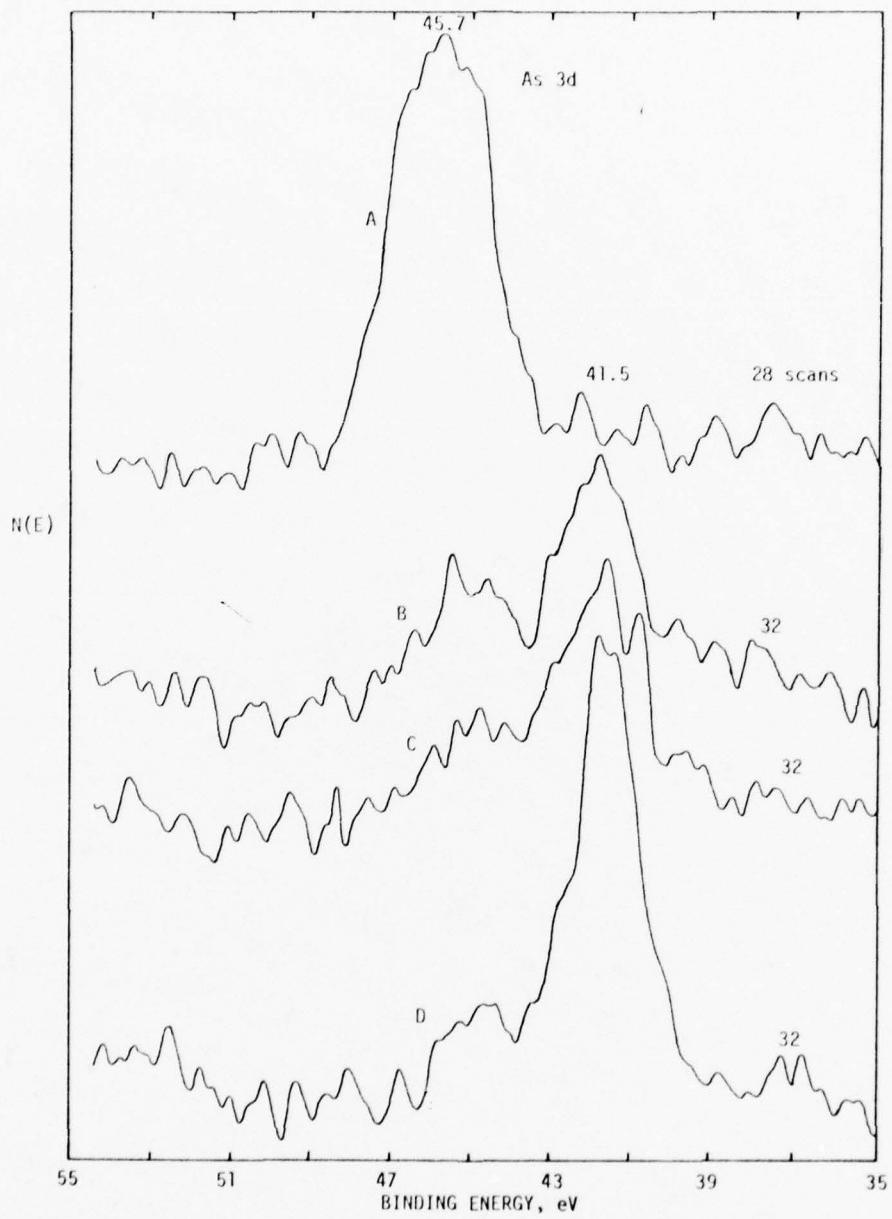
Figure 16. As 3d Photoelectron Peaks for the Thermally Oxidized GaAs
Specimen. Curve A is for the oxide surface; curve B is
after 30 Å removed; curve C is after 60 Å removed; and
curve D is after 120 Å removed. The number of scans is
indicated on each curve.

involving other reactive metals as well as aluminum and the possibility of utilizing such solid state reactions to develop a passivation method for GaAs devices have been considered in our program. Previous passivation methods are reviewed in chapter VII followed by an outline of a suggested method based upon the reduction of the initial gallium or arsenic oxide.

VI. OPTICAL METHODS:

In parallel with the previous studies an effort was initiated to characterize thin oxide films on gallium arsenide and other materials by the optical methods of ellipsometry and reflectivity. Oxide films on aluminum and tantalum, prepared by anodic oxidation or reactive sputtering, were studied to determine the optical constants and film thickness. With a series of these films with calibrated thicknesses one could in principle determine sputtering rates and thus obtain a more accurate value for the electron attenuation lengths in oxides. In fact, it would be desirable to incorporate a calibration specimen along with the specimen being examined by high resolution AES and XPS in order to insure that the sputtering conditions were the same for both type specimens.

The ellipsometer used in our investigations was a L117 Gaertner Production Ellipsometer equipped with a 2 mW helium-neon laser (6328Å) light source. The ellipsometric parameters that are measured are Δ and ψ. Δ is defined as $\delta_p - \delta_s$, the difference between the phase shifts for the component of the light wave parallel (p) to the plane of incidence and that perpendicular (s) to the plane of incidence. The relative amplitude attenuation is given by $\tan \psi$. Δ and ψ are related to the optical constants through the relation

$$\tan \psi \; e^{i\Delta} = r_p/r_s$$

where r_p and r_s are the Fresnel reflection coefficients for a surface film-absorbing substrate system. For such a system one obtains an expression relating five known parameters (λ, ϕ, n_1, Δ and ψ) to five unknown parameters (n_2, k_2, d, n_3, and k_3). We have used the computer program of Malin and

43

Vidam[19] to determine the optical constants for the thin film and absorbing substrate and the thickness of the oxide film from four sets of Δ and ψ values. We have also used the computer program of So[20] to determine the optical constants of the film and its thickness from only two sets of Δ and ψ values when the optical constants of the substrate are known. Obtaining the optical constants of a clean substrate is not a trivial matter. In our studies we used for this purpose an automated surface analysis apparatus developed by Wall and Stevenson of Georgia Tech[21] which provides real time acquisition and manipulation of optical reflectivity and Auger data. The apparatus consists of an ultra-high vacuum chamber/reflectometer equipped with a cylindrical mirror analyzer and integral coaxial gun for surface characterization by AES, an ion gun for surface cleaning by argon ion sputtering and a minicomputer for the collection and manipulation of the data. Computer programs were available to determine, from the reflectivity data, the optical constants, n and k, for the range of wavelengths used.

Gallium arsenide substrates were examined by both optical methods. The thickness of thin oxide films on GaAs after wet chemical cleaning was determined by ellipsometry and reflectivity measurements for clean and anodized GaAs were compared.

VII. GaAs SURFACE PASSIVATION - A PROPOSED METHOD:

Significant applications of GaAs devices and integrated circuits depend upon the development of an oxide or insulating layer with good dielectric properties, a minimum of fixed and mobile ions in the layer, and low surface or interface state densities at the insulator-GaAs interface. In the course of our fundamental investigations on GaAs surfaces we have also been cognizant of this need for surface passivation and have considered the application of our results to the passivation problem. A brief survey of the literature was made and a practical method was then outlined which utilizes the principle of the solid state reduction of an initial oxide on GaAs by Al to form Al_2O_3. A more detailed study would of course be necessary to explore this approach but the understanding of the surface physics and chemistry at insulator-GaAs interfaces is believed to be essential to the development of a successful passivation method.

7.1 Survey of Literature on Passivation

There have been a variety of techniques investigated for the growth of native oxides or other insulating films on gallium arsenide, including thermal, anodic, plasma oxidation and other methods. Some of these are reviewed by Schwartz[22] in a critical review of GaAs surface chemistry and by Wilmsen,[23] who compares the growth of thermal oxides on the III-V compound semiconductors with anodic oxides.

Thermal oxidation of GaAs has been the subject of several publications[23-32], and one Ph.D. research was devoted to the thermal oxidation of GaAsP.[33,34] Murarka[25] shows that amorphous oxide films are formed on GaAs heated in air and that the films have good adherence and can be removed by HCl, indicating that they might provide a useful mask for GaAs device technology. Navratil[27] studied the oxidation of GaAs in dry oxygen over the

temperature range 400-530°C and also obtained amorphous films. Later, Navratil, Ohlidal and Lukes[28] proposed a model for the growth of thermal oxides on GaAs within the temperature range 480-530°C and studied the system using optical reflectance measurements. In 1962, Minden[29] studied the oxidation of GaAs in pure oxygen and in water vapor containing oxygen at temperatures between 600°C and 900°C, and observed electron diffraction patterns which indicated that the films were crystalline and composed of β-Ga_2O_3. Later, Rubenstein[30] found that the thermal oxidation of GaAs in pure oxygen at temperatures between 700°C and 1130°C produced crystalline β-Ga_2O_3 and a small amount of crystalline $GaAsO_4$. Zaininger and Revesz[31] found that GaAs oxidized at 660°C in dry oxygen produced granular oxides free of arsenic. Also, Sealy and Hemment[32] concluded that some trace of arsenic was present in oxide films grown in oxygen at 610°C but those grown at 680°C contained no arsenic. Finally, Coerver[33,34] found that the thermal oxidation of GaAsP in dry oxygen in the temperature range between 600°C and 900°C comprised a mixture of crystalline β-Ga_2O_3 and $GaPO_4$. Using high energy resolution Auger and X-ray photoelectron spectroscopy (XPS or ESCA) techniques, we have shown (Chapter V of this report) that thermal oxides grown in oxygen at 600 °C were Ga_2O_3 and that they contained elemental arsenic throughout the bulk and a thin layer of As_2O_3 at the oxide-air interface.

The growth of anodic oxides on GaAs has frequently been investigated, principally by Schwartz at Bell Labs[35-37] and by Hartnagel and associates at the University of Newcastle upon Tyne.[38-43] Some of the basic ideas on

46

the anodic oxidation of metals and semiconductors were given in 1972 by Fehlner and Mott.[44] In 1976, Weimann and Schlapp[45] reviewed the two techniques which give homogeneous uniform films of low conductivity, constant voltage anodization in aqueous H_2O_2 (due to Schwartz) and anodization in a mixture of glycol and water (due to Hartnagel). These electrolytes were also compared with several non-aqueous electrolytes to determine the experimental conditions for stable and uniform films. Spitzer, Schwartz and Weigle[36] report that anodic films grown in hot concentrated (30%) H_2O_2 can be etched by HCl and H_2O but that their chemical stability is enhanced by heating in dry N_2 at 250°C for two hours, after which H_2O will no longer etch the oxide. They suggest that a device process for improved reliability might utilize an oxide growth-strip-regrowth cycle for removing surface contamination. Hasegawa, Forward and Hartnagel investigated other aqueous electrolytes than the mixture of glycol and water; these included tartaric or citric acid mixed with glycol[38] and a weak carboxylic acid with polyhydric alcohol in water.[39] In the second case, they obtained electrical properties of the anodic films by MOS capacitance measurements and found that the growth technique yields stable and reproducible layers with a breakdown strength of 5×10^6 volts/cm and resistivities of 10^{14}-10^{16} ohm-cm. Also, low temperature annealing in hydrogen improved the interface properties. In 1976, El-Safti, Weiss and Hartnagel[42] discussed the anodization of aluminum on GaAs and Weiss and Hartnagel[43] showed that GaAs surfaces cleaned in organic solvents, polished in bromine-methanol solutions and etched in HCl have a residual thin layer of oxide on them. This is consistent with the studies we have performed using AES to provide much more

47

detail on the composition of the residual film.

Schwartz, Ermanis and Brastad[37] recently demonstrated the anodic oxidation of GaAs in water of the proper conductivity and pH, and showed that, for device fabrication, a photoresist could be used to define restricted areas for oxidation and/or etching. Other electrolytes studied include a non-aqueous solution of ammonium pentaborate by Arora and Bidnurkar[46] and ammonium phosphate in water by Law and Lee.[47] Szpak[48] related the initial two-dimensional phase of anodic oxide growth to a distribution of oxide nuclei on the surface. Coleman, Shaw and Dobrott[49] obtained the oxygen concentration profile in anodic films using radioactive-labeled oxygen, while Guenthner, Rao, Thomas and Paulson[50] used simultaneous ion sputtering and Auger analysis to obtain composition profiles for anodic films grown on GaAsP in both aqueous and non-aqueous electrolytes, and changes in the profiles after annealing.

There have been few studies of the growth of oxides in GaAs in an oxygen plasma. Weinreich[51] used a technique similar to that of Ligenza[52] who studied the oxidation of silicon in a microwave-generated plasma. His films were amorphous and reached thicknesses of 3500Å in 100 minutes in an oxygen partial pressure of 0.2 Torr. However, Sugano and Mori[53] obtained polycrystalline films grown on (100) and (111) GaAs in a high frequency oxygen-discharge plasma, with a dependence on O_2 partial pressure and the high frequency field. Composition profiles were made of these films by simultaneous ion sputtering and Auger analysis.[54] Chang and Sinha[55] obtained amorphous layers by their plasma growth technique but they report that interface properties need to be improved before they can be used in

48

the passivation of devices. Chang, Chang and Sheng[56] recently used a new approach for growing insulating layers on GaAs; they first deposited aluminum on GaAs then oxidized the aluminum to Al_2O_3 in an oxygen plasma. The resulting films were analyzed by AES and transmission electron microscopy. Kauffman, Feldman, Poate and Chang[57] then used helium ion backscattering and ion-induced x-ray techniques to determine the composition profile but found unresolved discrepancies with the Auger data.

Lukes[58] studied the kinetics of the oxidation of gallium arsenide in air at room temperature and Loeschke and Kuehn[59] studied the oxidation kinetics and orientation dependence of the air oxidation of GaAs doped with tellurium or tin.

Two dielectric films which have proved successful on silicon, silicon dioxide, SiO_2, and silicon nitride, Si_3N_4, have been explored for the passivation of GaAs.[60-71] Lorenz[60] studied MIS devices using SiO_2 as the gate insulator. He observed considerable dispersion in the C-V curves with frequency and associated the high surface state density and distribution of time constants to the insufficient purity of water used in the cleaning operations prior to the SiO_2 deposition. Sato and Ikeda[61] used both SiO and SiO_2 in MOS capacitors. In 1970, Kern and White[62] reported on the first comprehensive study of silica films on GaAs. The SiO_2 films were deposited primarily by the pyrolysis of tetraethyl siloxane under various temperature and pressure conditions. C-V measurements of MOS capacitors were made as a function of several variables including the oxide deposition conditions, a post-deposition heat treatment, substrate dopant, the crystallographic orientation of the GaAs and the chemical treatment prior to deposition of SiO_2.

49

The lowest value of surface or interface state density of 10^{11} states cm^{-2} eV^{-1} was achieved by using (111) GaAs plus a combination of specific chemical treatments followed by rapid deposition of SiO_2 at a low temperature. Weissman[63] deposited both SiO_2 and Si_3N_4 in an R.F. glow discharge. From his C-V measurements he deduced that both types gave large densities of interface states. The density near the mid-gap was between $4-6\times10^{12}$ cm^{-2} eV^{-1} and near the band edges it was estimated to be greater than 10^{13} cm^{-2} eV^{-1}.

Ito and Sakai[64] fabricated inversion channel GaAs MISFET's using alloyed source and drain n^+ regions and a CVD double layer film of Al_2O_3 and SiO_2 for the gate oxide, for improved stability. Semushkina, Marakhonov and Seisyan[65] produced films of either Al_2O_3 or SiO_2 also by CVD techniques. Their C-V measurements indicated majority carrier (n) depletion due to electron capture by surface states supposedly introduced during the process heat treatment. The passivation of microwave Au-GaAs Schottky-barrier diodes by R.F. sputtered SiO_2 films was studied by Stareev, Piskorski and Majewski.[66] They formed windows in the oxide layer and vacuum deposited gold to form the Schottky barrier after cleaning the GaAs surface by ion sputtering. Messick[67] formed insulating films of silicon oxynitride on LPE layers on GaAs and fabricated MISFET's which showed little hysteresis and mobilities greater than 2000 cm^2/volt sec.

In addition to the studies of Si_3N_4 films by Weissman[63] and the silicon oxynitride films by Messick,[67] Sugano et al,[68] Ward[69,70] and Seki et al.[71] investigated the passivation of gallium arsenide with Si_3N_4. Sugano, Sakai and Mori[68] deposited Si_3N_4 films on GaAs surfaces at low temperatures using an R.F. glow discharge in a mixture of silane and nitrogen gas. However,

even though the technique is promising, the films were not dense enough to have sufficient insulating properties. Ward[69] and Cooper, Ward and Schwartz[70] reported on investigations of CVD-grown films of Si_3N_4 on GaAs including their evaluation by admittance-voltage measurements of MIS capacitors over a wide frequency range (10KHz to 50MHz). They interpreted their results in terms of large densities of surface states distributed across the interface into the insulator.

Insulating layers of Al_2O_3 show promise for good dielectric films on GaAs. Sugano, Sakai and Mori[68] who reported the growth of Si_3N_4 films in an R.F. glow discharge also investigated the growth of Al_2O_3 films on GaAs and found that their characteristics depended upon the growth rate. As mentioned earlier, Ito and Sakai[64] obtained improved stability of GaAs MISFET's by using double layer films of Al_2O_3 and SiO_2. Semushkina, Marakhonov and Seisyan[65] observed that the majority carrier (n) concentration was depleted at the surface for CVD Al_2O_3 films as it was for SiO_2 films, probably for the same reason, the substrate heat treatment. Singh and Hartnagel[72] were able to grow Al_2O_3 layers on GaAs by evaporating aluminum through a partial pressure of oxygen with a resulting interface state density that was lower than for native oxides. Siekanowicz, Huan, Hoffmann, Jolly and Chiang[73] applied aluminum oxide passivation to electron-beam semiconductor diodes and Wada, Yanagisawa and Takanashi[74] showed that heat treatment of Al-GaAs Schottky barrier diodes during and after Al deposition improved their characteristics with respect to surface states.

7.2 Proposed Method

Based upon the experience from previous insulating film studies, as reported in the literature, and upon the results of our fundamental investigations of solid state reactions at interfaces, we propose the following method for the passivation of GaAs surfaces for device applications.

The steps in the process would include:

(1) The choice of a particular orientation of the GaAs substrate and the use of semi-insulating Cr-doped substrates because of the desirability of fabricating field effect devices.

(2) The MBE growth of a semi-insulating or undoped buffer layer for isolation from substrate defects and surface contamination.

(3) The MBE growth of a doped layer which will become the conducting layer in field effect devices. The choice of dopant type and concentration profile may also be important for device applications.

(4) A wet chemical cleaning treatment. Appendix A gives the procedure we have used for cleaning GaAs substrates prior to MBE growth or prior to surface studies using AES.

(5) Growth of a thin anodic film as an aqueous electrolyte to displace the interface and to provide an initial film, e.g., Ga_2O_3.

(6) A possible heat treatment in dry N_2 to stabilize the initial film or in H_2/N_2 mixtures to improve interface properties.

(7) Deposition of pure aluminum to reduce or partially reduce the initial oxide film and to form Al_2O_3. Other metals may also prove to be feasible here if the thermodynamics is favorable.

(3)   Growth of thicker insulating layers of Al_2O_3 by a suitable
      deposition process, for example, reactive sputtering.

(9)   The possible low temperature growth of SiO_2 or other insulator
      on the Al_2O_3 film.

(10) A post-deposition heat treatment.

VIII. SURFACE/INTERFACE STATES ON ELEMENTAL AND COMPOUND SEMICONDUCTORS:
(A. Craig Kenton)

8.1 Introduction

Thus far we have considered problems associated with the physics and chemistry of surfaces or interfaces on semiconductors from a macroscopic point of view. In our studies during the last year we have focused on the microscopic or atomistic approach, especially in discussing the nature of interface reactions which will depend upon the local atomic arrangements and chemical bonds. The influence of these local effects on the electronic properties of the semiconductor is reflected in the energies and densities of surface or interface states.

A study was initiated under the program of theoretical techniques for describing the localized electronic structure at the atomic sites of a quasi-molecular complex comprising substrate and interface atoms. Three particular theoretical techniques appear promising. These are: (1) molecular cluster calculations; (2) the pseudopotential method; and (3) the generalized Wannier function method. Section 8.5 of this chapter reviews these localized theoretical approaches.

Of the several surface analytical techniques which probe the electronic structure of solids, photoemission and energy loss spectroscopy have provided the most lucid observations of intrinsic surface or interface states. Thus, data from photoemission and energy loss spectroscopy studies will be useful for comparison with the results of the theoretical studies. These experimental techniques and the interpretations of surface/interface states for silicon and gallium arsenide are reviewed in Sections 8.2 and 8.3.

The techniques of LEED and RHEED provide information on the crystallographic order and lattice damage of a clean surface or surface/adsorbate

system. The theoretical analysis of such data, however, is formidable due to complications arising from surface relaxation and/or reconstruction, multiple scattering processes and many body effects. Much progress, however, has been made recently in this area yielding useful model geometries that can be inserted into the electronic structure calculations. Models for the atomic geometry of gallium arsenide surfaces, based primarily on LEED data, are discussed in Section 8.4.

8.2   Surface/Interface States and Photoemission Spectroscopy

In principle, the photoemission experiment involves using electromagnetic radiation in the ultraviolet to X-ray range as an exciting probe to eject electrons out of a solid. The ejection of electrons will only occur if the exciting photon energy is sufficiently high. Once outside the solid, electrons may be analyzed in terms of their kinetic energy and emission angle. Photoemission probes the intrinsic electronic properties of the sample yielding a spectrum which will, in general, reflect both bulk and surface contributions. Surface sensitivity of photoemission spectra on surfaces can arise from two theoretical conditions resulting in a localized electronic wavefunction: (1) trapping at a surface state localized in a band gap; and (2) strongly damped final state wavefunctions.[75,76] The last condition arises from the inelastic electron-electron interactions which result in electron scattering lengths of ~ 5 Å, yielding emitted photoelectrons in the energy range 20 - 100 eV. This condition is responsible for the surface sensitivity of any electron spectroscopy, e.g., Auger Electron Spectroscopy (AES) or Low Energy Electron Loss Spectroscopy (LELS), in this range.

8.2.1   Studies on Silicon (Si) Surface/Interface States

Bardeen[77] first postulated the existence of surface

electronic states on semiconductor surfaces to explain band bending and
Fermi level pinning at a metal-semiconductor contact (Schottky barrier).
Allen and Gobeli[78] observed that the photoelectric threshold and work func-
tion of Si(111) remained constant as the Fermi level was swept through the
bulk band gap by varying the impurity concentration, i.e., the Fermi level
remained pinned at the surface due to the existence of surface states.
They deduced that the surface states existed in two bands, one above and
one below the Fermi level; however, since the photon energy was only about
1 eV above the valence band, the full energy distribution of the surface
states was not obtained. Chiarotti, et al.[79] observed optical absorption
for photon energies less than the bulk band gap by maximizing the surface
absorption sensitivity. After the cleaved surface was studied, it was then
exposed to oxygen and restudied. The differences in the clean and oxidized
absorption, shown in Figure 17, was assigned to surface states. Direct pho-
toemission evidence of filled surface states on Si(111) was first obtained
by Eastman and Grobman[80] and by Wagner and Spicer[81] for photon energies
more than 5 eV above the threshold. The results clearly showed a shoulder
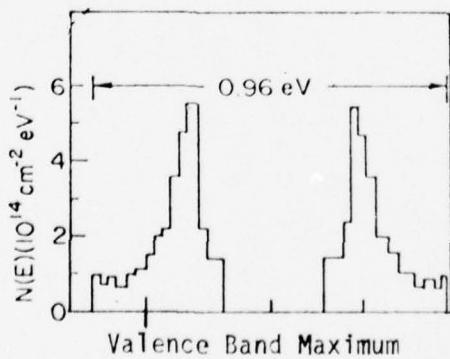
Figure 17. Model of Si Surface States as Determined by
Optical Absorption (after Chiarotti et al.[79]).

near the top of the valence band at the surface which disappeared after low

exposure to air or residual gas. Small differences in the location of peaks

have been attributed to the well known[82] (2 x 1) reconstructed surface of

Si(111) after cleavage and the (7 x 7) annealed structure.[86] Figure 18

illustrates the experimental spectra of several authors. Spicer[87] suggests

one method of identifying filled surface states is by varying the photon

energy and observing the shifting of bulk peaks. This is presently most

conveniently done by using continuously tunable synchrotron radiation. The

establishment of the pinning of the Fermi level[78] and verification by more

thorough photoemission studies[88] illustrates how band bending affects sili-

con surface states.
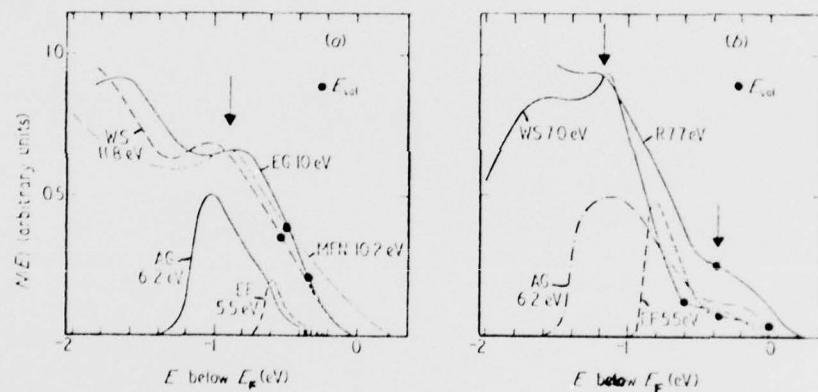
Figure 18. Comparison of Photoemission Energy Distribution Spectra
of a) Freshly Cleaved Si(111) 2 x 1 and b) Annealed
(> 850°C) Si(111) 7 x 7 Surfaces by Several Authors[80-88]
(after Feuerbacher and Willis[76]).

Figure 19 shows the shift of bulk states with respect to the surface Fermi

level and the relatively minor shift of the surface states. An experimental

approach of separating bulk and surface photoemission data by averaging over

the different surface structures and subtracting the average from the indi-

vidual spectra yielding the surface contribution is illustrated in Figure

20.[89-91] Justification of this procedure is that the averaged spectrum

57
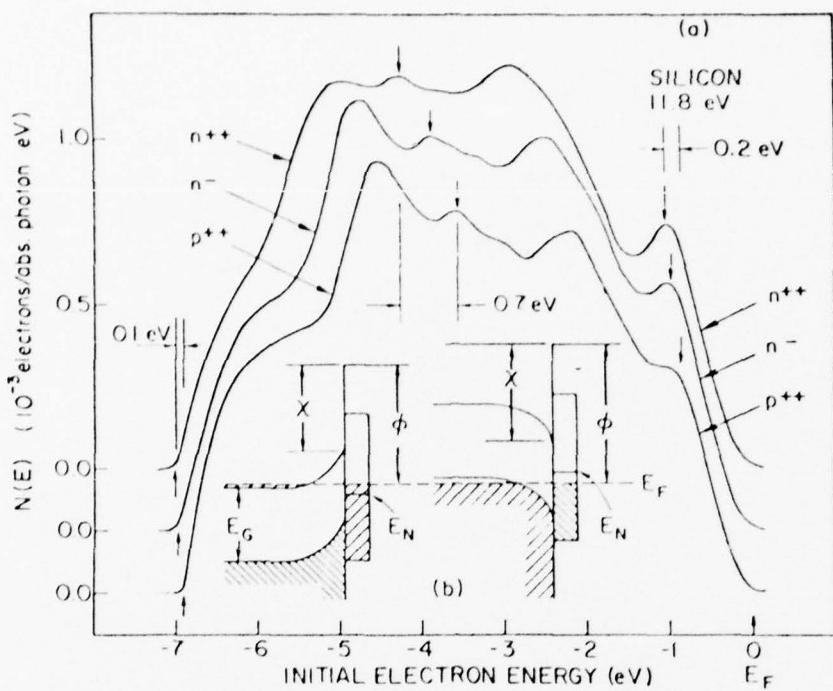
Figure 19.   (a) Energy Distribution Curves for Silicon. The high-
             energy peak is due to electrons in surface states. The
             pinning effect causes a 0.2 eV movement of this peak
             and a small shift in the work function edge (left).
             (b) Band Diagram for n++ (left) and p++ (right) Silicon
             Illustrating the Pinning Effect (after Spicer[88]).
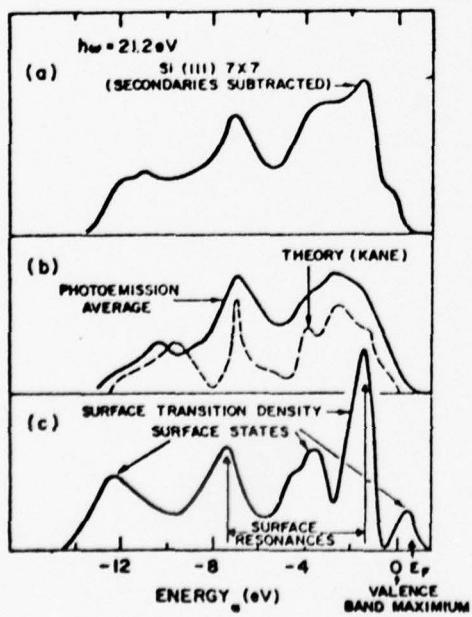
Figure 20.   (a) Photoemission energy
distribution from Si(111) 7 x 7 with
the estimated contribution from secondary
electrons removed. (b) Comparison of
"averaged" photoemission curve with the
density of states calculated by Kane[92].
(c) Surface transition density of states
obtained by Rowe and Ibach[89] by subtracting
the assumed bulk signal (curve b) from
the measured energy distribution (curve a).

58

is similar to a theoretical calculation of the density of states.[92] This appears most useful in identifying surface resonances, i.e. surface states which are degenerate with bulk states.

Theoretical progress on silicon has been achieved by several authors,[93-95] notably by Applebaum and Hamann,[96-98] where they have correlated one of the surface states in the band gap with "dangling bonds" of the surface atoms. Taking into account self-consistency and surface relaxation, two surface states are found.[97-99] The (2 x 1) reconstruction of freshly cleaved Si(111) has been theoretically studied by several authors.[98,100-103]

The use of angle-resolved photoemission, i.e. the energy analysis of ejected electrons in terms of their emission angle suggests new interpretations of the bonding mechanisms of surface species. Although many experimental and theoretical difficulties still exist, results for Si(111) indicate appreciable mixing of the dangling bonds and back bonds.[104,105]

In addition to conventional energy analysis of photoemission data, the technique of photoemission yield spectroscopy has been used to probe unfilled bulk and surface states. For Si(111), the work of Koma and Ludeke[109] and Bauer, et al.[110] is cited.

A widely used method for the characterization of surface states on semiconductors is by chemisorption to form surface bonds. The difference in the clean surface spectra and the chemisorbed spectra are then compared. In the case of silicon, it is found that the dangling bonds react with several active gases, preferentially oxygen, resulting in the disappearance of the observed intrinsic surface states. On n-type samples, oxidation removes the silicon surface states and destroys the Fermi level pinning. The pinning is not totally destroyed on p-type silicon even though the

surface state peak vanishes from the photoemission spectra. The remaining small density of surface states now become interface states resulting in the partial pinning on p-type samples.[88,111] This dramatic effect (see Figure 21) is the primary reason that the Si/SiO_2 interface is a passive structure-- providing reliable exterior surfaces for the countless devices utilizing silicon technology. Interface states have been studied theoretically and experimentally on the formation of the monohydride phase [Si(111) 7 x 7 → Si(111):H][113] and the trihydride phase [Si(111) 1 x 1 → Si(111):SiH_3][114]
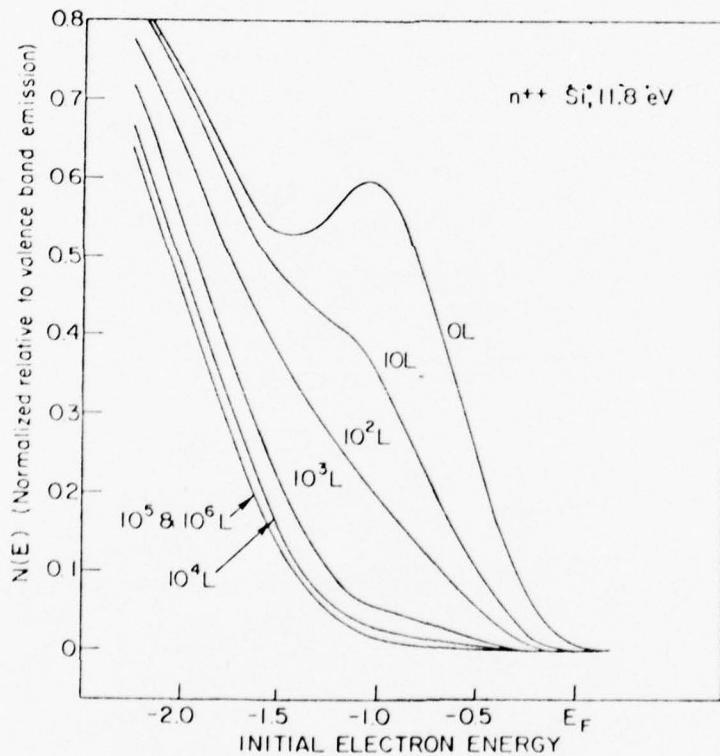
Figure 21. The Effect of Oxygen on the Si Surface States. The peak at about -1.0 eV (0 L) is due to surface states, which have almost entirely disappeared after 10^3 or 10^4L exposure. (1 Langmuir, L = 10^{-6}torr-sec.)(after Spicer[112]).

60

of silicon. The correlation between atomic geometry and electronic struc-
ture for this sytem has proved fruitful. Very recently, the atomic position
of Cl chemisorbed on Si(111) has been studied using angle-resolved photo-
emission with synchrotron radiation.[115] The electronic structure has been
correlated with the atomic structure by the pseudopotential method.

The study of silicon surface/interface states provides the concepts
by which we will extend our knowledge to more complicated systems, for ex-
ample, the compound semiconductors. The various techniques of photoemission
continue to play a crucial role.

8.2.2 Studies on Gallium Arsenide (GaAs) Surface/Interface States

Studies concerning surface and interface states on GaAs have
unquestionably practical significance -- the surface passivation of gallium
arsenide, for example, is one area receiving much current attention. Due to
the fact that GaAs is a compound semiconductor, one would expect it to be
much more complicated than the elemental semiconductors. Early work function
measurements indicated this fact by the absence of Fermi level pinning by
surface states.[116] A large band bending for n-type samples and the absence
of band bending on p-type samples further documented the complexity.[117]
Conclusions reached were that no arsenic-derived surface states existed with-
in the bulk band gap and that an unfilled band of gallium-derived surface
states existed in the gap. Eastman and Grobman,[118] using photoemission, con-
tradicted these results by observing a filled band of surface states for
GaAs(110) lying in the band gap. It was later shown that steps on badly
cleaved surfaces could induce extrinsic surface states in the gap.[119,120] Sub-
sequent photoemission results to date have generally agreed on the absence
of any filled intrinsic surface states within the band gap.[121-3] The

existence of the unfilled states in the band gap, however, has been the subject of much controversy. Huijser and Van Laar[124] concluded, by contact potential difference measurements, that no empty surface state band exists in the band gap of the GaAs(110) cleaved surface. This result contradicted several experimental[120-2,125-130] and theoretical[121,131-4] studies but now has been confirmed by photoemission experiments.[120,135-7] The present status of the GaAs(110) surface is perhaps best illustrated by the modified GSCH (Gregory-Spicer-Ciraci-Harrison) model shown in Figure 22.

In agreement with the absence of filled surface states in the band gap, no Fermi level pinning is observed for p-type GaAs(110)[120,122,138] supporting earlier studies.[116] Until recently, photoemission and other techniques favored the pinning of the Fermi level for n-type GaAs at the midgap.
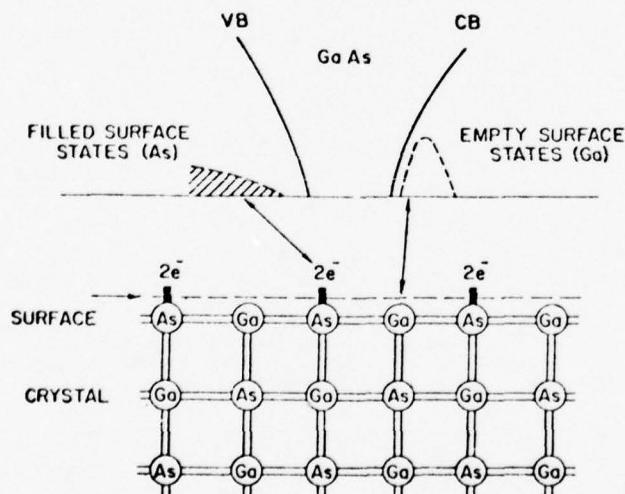
Figure 22. Schematic GSCH Model of the GaAs(110) Surface Showing the Energy Position of Filled and Empty Surface States and Their Association with the Ga and As Surface Atoms (after Lindau et al.[123]).

Huijser and Van Laar[124] persisted with the earlier views and maintained that their GaAs(110) cleaves on n-type material showed no pinning of the Fermi level. Furthermore, Chye, et al.[139] have shown the absence of pinning on both n- and p-type gallium antimonide (GaSb). Pinning was shown to occur if a small amount of oxygen was admitted to the system or if a Schottky barrier was formed. Gudat, et al.[137] have also found III-V n-type compounds with an absence of pinning. These facts motivated Spicer and workers[136,140-1] to study the question of n-type GaAs(110) in detail. In addition to surface defects, strain, or steps induced by cleaving, they found that a small amount of contamination on a good cleave would stabilize the Fermi level around the midgap. The substantiated result is that Fermi level pinning does not occur on cleaved n-type GaAs(110) due to intrinsic surface states. Pinning, however, does occur on these surfaces due to extrinsic causes. GaAs(110), therefore, does not possess intrinsic surface states of any type in the bulk band gap. This is in agreement with Figure 22.

It is noteworthy to state that the above revelations came about essentially by detailed studies on interface states, primarily concerning the uptake of oxygen on GaAs(110), using synchrotron radiation as the exciting source for photoemission.[136,140-2] Pianetta, et al.[142] suggest that the slight contamination which caused erroneous results on good cleaves was caused by the excitation of oxygen due to the ionization gauge and ion pump operating in the ultra-high vacuum (UHV) environment. Previous studies showed an oxygen uptake rate of 10^6 - 10^7 L ($1L = 1$ Langmuir = 10^{-6} Torr-sec) for a half-monolayer and a subsequent slow sorption rate. Taking the precautions of valving off the ion pump and using a cold-cathode (Redhead) gauge, Pianetta, et al.[142] have shown a marked exposure increase (10^7 - 10^{11} L) required for

half-monolayer coverage.   Also, the monitoring of the As-3d and Ga-3d photo-
emission core levels has shown that the As peak shifts but that the Ga peak
remains fixed for exposures to 10^{12} L. After this exposure, the Ga-3d peak
only broadens slightly, as shown in Figure 23. Previous experiments have
shown that the As peak shifts and that the Ga peak remains fixed up to
10^6 L exposure but that the Ga peak shifts at higher exposures, as shown
in Figure 24.

OXIDATION OF n-TYPE GaAs(110) AT $\hbar\omega$ = 100 eV
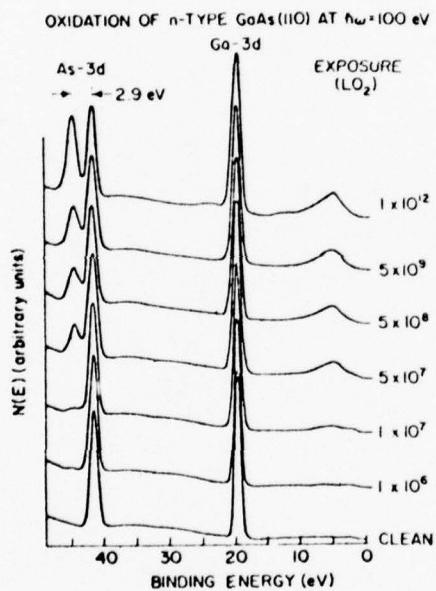
Figure 23.   Photoemission Spectra of Clean and Oxygen Exposed
            GaAs(110) Surfaces at a Photon Energy of 100 eV.   Note
            the 2.9 eV shifted As 3d peak and the high oxygen exposure
            10^{12}L, without any shift of the Ga-3d peak (after
            Pianetta et al.[142]).
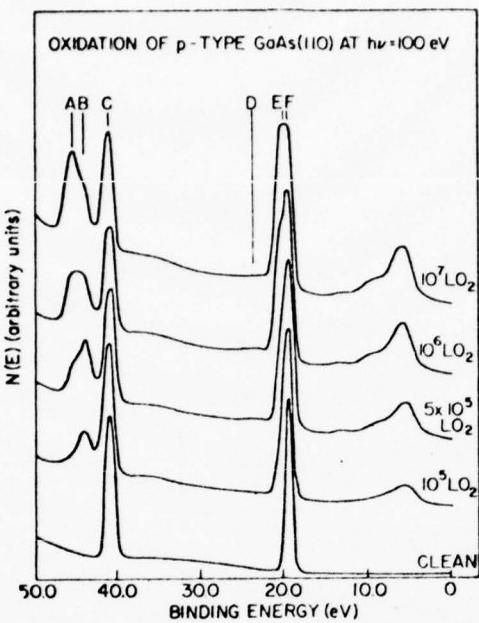
Figure 24. Photoemission Spectra of GaAs(110) Surfaces Exposed to
Activated Oxygen. Note the appearance of a second
shifted (ΔE = 4.5 eV) As-3d peak and a 1.0 eV shifted
Ga 3d peak (after Lindau et al.[123]).

The later data, Figure 23, suggest that a major charge transfer takes place

from arsenic to oxygen, illustrating that oxygen is preferentially bonded

to the As surface atoms and not to the Ga atoms on the truly clean surface.

The fact that the Ga peak remains fixed for the long exposure of 10^{12} L

(equivalent to atmospheric pressure of O_2 for 20 minutes) suggests that

the bonds between the surface atoms and the bulk are not broken. So, for

a short time, a freshly cleaved GaAs specimen at room temperature and atmos-

pheric pressure should possess stable back bonds.[123,136] The earlier results,

Figure 24, showing the shifting of the Ga-3d peak, are attributed to oxygen

65

broken up by a hot filament ionization gauge, attacking the bonds binding the surface atoms to the rest of the crystal.[145] The movement of the Fermi level in these studies has been monitored during the oxygen exposure and is shown in Figure 25 for a total of 10 cleaves. The figure shows that surface perfection and minute oxygen contamination dramatically affects the initial stages of oxidation. The inset in the figure shows that the valence band photoemission data from samples beginning with the Fermi level unpinned and moving to the midgap have much sharper features than the initially pinned-samples[123,140] Lindau, et al.[141] and Pianetta, et al.[140] have recently studied in detail the valence band structure, using photoemission, of cleaved and oxygen exposed GaAs(110). In addition to the results that have been mentioned, they emphasize that the chemisorption of small amounts of oxygen ($< 10^3$ L) produces long range ordering effects which sharpen the intrinsic valence photoemission spectra. This is attributed to rearrangement within the unit cell resulting in the relieving of surface strain.
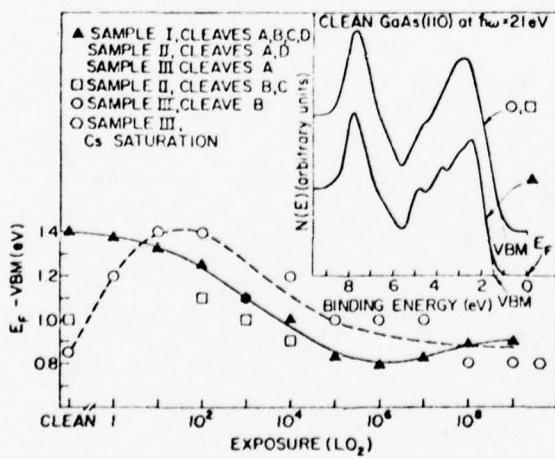
Figure 25. Fermi Level Pinning on GaAs(110) for Various Samples and Cleavage Qualities as a Function of Oxygen Exposure. Samples I and II are supplied by Laser Diode Corp. (doping 3×10^{17} cm^{-3}) and sample III by MCP Electronics, Ltd. (doping 1.7×10^{18} cm^{-3}). The insert shows representative photoemission spectra for samples with pinned and unpinned Fermi level (after Lindau et al.[123]).

66

In the study of the metal-semiconductor interface, the Bardeen[146] model, which correlates Fermi level pinning with the density of intrinsic surface states, has been used extensively.[147,148] However, the fact that a metal is added to a surface has raised many theoretical questions concerning the continued existence of surface states.[149-154] In the case of cleaved GaAs(110), the previous discussion has established that for both n- and p-type material, the surface Fermi level is unpinned. After a metal is added, however, the Fermi level is found to be pinned at the interface.[116] This suggests that the metal induces new interface states, now commonly referred to as metal induced gap states (MIGS). Heine[149] suggests that the new states are due to the tails of the metallic wavefunction decaying into the semiconductor. Inkson[151] suggests that the states are due to the narrowing of the semiconductor gap at the interface. Phillips[154] proposed that the states are due to elementary excitations and chemical bonding that pin the Fermi level. Perhaps the latest theory has been presented by Mele and Joannopoulos.[155] It correlates the Fermi level pinning to the formation of a dipole layer which is due to the filling of dangling bond states. Thus, the intrinsic surface states are still shown to play a vital role in the formation of the Schottky barrier. They point out that their theory is presently valid only for tetrahedrally coordinated semiconductors and suggest methods of extension.

The GaAs/Cs interface has been studied by photoemission by Spicer and co-workers[130,156-7] in several instances. However, the experimental studies that were undertaken are essentially invalid for a true metal-semiconductor junction due to their later conclusions regarding post-cleavage contamination of their surfaces. A detailed study of the variation in barrier height

of Schottky barriers as a function of the interface oxide thickness appears to be very feasible using photoemission techniques.

In summary, intrinsic surface states on cleaved GaAs(110) now are in concert with Fermi level measurements and do not lie in the bulk band gap. Oxidation studies on GaAs(110) have been characterized in terms of the initial and the long term uptake and are correlated well with the pinning of the Fermi level and the location of the bonding sites. Tunable synchrotron radiation provides a clean and wide range, stable energy source for photo-emission experiments under excellent vacuum conditions.

In the fabrication and passivation of elemental silicon for electronic devices, Fermi level pinning is substantially reduced when the surface undergoes oxidation. As a result, the devices are useful and reliable. The opposite behavior is encountered for the oxidation of GaAs(110), resulting in the Fermi level being pinned in the band gap. It is, therefore, not surprising that a good passivation scheme has not yet been developed.

8.3 Surface/Interface States and Electron Energy Loss Spectroscopy

Interest in Electron Energy Loss Spectroscopy (ELS) as a surface analytical technique has come into use within the last decade due to the ability to prepare reproducible surfaces in an ultra-high vacuum environment. Experiments using ELS have concerned collective vibrational states (phonons), normal vibrational states, and electronic states of clean and gas-covered surfaces. This discussion is related to the study of the excitation of electronic surface transitions on semiconductor surfaces.

Most theoretical results of ELS are based on the dielectric theory.[158] A high density of surface states may cause the dielectric constant for a surface to differ from that of the bulk. The surface is then modelled as a thin layer possessing a surface dielectric constant which depends on the

distance normal to the vacuum-solid interface. Anisotropic effects, how-
ever, have been experimentally observed.[159]

Typically, the energy-loss spectra are measured with a conventional
Auger single-pass cylindrical mirror analyzer (CMA) having an integral
coaxial electron gun. The primary electron beam strikes the sample at nor-
mal incidence with energies in the 50-1000 eV range. At these low energies
(typically < 500 eV) the escape depth of the secondary electrons, due to
inelastic scattering processes, is small, resulting in surface sensitive
spectra. When ELS is performed in this way, it is referred to as Low-
Energy Electron Loss Spectroscopy (LELS) and one operates in the reflection
mode of ELS. The energy resolution required for the CMA is ~100 meV based
on the magnitude of expected energy losses. To obtain this resolution,
modulation voltages are kept small (0.4 - 1.0 volts, peak-to-peak). To
increase the sensitivity, the second harmonic of the modulation voltage is
detected to obtain second derivative, $\frac{d^2N}{dE^2}$, spectra, using standard lock-in
techniques. It should be noted that the differentiation annihilates un-
structured loss intensity and overestimates sharp structures of low intensity.

Froitzheim, et al.[160] studied cleaved and annealed surfaces of Si(111)
for the first time, calculated optical absorption data, and compared it to
existing data.[161,162] They noticed the vanishing of intrinsic surface tran-
sitions after annealing. Ibach, et al.[163] studied the LELS spectra of Si(111)
and Si(100) 2 x 1 as a function of oxygen coverage up to a monolayer. They
noticed the disappearance of surface transitions of Si for the clean surfaces,
the appearance of surface transitions related to oxygen, the decrease in in-
tensity of bulk and the surface plasmons, and a splitting of the surface
plasmon, all as a function of increasing oxygen coverage.

69

Further LELS studies on Si[166-170] and Ge[160,164-8,171] show comparable results. Of particular mention are the combined photoemission and LELS experiments by Rowe, et al.[170] performed on Si(111) enabling an energy level model for occupied and unoccupied states to be developed.

Froitzheim and Ibach[172] have studied LELS for the cleaved and oxygen covered GaAs(110) surface and have not found any structure that can be associated with surface transitions. This has been attributed to low step densities and the lack of significant wavefunction overlap between As and Ga surface states. These results are in agreement with the latest photoemission experiments performed by Lindau, et al.[173] at Stanford.

In direct contradiction to these experiments, Ludeke, et al.[164-5,174-5] have observed transitions involving the narrow filled Ga-3d core levels as initial states and empty surface levels or conduction band levels as final states on GaAs(100), (111), and (110) surfaces. In Figure 26, their data show a peak at 21.3 eV for clean GaAs(100) and Ga-stabilized ($\overline{111}$) surfaces which is associated with excitations from the Ga-$3d_{3/2}$ core level into empty surface states. A weaker peak at ~20 eV is a similar transition from the Ga-$3d_{5/2}$ core level. This structure, attributed to spin-orbit splitting, disappears as the surface becomes As-stabilized and a strong peak appears at 1.7 eV associated with transitions from filled As surface states to empty conduction band states.

Room temperature oxygen adsorption on various surfaces was determined from the ratio of the peak-to-peak amplitudes of the O(510 eV) and Ga(1070 eV) signals in Auger dN/dE spectra as a function of exposure.[174,175] Monolayer coverage, as indicated by saturation in the O/Ga Auger ratio, is complete for exposures of the order of 10^9 L. The Ga-3d to surface state peaks

70
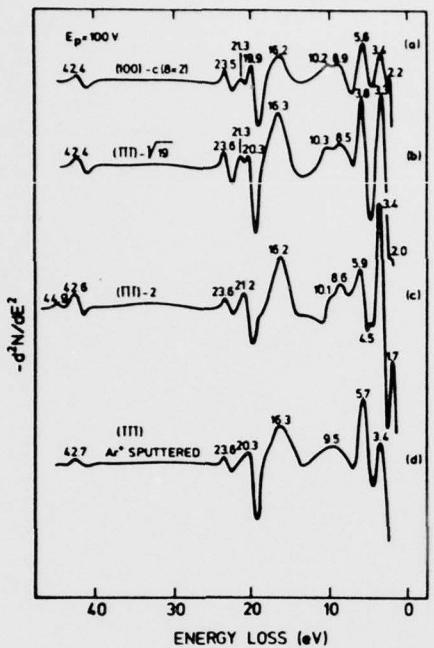
Figure 26. Second-Derivative Energy-Loss Spectra of GaAs: (a) (100) Surface, Ga Stabilized; b) ($\bar{1}\bar{1}\bar{1}$) Surface, Ga Stabilized; c) ($\bar{1}\bar{1}\bar{1}$) Surface, As Stabilized; d) ($\bar{1}\bar{1}\bar{1}$) Surface, Sputtered (after Ludeke and Esaki[164]).

are observed to diminish in intensity corresponding to the oxygen adsorption. This effect is interpreted as saturation of the unfilled Ga dangling bonds of the clean surface. Simultaneously with the disappearance of the above peaks, new peaks appear at 20.9 and 23.2 eV, which are believed to be due to excitations from the Ga-3d core levels into empty oxide-related interface states. No changes are observed in the loss peaks due to the excitation of As-3d core levels. It is thus concluded[168,174-5] that in the oxidation of (100) and (111) surfaces, as well as other GaAs surfaces in general, the oxygen is chemically bonded to Ga atoms and that the As atoms are not directly involved in the oxidation process.

The different GaAs surfaces were prepared either by Ar$^+$ sputtering and annealing or by molecular beam epitaxial techniques. The As and Ga surface

71

compositions of (100) surfaces were readily changed by treatments involving cooling a cleaned (100) surface below 200 °C in an arsenic vapor of 10^{-7} Torr (As rich surface), heating in ultra-high vacuum to 400 °C (As stabilized), or heating to about 500 °C (As depleted). Reflection high energy electron diffraction (RHEED) patterns establish the surface crystallography of these three different (100) surfaces[175] Low energy electron diffraction (LEED) could also be used to determine the surface reconstruction in each case. When the surfaces are prepared by Ar^+ sputtering and annealing, one would have to monitor the ratio of the Ga-to-As low energy (MVV) Auger peaks as a measure of the surface composition and the ratio of the Ga-to-As high energy (LMM) Auger peaks as a measure of the bulk composition.[176-177]

The previous conclusion concerning the site of oxygen chemisorption has been the subject of much controversy[178,179] since photoemission results clearly indicate that the As atoms are the initial bonding site[173] Lapeyre and Anderson[180] have presented strong evidence that excitonic effects are involved in the core level-surface state transition. They have proposed a direct recombination process, in which the core hole and electron recombine and transfer their total energy to valence electrons. This would require a strong localization of the initial electron-hole pair suggesting the excitonic nature of the empty surface state. An alternative model involving internal photon creation by the relaxation of the core level has also been proposed by J. C. Phillips. These observations suggest that the energy locations of the empty surface states of GaAs(110) must be modified.[181,182] When this is done, the results of LELS are in some accord with the recent photoemission experiments.[173] Photoemission results indicate GaAs(110) possesses no intrinsic surface states (filled or unfilled) in the band gap

72

and oxygen initially bonds to the As surface atoms. Mele and Joannopoulos[183] present a theoretical argument using an empirical tight-binding model which indicates that oxygen bonds mostly to the As surface atoms with some degree of mixing to the Ga species. Detailed points of the apparent controversy between the photoemission and LELS results are still unresolved.[178,179]

LELS studies on AlAs have also been performed.[184] This is an important compound due to the fact that the bulk lattice spacing (5.6622 $\overset{\circ}{A}$) is very close to that of GaAs (5.6532 $\overset{\circ}{A}$).[185] AlAs overlayers can also easily be grown on GaAs substrates by MBE, resulting in minimal interface distortion due to lattice mismatching.[177]

With respect to metal overlayers on GaAs, Rowe[186] has used a combination of ultraviolet photoemission spectroscopy (UPS) and electron energy-loss spectroscopy to study the effect of metal layers on (111) GaAs surfaces. UPS of direct bulk transitions gives information on changes in the surface potential on adsorption and energy-loss measurements show the resultant changes in the occupied and unoccupied intrinsic surface states. In addition, Gudat, Eastman, and Freeouf[187] report on empty surface states on the (110) surfaces of several III-V semiconductors, including GaAs, and the effect of metal overlayers on these states, using photoemission. In both of these studies there is a correlation between the surface state energies and the position of the Fermi level (or value of the surface potential) at the metal-semiconductor interface. Thus, it is concluded, as a number of model studies suggest, (see, for example, the recent paper by Borrego, Gutmann, and Ashok)[188] that the intrinsic surface or interface states still play an important role in determining Schottky barrier heights.

The relatively new method of LELS yields another surface analytical

technique which is important in the analysis of the microstructure of solid surfaces. The contradictions that have arisen, in comparison to other experiments, have required a closer scrutiny of the effects of some standard experimental procedures and have motivated better explanations of the spectra from theorists. LELS, still in its infancy, will most likely provide useful experimental inputs into the complex theories of low energy electron scattering.

8.4 Surface Atomic Geometry of GaAs (110)

In every useful theoretical model which seeks to calculate local properties of matter, a detailed knowledge of the geometrical configuration of atomic species at the surface or interface region is required. The analysis of elastic low-energy electron diffraction (ELEED) data has provided most of this knowledge to date.

Surface atomic geometry, in principle, can be determined from the analysis of LEED intensities.[189] Surface sensitivity is achieved because of the strong interaction of low energy electrons with the first few atomic layers of a solid. This introduces the problem of multiple scattering effects which makes dynamical LEED calculations complex and lengthy. In practice, there exists a multiplicity of possible geometries which will yield a particular LEED structure. The usual procedure is then to calculate the LEED intensities from probable geometries and compare the results to experimental intensities. The atomic geometry which best fits the experimental data is then selected. Even though the GaAs (110) surface has the ideal 1X1 LEED structure, two factors suggest that the atomic arrangement of the surface is different than that of the bulk.[190] The (hk) and (hk̄) beams exhibit extreme asymmetry in intensity and the (10) and (1̄0) beams possess strong intensity. If the surface was an ideal termination of the bulk zincblende

lattice, the (10) and ($\bar{1}$0) beams would be very weak.

The following discussion will outline the model for the GaAs (110) re-constructed surface proposed by Duke, et al.[191] Assuming that covalent bonds are relatively incompressible, one can model the surfaces of covalent semi-conductors by altering bond angles while keeping bond lengths fixed. In support of this assumption, the reduction in surface Madelung energy and the breaking of surface covalent bonds suggest a reduction of charge transfer in the surface region compared to the bulk. For GaAs (110) 1X1, these assump-tions lead to the hypothesis[192,193] that the As atoms rotate outward from the surface toward a prismatic coordination and that the Ga atoms rotate inwards toward a three-fold planar (sp^2) coordination. The rearrangement occurs only in the first layer, as shown in Figure 27, and is completely characterized by a single parameter, θ_T, the tilt angle. This is the angle between the (110) surface and the plane, S, passing through the nearest neighbor surface Ga and As atoms. The figure shows the ideal 1X1 structure ($\theta_T = 0$) alongside the reconstructed 1X1 model. Some interatomic distances are shown along with the 1X1 surface net in the top view. In the side view, the decrease in the average interlayer spacing between the surface and second layer is denoted as Δ (which is directly related to θ_T in this model). This rearrangement preserves not only the bond lengths but also the periodicity parallel to the surface. This simplification is very important as several theoretical me-thods (e.g., the pseudopotential method) rely on surface translation symme-try in order to perform "layer" calculations. Indeed, Duke, et al.[191] found that their exact multiple-scattering computer programs[194] required too much memory for zincblende or wurtzite cleavage face calculations. New programs were developed, based on the layer iteration method, where individual layer

75

scattering amplitudes, reflection matrices, and transmission matrices are first calculated.[195][196]

ATOMIC STRUCTURE OF GaAs(110)1x1 SURFACE
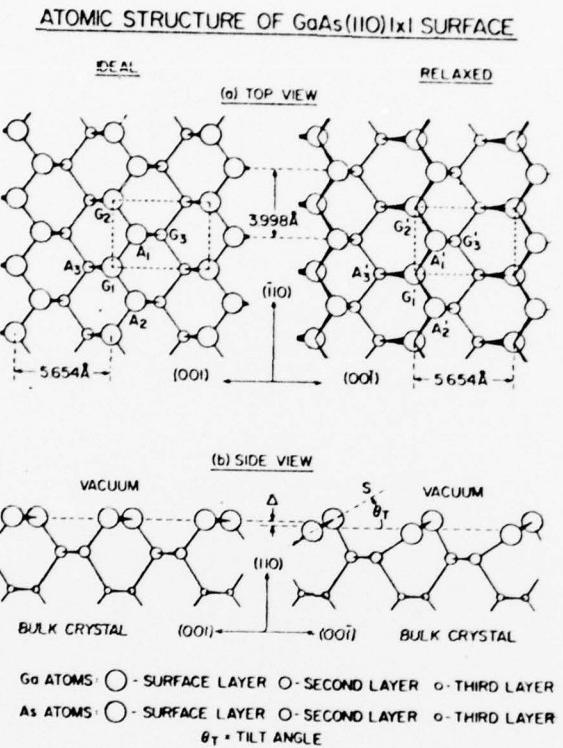
Figure 27. Atomic Structure of Ideal and Relaxed GaAs(110)1 x 1 Surfaces. The ideal surface is obtained by truncating the bulk lattice. In the relaxation model, Ga atoms move into and As atoms move out of the crystal (after Duke et al.[191]).

From their calculations, Duke, et al.[191] determined the best agreement with experiment occurred for the range of the tilt angle $27° \leq \theta_T \leq 34.8°$, with the larger angles being statistically preferred.

Duke, et al.[191] also suggest a correlation between the local electronic structure and the atomic geometry of the surface region mainly due to the character of the chemical bonding, i.e., the percent ionicity of covalency of the bond. Pandey, et al.[197] have used the previously discussed geometric model in tight-binding calculations to generate the local density of states for the GaAs (110) 1X1 surface. Studying two values of the tilt angle, $\theta_T = 19°$ and $\theta_T = 35°$, they concluded that $\theta_T = 19°$ compared more favorably with various photoemission experiments. It is of interest to note that their local density of states curves, shown in Figure 28, show a sharp peak just below the conduction band minimum (E_c) for their best choice of $\theta_T = 19°$.
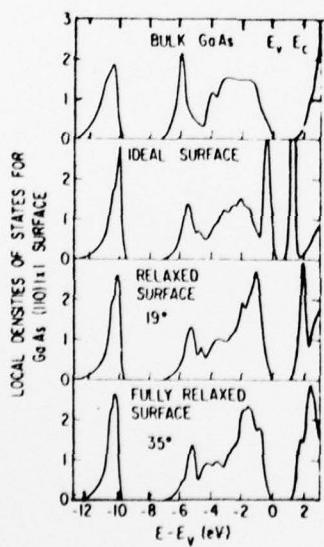
Figure 28. A Comparison of the Bulk Density of States with the Local Densities of States at the Surface for the Ideal, the Relaxed(19°), and the Fully Relaxed (35°) Models of GaAs(110) 1 x 1 Surface (after Pandey et al.[197]).

77

This is in disagreement with the latest photoemission data,[198] which shows no intrinsic surface states in the bulk band gap. However, the fully relaxed surface, $\theta_T = 35°$, shows the movement upward and broadening of this surface state, in agreement with photoemission data and the LEED calculations of Duke, et al.

Very recently, Tong, et al.[199] have compared their experimental LEED intensity data with curves calculated by the combined space method (CSM).[200] This dynamical method for calculating LEED intensities is specifically designed for closely spaced noncoplanar surface layers. Extending the previously described model, they have found that intensity curves are sensitive not only to the tilt angle but also to the vertical height of the surface atoms from the second layer. This corresponds to viewing Δ as an independent parameter in the previous model. The best agreement with experiment, determined from 11 relaxed structures, was found to have a $\theta_T = 27°$ and a surface layer separation distance of 1.452 $\overset{\circ}{A}$ ($\Delta = 0.233$ $\overset{\circ}{A}$). This distance corresponds to a slight compression of the surface layer Ga and As back bonds. The bond lengths of the surface atoms to one another remain fixed for this model.

For comparison to previous calculations, Tong, et al. studied the geometries with tilt angles $\theta_T = 19°$ and $\theta_T = 34.8°$. They found considerable disagreement with the published results, attributing it to an inaccurate method in calculating the multiple scattering effects.

The basic model that was described by Duke, et al. and extended by Tong, et al. remains intact to date and provides the best information known on the structure of the GaAs (110) 1X1 surface. With all the bond lengths fixed, it has been used for various theoretical calculations; in particular,

the pseudopotential simulation of the GaAs (110) 1X1 surface.[201]

The importance of the geometrical structure cannot be underestimated in theoretical calculations. Better theoretical models and subsequent calculations of LEED intensity curves appear to be the most useful endeavor, especially to understand the differences in the results of the present calculations. The strong correlation between surface atomic geometry and local electronic structure are increasingly becoming a method by which assumed model geometries are conceived and tested by LEED calculations. Recently, Lindau, et al.[202] have suggested that the surface electronic structure may provide more detailed information on rearrangement of surfaces, especially GaAs (110), than LEED. This assertion needs to be substantiated by quantitative calculations.

8.5   Theoretical Modeling of Localized Electronic States

8.5.1   Hartree-Fock Molecular Cluster Calculations

The evolution of experimental and theoretical surface analytical techniques over the past twenty years has resulted in significant increases in resolution, sensitivity, and accuracy. In conjunction with this trend, the concepts incorporated into the band theory of solids, primarily developed to understand gross and bulk features of crystalline matter, have necessarily been modified in order to accomodate microscopic phenomena such as impurities, lattice vacancies, etc. Furthermore, macroscopic phenomena such as crystal surfaces, have required extensive reformulation of several aspects of band theory. The band theory approach has been and will continue to be highly successful. On the other hand, approaches dealing with the assemblage of atoms to form a solid from "first principles" are conceptually and intuitively attractive. The ultimate success of both techniques would

be their ability to simultaneously model a particular experimental system. The advent of high speed computers has moved theoretically-established first principle calculations of practical systems into the realm of possibility.

The most important and useful model that has been developed for electronic structure calculations is the *Hartree-Fock* (HF) *method*, which is intimately connected with the one-electron theory of matter. P. W. Anderson[203] has stated that the main usefulness of the fundamental many-body theory is predicting the range of application and flexibility of the Hartree-Fock theory. In calculating the total energy of an atom in its ground state, the error in the actual experimental energy and the calculated Hartree-Fock energy is defined as the correlation energy. The percentage error in the correlation energy steadily decreases from ~1% for He($Z=2$) to ~0.1% for Ar($Z=18$) and appears to continue its downward trend for heavier elements.[204] The fact that such a small correction is all that is necessary to yield experimental results shows that the Hartree-Fock method is a very good approximation to the many-electron problem.

In extending the Hartree-Fock method to molecules, the major pitfall is the destruction of the spherical symmetry of the system. Solutions of the central-field problem (i.e. atomic orbitals) then become invalid and molecular orbitals must be introduced. The general procedure for handling polyatomic problems can be traced back to Roothaan's method, also referred to as the *analytic Hartree-Fock method*.[204] In this method, electron wavefunctions are modeled as a linear combination of a finite number of suitably chosen basis functions. The problem then becomes one of algebraically determining the coefficients of the basis functions in each wavefunction expansion. The procedure commonly used for solving the Hartree-Fock equations

is the method of the self-consistent field (SCF). This iterative procedure can be carried out to any predetermined degree of accuracy by comparing successive calculations of the set of coefficients for the basis functions.

The choice of a suitable set of basis functions to model the one-electron wavefunction has been the subject of extensive investigation.

Perhaps the most well known basis function occurs in the "minimal-basis set," and is referred to as a Slater-type orbital (STO):

$$r^{n-1} e^{-\alpha r} Y_{\ell m}(\theta, \phi),$$

where $Y_{\ell m}(\theta, \phi)$ is a spherical harmonic. For a central-field problem, such as a single atom or a molecule having infinite separation between atoms, modeling of a single one-electron wavefunction by a STO is very appropriate.[204] In order to model a real molecule, which possesses finite internuclear distances, the parameter α (the orbital exponent) has been introduced. A single one-electron wavefunction, in this case, is still modeled by one STO but now α is optimized by minimizing the energy of the system.

A logical extension of this method is the "double-zeta" basis set. Here, a single wavefunction is modeled as a linear combination of two STO's. If reasonable, but different, orbital exponents are selected for the two STO's, a simpler linear optimization of the coefficients of the STO's is all that is necessary to give comparable results to a minimal basis set calculation.

The basis functions that have been discussed can be extended to include "polarization functions" (basis functions with higher angular quantum numbers), which allow charge buildup in the bonding region.[205] It is now clear that the flexibility introduced by this refinement is important in geometrical structure predictions.

81

Furthermore, completely general functions can be used for a single orbital allowing greater flexibility, but with a considerable increase in computational difficulties.[207]

STO's have been used with great success in atomic and molecular calculations. In the molecular problem, however, one is faced with the additional complication of assigning the one-electron orbitals to particular geometric centers associated with the equilibrium sites of the atoms. The analytic Hartree-Fock procedure then requires one to calculate two-electron integrals over all orbitals in the system.[208] This presents a tremendous calculational, but tractable, problem for functions like the STO's in calculating the many-center two-electron integrals for a molecular problem. To facilitate this difficult problem of integral computation, S. F. Boys[209] suggested the use of the cartesian Gaussian functions of the form: $X^\ell Y^m Z^n e^{-\alpha r^2}$. The distinct advantage of the Gaussian functions as a basis set relies on the elegant theorem that a product of two Gaussian functions is also a Gaussian. As a result, the most complicated four-center two-electron integrals can be reduced immediately to two-center cases which can rapidly be evaluated by simple formulas. However, Gaussian functions are less appropriate than functions such as STO's for representing one-electron orbitals. As a result, a linear combination of Gaussian-type orbitals (GTO's) must be used for obtaining comparable accuracy. Typically, 3-8 GTO's are used for a particular one-electron wavefunction expansion. The use of GTO's, then, creates a substantial increase in the number of integrals to be evaluated. For two-electron integrals, the increase varies as the fourth power of the number of GTO's in an expansion. Furthermore, the final calculation of the electronic wavefunction is proportional to the number of integrals. Even

with the increase in the number of calculations, it generally pays to use GTO's rather than STO's for efficient molecular calculations due to the significant decrease in the time per calculation.

Satisfied with using a linear combination of GTO's as a basis set for efficient calculations, one still must determine the exponents and coefficients to describe a one-electron orbital. One method of doing this is by expanding a minimum basis STO into a linear combination of K GTO's.[210] The resulting basis sets are denoted by STO-KG (Slater-type orbital at the K-Gaussian level). These are documented for K=2 through 6 for several elements.[211] As K increases, the STO-KG will approach the true STO. STO-3G and STO-4G yield comparable results to a full STO calculation.

To combat the large number of Gaussian basis functions that accumulate as one studies a heavier atom or a larger molecular cluster, several "contraction" schemes have been introduced.[212] Contracted functions are formed by taking fixed linear combinations of the Gaussian basis functions, now called primitives. Care must be exercised in constructing compact and flexible contractions. Generally, inner shell orbitals are contracted to some degree while leaving outermost orbitals uncontracted. This procedure is called a segmented contraction scheme. A general contraction scheme has been used by Raffenetti[213] which reduces all core orbitals to a single function. The valence orbitals are modeled by a linear combination of core primitives and the innermost valence function. The remainder of the valence orbitals are left uncontracted.

Optimized atomic Gaussian basis set expansions are presently available through xenon (Z=54).[214] Segmented contraction schemes which give good results have been established through copper (Z=29).[212]

One-electron wavefunctions, in general, possess a spatial and spin co-ordinate dependence. If there are no constraints placed on the total Hartree-Fock wavefunction (other than orthonormality) and the electron wavefunction is denoted by the antisymmetric combination of a spatial wavefunction times a spin eigenfunction, the version of the theory is referred to as *unrestricted Hartree-Fock* (UHF). If the wavefunctions are constrained to be the same for different spins, i.e. spin is neglected, the version of the theory is called *restricted Hartree-Fock* (RHF). In cases where a system has unpaired electrons, the UHF theory usually leads to an energy lowering. For larger atoms or molecules, the UHF method has been shown to properly model the contraction and localization of higher angular momentum electrons. In particular, for transition metal hydrides, UHF calculations[215] show the proper localized behavior of d-electrons, while other methods such as RHF[216] and SCF-Xα-SW[217] (Self-Consistent Field X-alpha scattered wave) calculations show considerable s-p-d mixing.

Efficient computer programs, developed by Dr. Isiah Shavitt and his group at Battelle Columbus Laboratories, are presently available at Georgia Tech for calculating the complete electronic structure of a molecular cluster of atoms. The code is designed to perform RHF, UHF, and MCSCF[218],[219] (multiple configuration SCF) calculations using Gaussian functions as a basis set. Some of the features of the program are: (1) the ability to internally generate Gaussian expansions of STO's; (2) the ability to flexibly input any desired segmented contraction scheme of given primitive Gaussians; (3) the exact treatment of the exchange interaction; (4) the performance of charge-conserving integral approximations;[220] (5) the efficient calculation of two-electron integrals;[220] and (6) a contour and perspective graphical package

1.0

28   25

32   2.2

3.6

4.0   2.0

1.1

1.8

1.25   1.4   1.6

MICROCOPY RESOLUTION TEST CHART

NATIONAL BUREAU OF STANDARDS-1963-A
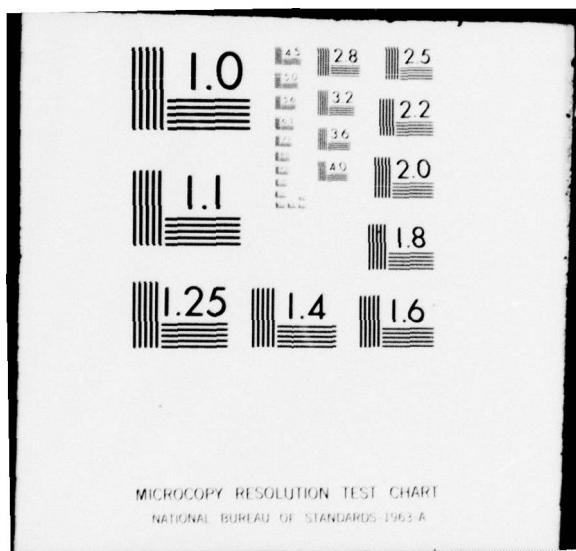
for visualizing the results. In conjunction with the above, there is an option also available which allows replacement of the core orbitals with an *ab initio* effective core potential. This technique, developed and implemented primarily by L. Kahn, enables one to consider only detailed calculations involving the valence electrons, significantly reducing computation time.[221-224] Using this method, feasible self-consistent calculations of valence orbital wavefunctions and energies can be made for heavier atoms and larger molecular clusters.

The basis of the molecular cluster approach in modeling surface/interface electronic states at a semiconductor surface relies on the assumption that the electronic structure can be reasonably described by the local atomic arrangement. As the cluster size is increased, the results should approach that of a semi-infinite solid as described by band structure calculations. Unfortunately, practical limitations on computation time restrict the size of a cluster greatly. Finite size clusters add the additional complication that important differences may be observed between the electronic structure of a cluster and a semi-infinite solid. This is primarily due to the fact that most atoms are at, or are very close to, the surface of a feasible cluster. One particular method that has been used for silicon to reduce effects of the cluster edges is to introduce hydrogen atoms to tie up the "dangling bonds".[225,226] The hydrogen atom is expected to saturate the bonds for silicon since its electronegativity matches that of the sp^3 hybridized bonding orbitals and, thus, preventing any unwanted charge transfer at the outermost cluster sites. Another method of reducing unwanted cluster edge effects has recently been used by Nishida.[227] He points out

that using H atoms for saturating semiconductor bonds is not general and is not satisfactory for germanium and other semiconductor surfaces. In his extended Hückel theory (EHT)[228,229] calculations, he has chosen an appropriate basis set and Hamiltonian to exclude the surface sp^3 orbitals of silicon and germanium clusters. Hydrogen chemisorption on Si(111) and Ge(111) surfaces as well as the clean GaAs(110) ideal and relaxed surface was studied. The results obtained by EHT show evidence of surface and interface electronic states due to charge localization. The major drawback of EHT calculations is that it is a non-SCF procedure. Nevertheless, it has proven the feasibility of performing cluster calculations on semiconductor surfaces.

There are several methods by which the results of cluster studies may be applied to experimental and other theoretical studies.

The comparison of energy levels of the molecular cluster to band structure results has been the predominantly used procedure. One can determine the band gap and valence-band width as a function of cluster size. Figure 29 shows this comparison for the EHT cluster calculations of silicon. Furthermore, the grouping of energy levels suggest the coagulation of bands. Figure 29 shows this grouping for silicon. For adsorption studies on metals, such as CO on Ni, Figure 30 shows how the density of energy levels is qualitatively compared to photoemission band structure results. Comparison with gas phase energy spectra, of CO in this case, shows the non-trivial identification and resequencing of energy levels upon adsorption.[230]

By analyzing the molecular wavefunctions resulting from a cluster calculation, one may calculate the local density of states (LDOS). This may better be compared to surface sensitive photoemission results and other

86
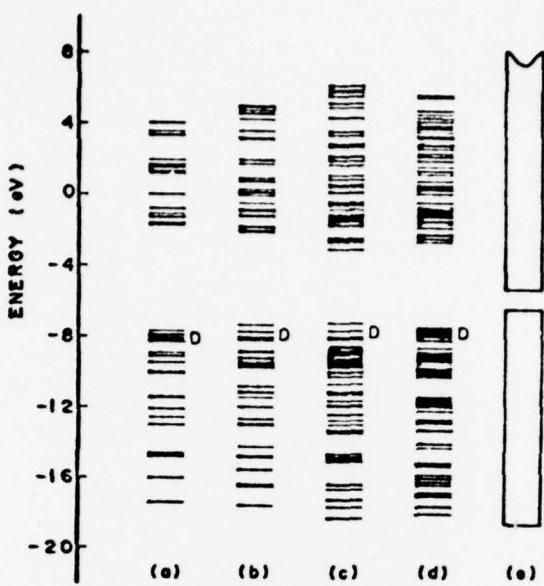
Figure 29.   Energy Level Diagrams for Ideal Si(111) Clusters
             as a Function of Cluster Size: (a) Si_{19}; (b) Si_{26};
             (c) Si_{45}; and (d) Si_{55}.   The result for the in-
             finite cluster is shown in (e) and originates from
             a band structure calculation.   Levels labelled by
             D correspond to sp^3 dangling bond orbitals (after
             Nishida[227]).
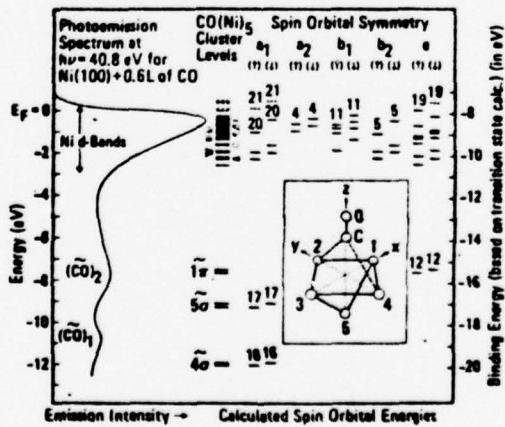
Figure 30.   Comparison of Theoretical Energy Levels for the
             $CO(Ni)_5$ Cluster and the Experimental Photo-
             emission Spectrum of CO Chemisorbed on Ni(100).
             The inset shows the model cluster (after Batra
             and Bagus[230]).

87

theoretical models. Figure 31 shows the EHT LDOS calculations for a GaAs(110)
cluster which is in agreement with pseudopotential layer calculations[231]
and tight-binding calculations,[232] but not in present agreement with pre-
viously discussed recent photoemission results in Section 8.2.2. Further
analysis of the molecular wavefunctions will give information on their angu-
lar dependence and allow comparison to angle-resolved photoemission studies.
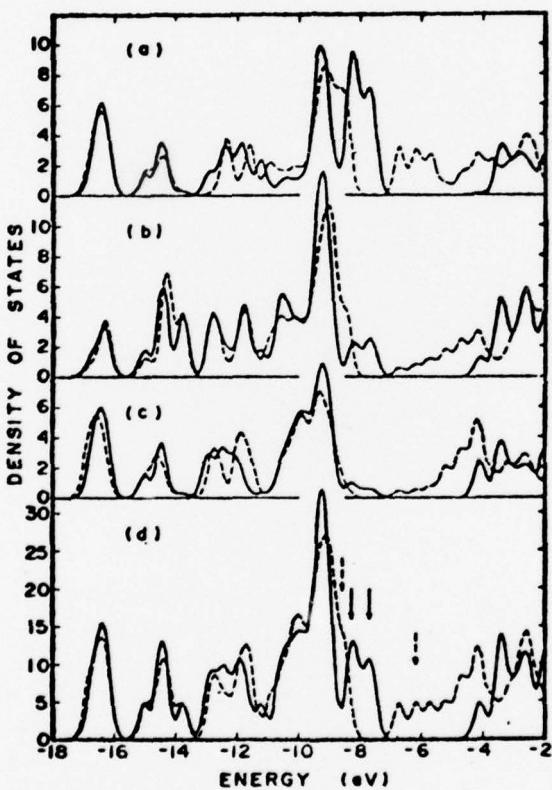
Figure 31. Extended Hückel Theory Calculations for Ideal (solid lines)
and Relaxed (dashed lines) GaAs(110) Surfaces Modeled by a
$Ga_{14}As_{14}$ Cluster. First layer (a), second layer (b), and
third layer (c), LDOS's are shown. In (d), the total density
of states is shown, with prominent surface states indicated
by arrows. (after Nishida[227]).

A very important application of the cluster method is predicting struc-
tural geometries of a system.[210] Applications of this type that have re-
cently begun to appear in the literature are primarily concerned with the
chemisorption of a single adatom onto a surface. A study of H chemisorp-
tion on a NiO surface[233] has been carried out using RHF, UHF, and the
generalized valence band (GVB)[234] methods. Figure 32 shows the total energy
of the chemisorption system versus the distance the H atom is from the sur-
face plane for different adsorption sites. The minima of the potential
curves yield the binding energy and equilibrium distance for the H-O or
H-Ni bond. A similar study of the chemisorption of O on the Li(100) surface
has been performed using RHF.[235] Three sites were considered for the
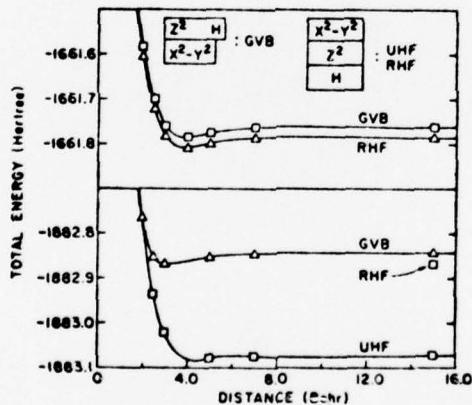
Figure 32. Potential Energy Curves for a H Atom Approaching a Surface
            of NiO. The upper curves correspond to H chemisorption
            on the O sites of NiO; the lower curves correspond to H
            chemisorption on the Ni sites of NiO (after Bobrowitz
            and Goddard[234]).

89

sorption, as shown in Figure 33A. Binding energy versus surface distance

results were obtained for different cluster sizes, as shown in Figure 33B,

C and D. The bridge site for this system was determined to yield the more

stable configuration, thus predicting a suitable geometry for subsequent study.

A

B

C

D
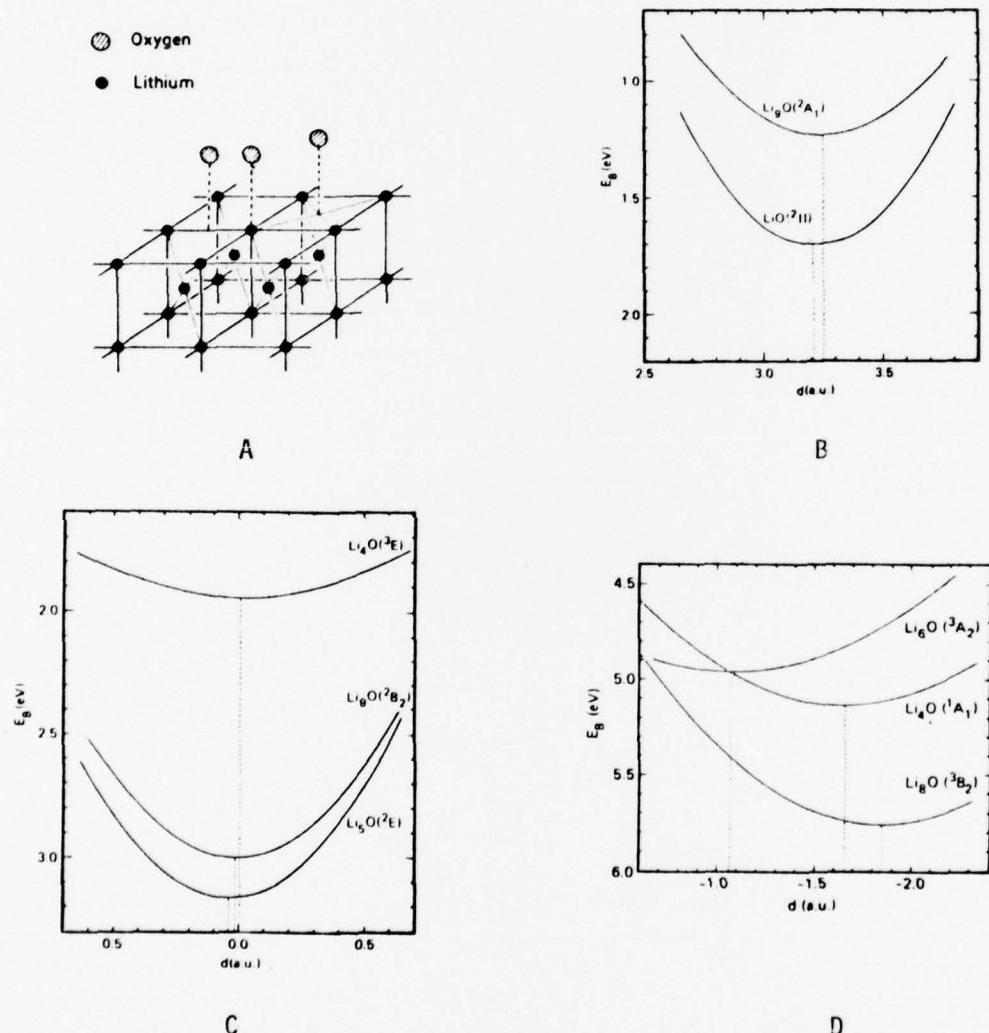
Figure 33. Chemisorption of O on the Li(100) Surface. A shows the
three high-symmetry surface adsorption sites; B, C, and
D show the oxygen binding energy as a function of distance
from the surface plane for the on-top, central, and bridge
site, respectively (after Hermann and Bagus[235]).

A thorough study of the HF method, especially concerning selection of basis functions and cluster convergence properties, has recently been done for H chemisorption on the Be(0001) surface.[236] It was found that even a 22 atom Be cluster did not have properties of a bulk metal. They established that the interaction of a H adatom with the substrate is predominantly determined by nearest Be neighbors. Properties associated with chemisorption are, therefore, expected to converge rapidly with respect to cluster size. Predictions on the stable geometrical location of the adatom were carried out, as previously described, by studying the binding energies.

As a result of the feasibility of cluster calculations, RHF and UHF studies were initiated under our ONR-sponsored program on model semiconductor surfaces using the previously mentioned computer codes. The following path of approach has been established. The compound semiconductor GaAs has been selected primarily because of current fundamental interest and the existing difficulties in passivating the surface for device applications. Initial calculations are presently being carried out on various atoms of interest, e.g. Ga, As, O, Al, Ta, and H, to determine suitable basis sets and *ab initio* core potentials. Full optimized GTO basis sets have been obtained for elements up to $Xe(Z=54)$.[237] The next calculations will involve clusters of Ga and As atoms arranged in various crystallographic orientations, i.e. GaAs(110), (100), (111) and ($\bar{1}\bar{1}\bar{1}$) along with attempts to reduce cluster edge effects. Vacancies in the lattice, for example, resulting from arsenic depletion during a heat treatment, can be considered by removing strategic atoms from the cluster. Subsequent calculations would identify the effect of chemisorbed atoms, e.g. Ga_xO_y, Al_xAs_y, Al_xO_y, Ta_xO_y, H, etc., representing surface "quasi-molecular" clusters from the passivation film or interface.

In accomplishing this, the particular angular orientation of the electronic structure of the added atoms must be correlated with the underlying crystal structure. These will be assumed, mostly based on previous experimental (AES, LEED, XPS, UPS, etc.) results, some of which have been described in this report. Comparison of these calculations should show detailed interface electronic structure differences due to changes in bonding configurations at the surface of the initial cluster. The results will be compared to existing atomic energy level data and, in particular, photoemission data. Based on these comparisons, coupled with binding energy calculations for chemisorbed clusters, predictions can be made on the goemetrical arrangements of the surface and interfacial layers. In line with the prediction by Lindau (see Section 8.4) that surface electronic structure may provide better information on the geometrical rearrangement of surfaces, the HF cluster model may reveal an important theoretical link by which detailed rearrangements may be assumed and efficiently compared with experimental surface/interface data.

The HF molecular cluster model provides a "first principles" evaluation of electronic structure. The use of this method for the heavy atoms, such as Ga and As, will require developing optimum small clusters for modeling crystal surfaces in order to achieve a practical computation time. The model is expected to yield relevant information on the *local* electronic environment of the interfacial species and, hence, enable choices of an optimum geometric and electronic configuration. For passivation purposes, the optimum configuration would seek to reduce interface electronic states.

8.5.2 Localized Electronic Structure Calculations Using Wannier Functions

In studying the energy spectrum in an excited electron in ideal crystal, Gregory Wannier constructed "orthogonal atomic functions," now called Wannier functions.[238] The motivation for this was that atomic functions, rather than delocalized Bloch functions, had been shown to be more effective for studying the behavior of electrons in crystals.[239] The problem with atomic functions, however, is that they are not orthogonal. We postulate a function, $a_n(\vec{r})$, such that a Bloch function in the nth band is given by:

$$\psi_{\vec{k},n} = \frac{1}{\sqrt{N}} \sum_{\vec{\ell}} e^{i\vec{k}\cdot\vec{\ell}} \, a_n(\vec{r}-\vec{\ell})$$

yielding an inversion formula

$$a_n(\vec{r}-\vec{\ell}) = \frac{1}{\sqrt{N}} \sum_{\vec{k}} e^{-i\vec{k}\cdot\vec{\ell}} \psi_{\vec{k},n}(\vec{r}) \quad .$$

It can easily be shown, using the orthogonality of the Bloch functions, that the Wannier functions, $a_n(\vec{\ell})$, are orthogonal for different bands and for different sites. Phenomena involving localized electronic levels are thus conveniently represented in terms of Wannier functions. Surface states have been studied utilizing these methods.[240] Theoretical progress has been made, notably by Kohn[241] and Cloizeau.[242] The properties of Wannier functions in relation to energy bands are firmly established in these studies. Useful quantitative calculations had not appeared until 1972 when Kohn[243] adapted an *ab initio* variational technique -- calculating Wannier functions for several bands of the diamond structure. Once Wannier functions are found,

Bloch functions, energy eigenvalues, and moments of the density of states
are easily calculated. This method, then, provides an alternative approach
to conventional bulk band structure calculations.

A milestone occurred when Kohn and Onffroy (1973)[244] introduced the
concept of Generalized Wannier Functions (GWF) in studying a one-dimensional
periodic lattice with a point defect. They have shown that the GWF's have
the same localized properties as the Wannier functions of the perfect lat-
tice. Furthermore, as the localized site index of the GWF's moves away from
the defect site, the GWF's exponentially approach the perfect lattice Wannier
functions. Then, only a few perturbed Wannier functions will differ from
the perfect crystal Wannier functions. Kohn and Onffroy introduce an *ab
initio* method for calculation of the GWF's and comment that this procedure
is easier than attempting to calculate eigenfunctions of a non-periodic sys-
tem. This theory has also been applied to a localized impurity state between
two bands and the determination of which band this state belongs to.[245] Gay
and Smith[246] have extended Kohn and Onffroy's work to the study of localized
bulk defects in three-dimensional solids. They have pointed out the particu-
lar usefulness of the GWF method to study the well localized deep traps,
complementing the effective mass formalism for shallow impurity levels in a
band gap material. Lattice vacancies are also considered in terms of a de-
fect model. In contrast to the Koster-Slater method of handling localized
impurity problems, the GWF method does not require the knowledge of the im-
purity potential and the full set of energy eigenvalues and eigenstates of
the perfect crystal. Gay and Smith also show the ease of self-consistently
calculating the charge densities and local density of states (LDOS) knowing
only the GWF's. Since the charge density changes in the region around a

94

defect, self-consistency has been shown to be of critical importance.[247] In terms of the bond concept in solids, the GWF's, due to their orthonormality, decay smoothly in regions where no other functions would exist. At a surface, the decaying tails of the GWF's form the dangling bonds of surface chemistry.

Studies of the application of GWF's to crystal surfaces have been done by Rehr and Kohn[248] and by Smith and Gay.[249,250] The importance here is the detailed characterization of the electronic structure of the surface in the chemisorption process. GWF's are applicable to surfaces because of the ample experimental evidence that the strong variation of electrical properties in the surface region decays rapidly into the bulk. Describing the surface electronic structure in terms of orthonormal local functions which can be calculated directly (GWF's) is surely an advantage over using the delocalized functions for localized surface states.

Smith and Gay[249,250] test the GWF formalism on exactly soluble one-dimensional Mathieu potential surface problems.[251-253] The type analytic model potential that was used is shown in Figure 34. The GWF trial functions
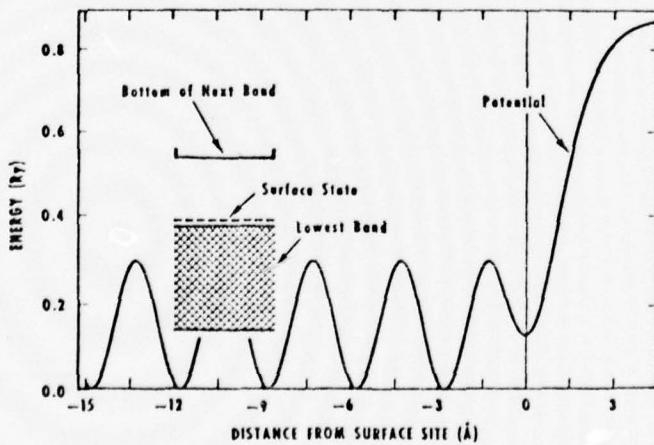
Figure 34. Model Surface Potential Plot. The inset shows the relevant part of the energy spectrum of the potential. (after Gay and Smith[250,254])

were chosen as modified gaussians with a variational parameter and are shown for the first three lattice sites in Figure 35. This shows dramatically how the GWF's rapidly approach the symmetric Wannier functions of the bulk and the smooth exponential decay of the surface site GWF into the vacuum.
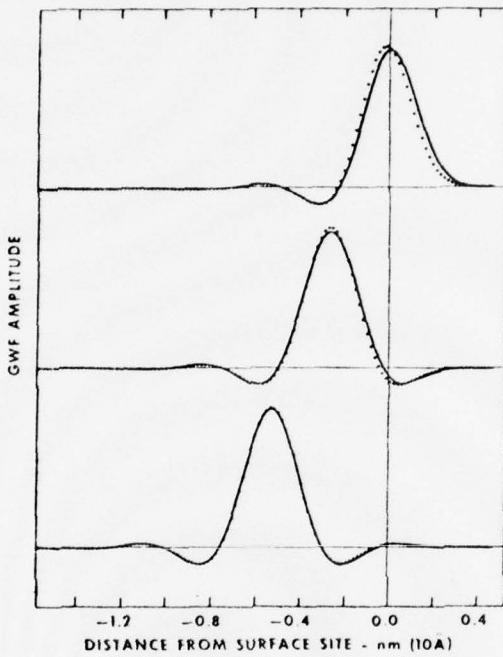
Figure 35.   Generalized Wannier Functions Computed with Gaussians for the First Three Lattice Sites. The rapid approach to the symmetric bulk Wannier function by the third site is illustrated. (after Gay and Smith[250])

The comparison of the exact wave functions to the approximate wave functions calculated from the GWF's is shown in Figure 36, illustrating the accuracy of results using simple trial functions. The theory for three-dimensional surfaces and their complications is discussed in reference 246. The use

of GWF's with respect to other methods of electronic structure calculations

has been suggested by J. R. Smith.[254]
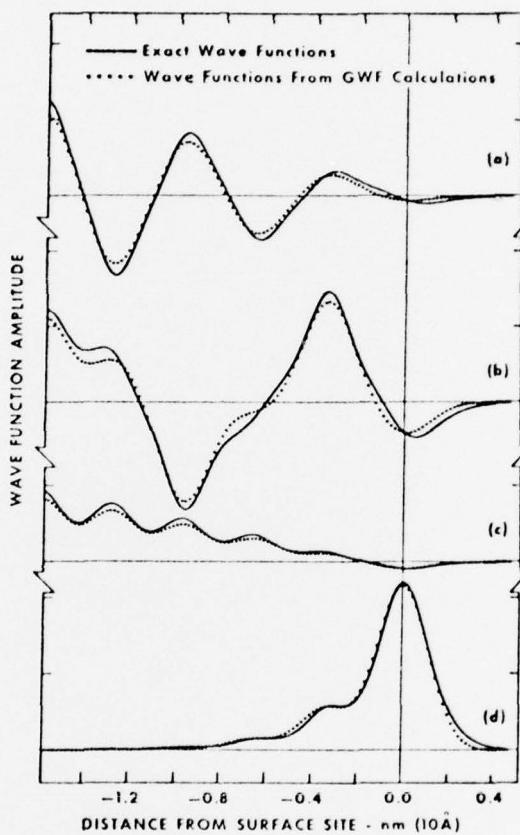
Figure 36. Comparison of Approximate with Exact Wavefunctions
for the Mathieu Surface Potential. The approxi-
mate wavefunctions are calculated from GWF's. The
top three plots compare wavefunctions near the
(a) top, (b) middle, and (c) bottom of the lowest
band. The bottom plot compares the approximate
and exact surface state wavefunctions. (after Gay
and Smith[250])

Needed work has not been done on the practical application of General-
ized Wannier Functions applied to two- and three-dimensional models, es-
pecially involving surfaces and interfaces. Some work has been done by
Pei and Kohn for calculating interface energies concerning stacking faults
in nickel, resulting in practical applications to transition metals.[255]

In a private communication with J. R. Smith, he suggested the feasibi-
lity of applying the method to various semiconductor surfaces, in particular,
silicon with its bulk diamond structure. Calculations for various gallium
arsenide surfaces also seem feasible. Experimental evidence by photoemis-
sion and low-energy loss spectroscopy has generally shown the existence
of surface states localized predominantly on the arsenic atoms. Calculating
the GWF's for the polar faces (either arsenic-rich or gallium-rich surface)
and the subsequent calculation of the charge density and LDOS at surface
sites would help corroborate experimental results and contribute to theore-
tical predictions.

The effort that has been undertaken in the study of the Wannier function
techniques has shown that, until recently, the technique has been dormant
for several years -- overshadowed by extensive band structure calculations.
The concepts behind the theory suggest that the GWF's are a logical exten-
sion to the non-orthogonal atomic functions while preserving the idea of
Bloch functions; that is, explaining the nature of electrons in crystals.
The ability to calculate GWF's from an *ab initio* procedure is superior to
any empirical band structure procedure. Also, the ability to calculate
various parameters, even the Bloch functions, directly from Wannier func-
tions, reflects its generality. Wannier functions normally have been most
useful for wide band gap materials, such as insulators, but have been

applied to surfaces, incorporating strong and weak perturbations there. The essential ingredients of the theory show that it can effectively be applied to any system which possesses spatially localized states. The realm of III-V compound semiconductors, such as GaAs, fits this application, as well as various interfacial structures, such as oxygen chemisorption on GaAs. Photoemission results have clearly shown the retention of interface states at the GaAs/oxygen interface. It is hoped that calculations such as the ones mentioned here will provide a theoretical basis for practical interface processes, such as the passivation of elemental and compound semiconductors.

8.5.3 Localized Electronic Structure Calculations Using Pseudopotentials

In an attempt to understand the behavior of electrons in crystals, the pseudopotential method was developed as a modification of Herring's orthogonalized plane wave (OPW) formalism.[256] The method relies on the assumption that the effective potential for the core electrons may be separated from that of the valence electrons. This is in line with the view that the valence electrons are solely responsible for all of the ordinary chemical and physical properties of the system. The pseudopotential, then, seeks to describe the interaction of a valence electron with the core ion and the surrounding cloud of other valence electrons. Furthermore, in contrast to the view of the Hartree-Fock self-consistent field, a wide range of solid state properties may be calculated directly using the pseudopotential. Thus, results of pseudopotential calculations may readily be compared to experimental results which then, in turn, could be used to modify and refine the original pseudopotentials, i.e. the interaction of the valence

electron. The pseudopotential can be thought of as inherently containing the effect of the core structure while retaining the detailed structure of the valence electrons. The lowest states of the pseudopotential, therefore, correspond to the lowest states of the valence electrons. The pseudopotential models the crystal structure as a weak periodic perturbation and allows the valence structure to be considered by the well known nearly-free electron (NFE) formalism. Band structures are, therefore, easily obtained.

Rapid theoretical progress coupled with applications emerged in the early 1960's, notably by Austin, Heine, and Sham,[257] who recast the theory into the form which essentially prevails today. This era ended in the famous paper by Cohen and Bergstresser[258] in which they documented and illustrated pseudopotential results for a total of fourteen elemental and compound semiconductors. Several of the bulk band structures were found to be well correlated to optical reflectivity and photoemission data existing at that time.[259]

Harrison's book in 1966 reviewed and contributed to the pseudopotential theory, particularly for metals, up to that time.[260] It was essentially replaced by the authoritative reference by Heine, Cohen, and Weaire in 1970.[261] Most present day work is based on the foundations laid in this book which includes reviews of the entire theory relating to the various types of pseudopotentials in use as well as the detailed fitting of pseudopotentials to experimental data. Also a large section on cohesion and structure is included.

It is worthwhile to emphasize that in most applications of the pseudopotential technique, persisting to the present day, the pseudopotentials are empirically derived. The reason for this is that considerable success

has been achieved in fitting pseudopotentials to one experiment and then using the results on another type of experiment. Reference 261 cites several instances of this occurrence.

In more recent times, a useful self-consistent pseudopotential method for handling surfaces has developed.[262] In the model, periodicity is retained parallel to an interface and electronic screening of the interface is properly taken account of by self-consistency. The partial periodicity allows one to apply standard pseudopotential theory as outlined in reference 261. A particular surface structure is built up by considering a unit cell as an infinite "slab" of the crystal, i.e. a structure possessing a surface on each side of the slab. As the slab is periodically repeated, the surface layers are built maintaining a two-dimensional periodicity. One need only to consider enough layers so that the two surfaces of the periodically repeated system do not appear to affect one another, i.e. by allowing enough layers for one surface's effect to decay into the "bulk".

The self-consistent pseudopotential method described here requires three inputs: (1) the empirical pseudopotential, V_{EMP}, usually constructed from fitting bulk energy spectra; (2) the geometrical arrangement of the slab; and (3) atomic ion core pseudopotentials, V_{ION}. The parameters of V_{ION} are fit to a Heine-Abarenkov core potential as outlined in reference 261.

The entire procedure will now be outlined briefly by resorting to the block diagram in Figure 37. V_{EMP} initiates the self-consistent loop. The total charge density, $\rho(r)$, is then calculated followed by a Hartree screening potential, V_H, and a Slater statistical exchange potential, V_X. V_H and V_X are added, resulting in the screening potential, V_{SCR}, which is then added to V_{ION} to yield a __total__ pseudopotential, V_T. V_T is then retained for

comparison to the next iteration until self-consistency is achieved.[262]

STEPS IN ACHIEVING SELF-CONSISTENCY
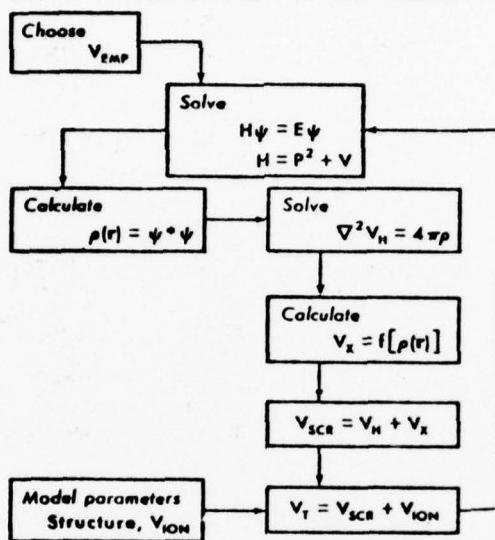
Figure 37. Block Diagram Indicating the Basic Steps in
Obtaining a Self-Consistent Psendopotential
(after Schlüter, et al.[262]).

The Si(111) ideal, relaxed (inward 0.33 A), and (2 x 1) reconstructed
surfaces were the first applications of this method to a semiconductor sur-
face.[262,264] The ideal and relaxed surface models show general agreement
with theoretical results.[265] We illustrate Cohen and his group's calcula-
tion of the local density of states (LDOS) and total charge of the relaxed
Si(111) 12-layer slab surface model in Figure 38. Layer 1 is deep within

the bulk and is typical of the silicon bulk density of states. Surface

features reveal themselves as the top slab (layer 6) is approached showing

the prominent Si(111) dangling bond state surface state. The other shaded

peaks are correlated to the four back-bond surface states. The Si(2 x 1)

reconstructed surface model was found to give splitting of the dangling

bond state into two bands, consistent with photoemission data and other

theoretical results.[265]
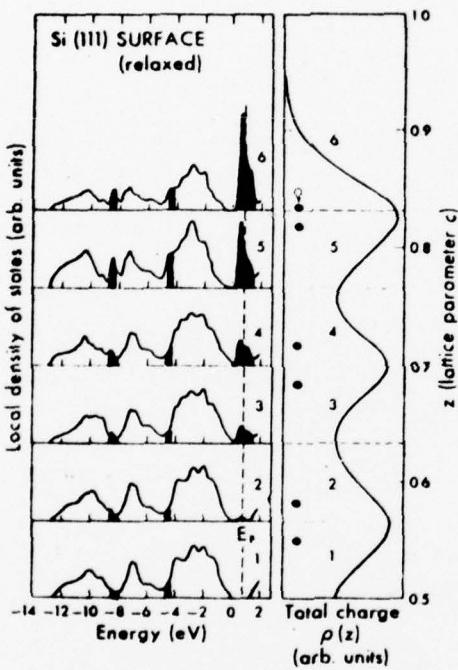
Figure 38. Local Density of States for a Relaxed Si(111)
Surface. The most prominent surface states
are indicated. The total valence charge as
a function of the coordinate z perpendicular
to the surface is shown for reference. (after
Louie, et al.[264]).

The electronic structure of GaAs(110) ideal and relaxed surfaces has also been studied using the pseudopotential method.[264,267,268] For the ideal surface, Figure 39 shows the total valence charge density terminated for each type of atom. Figure 40 shows the charge densities for the dangling bond surface states and Figure 41 shows the LDOS with a corresponding table correlating the positions of the identified surface features (shaded) with respect to the top of the bulk valence band.[267] The fact that recent photoemission data does not agree well with the location of the anion and cation derived surface states, a relaxed GaAs(110) surface was considered. Figure 42 shows the LDOS obtained by the pseudopotential calculations for this structure.
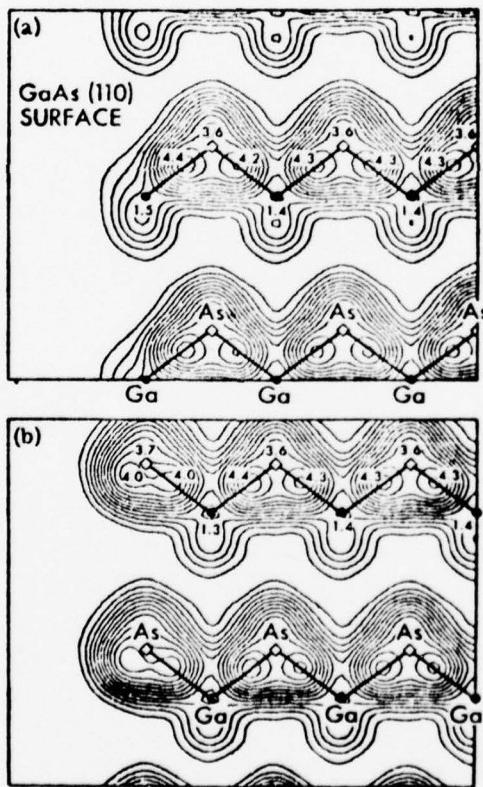
Figure 39. Total Valence Charge Density for the GaAs(110) Surface Plotted in the (1$\bar{1}$0) Plane Terminated on the (a) Ga Atom and (b) As Atom. The charge density has been normalized to one electron per unit cell volume $\Omega_{cell} = 812$ Å^3. The contour spacing is in units of 0.35. (after Chelikowsky and Cohen[267]).
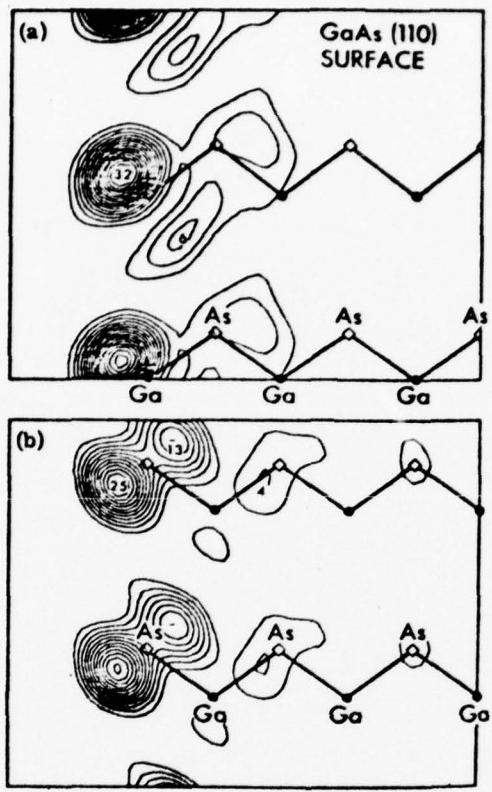
Figure 40. Charge Density of the GaAs (110) Surface for the
(a) Ga Dangling-Bond and (b) As Dangling-Bond
Surface States in the Same Plane and Normalization
as in Figure 39. The contour spacing is in units
of 2.0. (after Chelikowsky and Cohen[267]).

GaAs (110) SURFACE
Local density of states

TOTAL

LAYER 5

LAYER 3

LAYER 2

LAYER 1
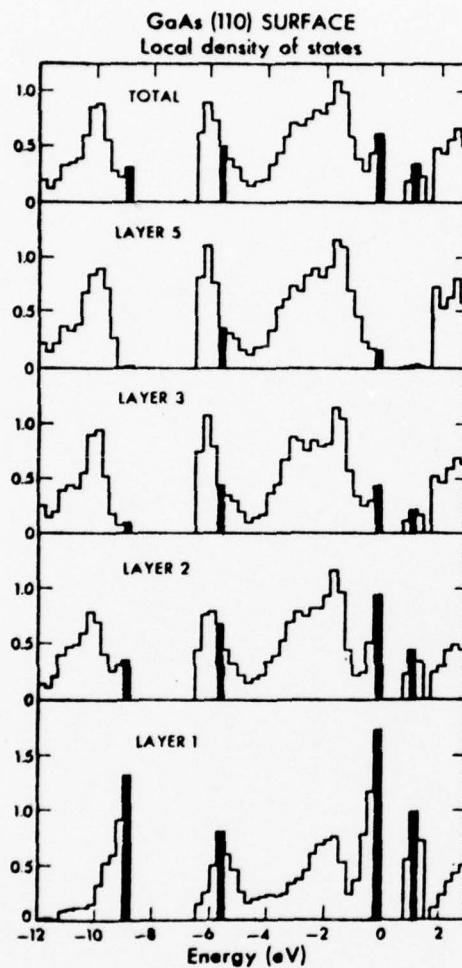
Energy (eV)

Feature	Energy (eV)
As s-like	−9.0
Ga s-like	5.75
As back bond	−2.0
As parallel bond	−0.5
As dangling bond	−0.25
Ga dangling bond	+1.0

Figure 41. Local Density of States for the GaAs (110) Surface (in arbitrary units). The total density of states was obtained by summing over all layers. Prominent surface features are shaded in the spectra and identified in the table. (after Chelikowsky, et al.[267]).

106
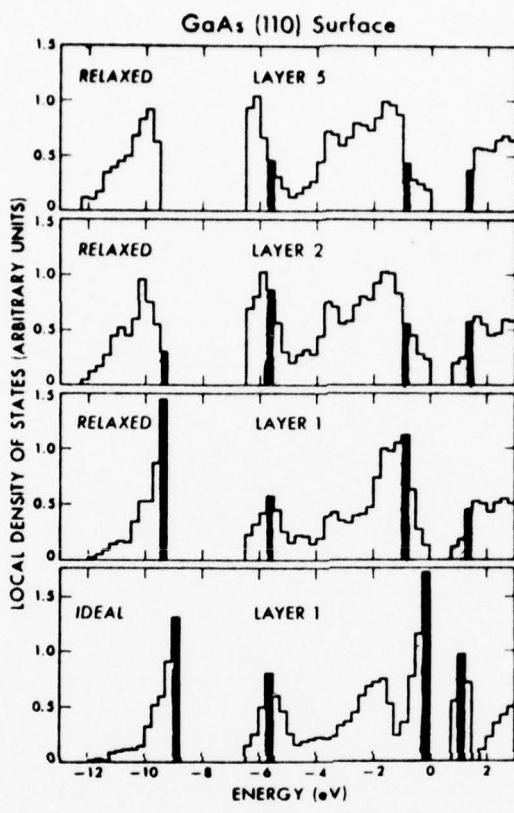
Figure 42. Local Density of States for a Relaxed (110) Surface of GaAs. The LDOS at the surface layer for the ideal case is also displayed. (after Louie, et al.[264]).

The effect of the relaxation is shown to move the filled As surface states down about 1 eV and to disperse the empty Ga surface state. These results are more compatible to partial-yield photoemission data than the results for the ideal surface.[270] Surface states, however, still are found in the energy gap which is in contradiction to experimental evidence. It is, of course, suggested that a more suitable geometry could be chosen that would improve results.

A pseudopotential study of metal-semiconductor interfaces has been undertaken by Cohen and his group using the jellium model to describe the metal.[264] M/Si, M/GaAs, M/ZnSe, and M/ZnS models have been studied because of their increasing ionicity. Pseudopotential results show that the dangling bond surface states are removed by the presence of the metal, but are replaced by metal-induced gap states (MIGS). In contrast to the Bardeen model, intrinsic surface states are shown not to play a dominant role in determining the barrier height of a Schottky interface. Calculated barrier heights, due to the MIGS, are found to be in good agreement with experimental values. A simple model is postulated that quantitatively correlates the barrier heights for different metals on semiconductors of varying ionicity.[271]

It is noteworthy to mention that recent theoretical work[272] using an empirical tight-binding Hamiltonian for GaAs(110) corroborates with most of the self-consistent psendopotential calculations. The pseudopotential method has also been recently applied to GaAs-AlAs heterostructures [which can be grown by molecular-beam epitaxy (MBE)] with new fitting parameters for Ga, Al, and As.[273]

In conclusion, the pseudopotential method has recently been the subject of several investigations on surface/interface electronic states.

Calculations have shown surface features that are in relatively good agreement with experimental data concerning band structure. Also, a model has been suggested, based on pseudopotential results, which puts the explanation of Schottky barriers on a firmer footing. As experimental data becomes more accurate, the pseudopotentials can likewise be refined. As results of pseudopotential studies advance, insight should be seen into the problem of passivation of semiconductors, particularly GaAs. The present requirements of two-dimensional periodicity and using identical slabs may turn out to be too stringent to understand the details of, say, oxygen chemisorption. The continued analysis of intrinsic surface states by pseudopotentials, using better geometrical models, may presently prove to be the most useful effort in this area.

IX. SURFACE INSTRUMENTATION:

The principal analytical techniques used during the program were Auger
electron spectroscopy (AES) and X-ray photoelectron spectroscopy (XPS). The
advantages of high resolution AES and XPS were pointed out earlier in this
report. Most of the facilities required to conduct the program were avail-
able in laboratories of the Applied Sciences Laboratory of the Engineering
Experiment Station or in the School of Physics. The high resolution AES
and XPS studies were performed during visits to the Applications Laboratory
of Physical Electronics Industries in Eden Prairie, Minnesota.

At the beginning of the program in 1975 the ultra-high vacuum system
that was available provided combined LEED and Auger capabilities with a re-
tarding grid analyzer, sputter-ion gun and a quadrupole residual gas analy-
zer. This system was also equipped with a turbo-molecular pump, a titanium
sublimation pump, a large ion pump and a gas manifold.

During the first year system modifications were made to improve the
detection sensitivity of the Auger technique. These modifications included
the addition of a PHI Model 10-155 Cylindrical Mirror Analyzer, a Model
11-010 Electron Gun Control Unit and a Model 11-500A Auger System Control
Unit.

During the second year a PHI Model 04-191 Sputter Ion Gun and a Model
20-115 Control Unit were added to provide higher ion energies and a raster
capability for more uniform sputter etching of larger areas. Also an auxi-
liary titanium sublimation pump, adapted from an Electro-Ion pump, was
installed directly on the chamber for increased pumping speed. Improved
data handling was accomplished by using a Nicolet Model 535 Signal Averager,
purchased under the contract. This unit has been particularly useful for

increasing the signal-to-noise ratio of weak Auger derivative signals without sacrificing resolution and it has been used to obtain N(E) data for energy loss measurements. Fabrication of MOS and Schottky barrier test structures within the Auger system was made possible by using an evaporator mounted on the rear flange of the system. This _in situ_ evaporator, pictured in Figure 14 of our Interim Report dated 28 January 1977, provided a capability for aluminum or gold evaporation with appropriate shuttering and thickness control with a quartz crystal thickness monitor.

During the third year another evaporator was designed for inclusion in the system when the LEED optics was also in place on the back flange. With this arrangement surface characterization of GaAs samples before metal deposition can include crystallographic information from LEED as well as the measurement of surface contamination and stoichiometry from AES.

The current LEED/Auger ultra-high vacuum system is shown in the photograph of Figure 43.

The majority of the improvements in the instrumentation for surface studies can be attributed directly to this ONR-sponsored program. We anticipate acquiring in the near future, under a National Science Foundation equipment grant, a multiple technique surface analysis instrument which will include high spatial resolution (<0.2 µm) SAM, a high energy resolution analyzer for AES and XPS, and a SIMS attachment. This equipment will greatly aid investigations of the type described in this report.

Figure 43. Surface Analysis Instrumentation Used for LEED, AES, LELS and Other Surface Studies.

X. IDENTIFICATION OF PERSONNEL:

The following personnel participated in the program during the period 1 May 1975 to 30 April 1978.

E. J. Scheibner, Research Professor of Physics and Head of the Surface Physics and Chemistry Laboratories of the Solid State Sciences Division, was Principal Investigator of the program. He received his Ph.D. in Physics from Illinois Institute of Technology in 1955, has an M.S. degree in Physics from Illinois Tech and a B.S. degree in Physics from Georgia Tech. Dr. Scheibner is primarily responsible for surface analytical instrumentation including low energy electron diffraction (LEED) and Auger electron spectroscopy (AES). He has extensive experience in thin films, semiconductors, ultra-high vacuum and surfaces. His current research interests relate to surface or interface effects in solid state devices and applications of AES. He regularly teaches a graduate course on surface physics as part of an interdepartmental academic program in surface science and technology, and directs the thesis research of Ph.D. students in Physics.

M. W. Ribarsky, a Research Scientist in the School of Physics, was involved in the theoretical phases of the program, particularly the analysis of Auger and X-ray photoelectron spectra and the development of methods for calculating energy levels for clusters of atoms at the surface. Dr. Ribarsky received his Ph.D. in Physics from the University of Cincinnati in 1974 and his M.S. and B.S. in Physics from the same institution in 1970 and 1967, respectively.

Walter H. Hicklin, Research Engineer, had direct responsibility for operating and maintaining the LEED/Auger equipment. He is highly competent in the operation of several other analytical instruments including the scanning

113

electron microscope, transmission electron microscope, and X-ray and electron diffraction units. In addition, he has experience in producing films of a variety of metals, insulators and semiconductors by evaporation, sputtering, electroplating, chemical vapor deposition and molecular beam epitaxy techniques.

James M. Hill, III, a graduate student in Physics, was involved in the early work on GaAs surfaces. Mr. Hill received his M.S. Degree in Physics in December 1976 and accepted employment in Texas.

Richard Marucci, a student in Electrical Engineering, was involved in measurements on silicon MOS devices and in the development of Auger instrumentation. Mr. Marucci received his B.S. degree in Electrical Engineering in December 1976 and has accepted an electronics position in another division of the Engineering Experiment Station.

Charles S. Brown, a graduate student in Physics, was involved in the preparation and analysis of thin oxide films on tantalum, aluminum and gallium arsenide by optical methods. Mr. Brown successfully passed the comprehensive examination in the Spring of 1977 and is now engaged in his Ph.D. thesis research.

A. Craig Kenton, a graduate student in Physics, was involved in Auger studies of GaAs surfaces and in the analysis of Schottky barriers on GaAs. He also initiated theoretical studies of surface states on GaAs by cluster methods. Mr. Kenton successfully passed the comprehensive examination in the Spring of 1977 and is now engaged in his Ph.D. thesis research.

XI. PRESENTATIONS, REPORTS AND PAPERS:

E. J. Scheibner, "Solid State Reactions on Semiconductor Surfaces," presented at Workshop on Solid-Phase Epitaxial Reactions held in Hughes Research Laboratories, Malibu, California, August 8, 1975.

E. J. Scheibner, "Studies of Solid State Reactions on Elemental and Compound Semiconductor Surfaces," Interim Technical Report, Contract No. N00014-75-C-0909 with Office of Naval Research, January 21, 1976.

E. J. Scheibner, "Interface Structures in MOS Devices and Their Effect on Reliability," presented at the meeting of the International Society of Hybrid Microelectronics, Huntsville, Ala., January 28, 1976.

M. W. Ribarsky and E. J. Scheibner, "Analysis of High Resolution Auger and X-ray Photoelectron Spectra from Thin Oxide Films on Aluminum," presented at Amer. Phys. Soc. meeting in Atlanta, March 20 - April 1, 1976, Bull. Amer. Phys. Soc., 21, 432 (1976).

E. J. Scheibner and W. H. Hicklin, "Characterization of Metal-Oxide Systems by High Resolution Electron Spectroscopy," presented at the 30th Annual Symposium on Frequency Control, Atlantic City, N.J., 2-4 June 1976; Proceedings 30th Annual Symposium on Frequency Control, U. S. Army Electronics Command, Fort Monmouth, N.J. (1976) pp. 240-248.

E. J. Scheibner, "Studies of Solid State Reactions on Elemental and Compound Semiconductor Surfaces," Interim Technical Report, Contract No. N00014-75-C-0909 with Office of Naval Research, January 28, 1977.

Y. E. Strausser, E. J. Scheibner and J. S. Johannessen, "Observations of Al_2O_3 and Free Si in the Interface Between Al Films and SiO_2," accepted for publication in Thin Solid Films.

M. W. Ribarsky and E. J. Scheibner, "Analysis of Auger and X-ray Photoelectron Spectra with Application to Thin Oxide Films on Aluminum," unpublished report.

XII. SUMMARY AND RECOMMENDATIONS:

The physics and chemistry of interfaces in composite planar structures
on silicon and gallium arsenide single crystals were investigated. In the
study of interface chemistry the direction of oxidation-reduction reactions
was predicted from the bulk thermodynamic values of the free energy changes
on forming the various inorganic oxides. Thus, observations were made of
the reduction of SiO_2 on silicon by Al to form Al_2O_3 and the reduction of
Ga_2O_3 by Al to form Al_2O_3. Other metals were predicted to behave similarly
to Al. The identification of the separate solid state phases in the compo-
site structures was made by high energy resolution Auger electron spectros-
copy (AES) and X-ray photoelectron spectroscopy (XPS) techniques. Further
studies of this type are recommended. In particular, investigations should
be made of oxidation-reduction reactions involving metals other than Al. The
dependence of the width of the reaction zone on initial oxide thickness and
the elemental distribution, e.g. Si, Ga or As, within the metal and the oxide
should be determined.

Experimental MOS and Schottky barrier test devices were fabricated from
planar composite structures prepared in the ultra-high vacuum system and
having well-characterized interfaces. Because of the importance of these
type devices in advanced electronic systems further efforts should extend
the fundamental studies towards new device technologies including a considera-
tion of device reliability from the materials, rather than the statistical,
viewpoint.

The attenuation length of ~1400 eV electrons in thin oxide films on
aluminum was studied with high energy resolution AES and XPS. Theoretical
interpretation of the data involved the removal of background and instrument

116

resolution effects and separation of the oxide and metal peaks into Lorent-
zian and Gaussian components. Measurements of the integrated intensities
of the peaks as a function of oxide thickness fitted to predicted curves
gave values for the attenuation length. Since relatively little data exist
for electron attenuation in oxides it is strongly recommended that these
studies be continued. In particular the importance of establishing accurate
sputtering rates for oxides should be noted and measurement schemes should
be devised for obtaining attenuation length data for a range of electron
energies.

The passivation of compound semiconductor surfaces on devices has proved
to be much more difficult than that of silicon surfaces, yet it is necessary
for achieving stable, reliable devices. We have reviewed the voluminous
literature on the subject of GaAs surface passivation and have suggested a
possible method based upon the solid state reactions occurring at interfaces.
The main point is that attention to the fundamental physics and chemistry
of interfaces is likely to be equally, if not more fruitful than the previous
empirical approaches to passivation. In future efforts, consideration of
the electronic factors, e.g. the distribution of interface states, which
are required for a good passivation method should be stressed. In addition
more directed studies of interface chemical reactions should be carried out.

Localized theoretical models for predicting the electronic structure
of groups of atoms in the vicinity of interfaces have been examined briefly.
The particular techniques included are: (1) molecular cluster calculations
based upon an unrestricted Hartree-Fock method; (2) the pseudopotential
method; and (3) the generalized Wannier function method. Data resulting
from photoemission and energy loss spectroscopy will provide the experimental

verification of the assumed parameters in the models. For example, it is expected that precise atomic geometrical arrangements will be required in most of the theoretical calculations to give good agreement with the distributions of surface/interface states obtained experimentally. However, a sensitivity analysis will have to be made for each of the theoretical methods. It is strongly recommended that studies of the localized electronic structures be continued with emphasis on the atomic composition and arrangement at interfaces.

XIII. REFERENCES:

1. A. Christou and H. M. Day, J. Appl. Phys., 47, 4217 (1976).

2. A. Christou and K. Sleger, Int. Phys. Conf. Ser., 33b, 191 (1977).

3. H. K. Henisch, Rectifying Semiconductor Contacts, Oxford University Press, Oxford (1957).

4. S. M. Sze, Physics of Semiconductor Devices, Wiley-Interscience, New York (1969).

5. A. van Oostrum, J. Vac. Sci. Technol., 13, 224 (Jan/Feb 1976).

6. B. R. Pruniaux and A. C. Adams, J. Appl. Phys., 43, 1980 (1972).

7. P. Pianetta, I. Lindau, C. M. Garner, W. E. Spicer, Phys. Rev. Lett., 37, 1166 (1976).

8. R. Ludeke and A. Koma, CRC Crit. Rev. Solid State Sci., 5, 259 (1975).

9. R. Ludeke and A. Koma, J. Vac. Sci. Technol., 13, 241 (Jan/Feb 1976).

10. A. Koma and R. Ludeke, Phys. Rev. B, 13, 739 (1976).

11. O. Wada, S. Yanagisawa and H. Takanashi, Japan J. Appl. Phys., 12, 1814 (1973).

12. P. W. Palmberg, J. Vac. Sci. Technol., 12, 379 (Jan/Feb 1975).

13. C. D. Wagner, presented at the Discussions of the Faraday Society, Vancouver, Canada, July 1975.

14. E. J. Scheibner, Interim Technical Report, Contract No. N00014-75-C-0909 with Office of Naval Research, January 28, 1977.

15. E. A. Stern and R. A. Ferrell, Phys. Rev., 120, 130 (1960).

16. F. K. Wertheim, M. A. Butler, K. W. West and D. N. E. Buchanan, Rev. Sci. Inst., 45, 1369 (1974).

17. P. H. Citrin, G. K. Wertheim and Y. Baer, Phys. Rev. Lett., 35, 885 (1975).

18. J. C. Shelton, J. Elec. Spect. and Rel. Phenom., 3, 417 (1974).

19. M. Malin and K. Vidam, Surf. Sci., 56, 49 (1976).

20. S. S. So, Surf. Sci., 56, 99 (1976).

21. W. E. Wall and J. R. Stevenson, On Line Optical and Auger Data Acquisition, unpublished (1977).

22. B. Schwartz, "GaAs Surface Chemistry," CRC Crit. Rev. in Solid State Sci., 5, 609-24 (1975).

23. C. W. Wilmsen, "Oxide Layers on III-V Compound Semiconductors," Thin Solid Films, 39, 105-17 (Dec. 1976).

24. A. V. Emel'yanov, A. V. Nikitin, V. N. Timofeev and A. N. Shokin, "Nature of Gallium Arsenide Thermal Oxidation Products," Kristallografiya, 20, 611-14 (1975).

25. S. P. Murarka, "Thermal Oxidation of Gallium Arsenide," Appl. Phys. Lett., 26, 180-1 (1975).

26. F. Koshiga and T. Sugano, "Thermal Oxidation of Gallium Arsenide," Proc. Conf. Solid State Devices, 8, 465-9 (1977).

27. K. Navratil, "Thermal Oxidation of Gallium Arsenide," Czech. J. Phys., B18, 266 (1968).

28. K. Navratil, I. Ohlidal and F. Lukes, "A Model of Oxide Film Originating at Thermal Oxidation of GaAs," Czech. J. Phys., B27, 672-81 (1977).

29. H. J. Minden, "Thermal Oxidation of GaAs," J. Electrochem. Soc., 104, 733 (1962).

30. M. Rubenstein, "The Oxidation of GaP and GaAs," J. Electrochem. Soc., 113, 540 (1966).

31. K. H. Zaininger and A. G. Revesz, "Ellipsometric Investigation of Oxide Films on GaAs," J. Phys., Paris, 25, 208 (1964).

32. B. J. Sealy and P. L. F. Hemment, "Structure and Composition of Native Oxides on GaAs," Thin Solid Films, 22 539 (1974).

33. L. E. Coerver, "Thermal Oxidation of Gallium Arsenide Phosphide," Ph.D. Thesis, Univ. of New Mexico (1974). Available Univ. Microfilms, Order No. 74-20,349.

34. D. H. Phillips, W. W. Grannemann, L. E. Coerver and G. J. Kuhlmann, "Fabrication of GaAsP MIS Capacitors, Using a Thermal Oxidation Dielectric Growth Process," J. Electrochem. Soc., 120, 1087 (1973).

35. R. A. Logan, B. Schwartz and W. J. Sundburg, "Anodic Oxidation of Gallium Arsenide in Aqueous Hydrogen Peroxide Solution," J. Electrochem. Soc., 120, 1385-90 (1973).

36. S. M. Spitzer, B. Schwartz and G. D. Weigle, "Preparation and Stabilization of Anodic Oxides on GaAs," J. Electrochem. Soc., 122, 397-402 (1975).

37. B. Schwartz, F. Ermanis and M. H. Brastad, "The Anodization of GaAs and GaP in Aqueous Solutions," J. Electrochem. Soc., 123, 1089-97 (1976).

38. H. Hasegawa, K. E. Forward and H. L. Hartnagel, "Improved Method of Anodic Oxidation of Gallium Arsenide," Electron. Lett., 11, 53-4 (1975).

39. H. Hasegawa, K. E. Forward and H. L. Hartnagel, "New Anodic Native Oxide of GaAs with Improved Dielectric and Interface Properties," Appl. Phys. Lett., 26, 567-9 (15 May 1975).

40. H. Hasegawa and H. L. Hartnagel, "Anodic Oxidation of Gallium Arsenide in Mixed Solutions of Glycol and Water," J. Electrochem. Soc., 123, 713-23 (1976).

41. H. Hasegawa, K. E. Forward and H. L. Hartnagel, "New Anodic Oxidation of Gallium Arsenide," Thin Solid Films, 32, 65-7 (1976).

42. A. F. A. B. El-Safti, B. L. Weiss and H. L. Hartnagel, "Analysis of Multi-component Thin Films on Gallium Arsenide by Anodic Processes," Electron. Lett., 12, 322-5 (1976).

43. B. L. Weiss and H. L. Hartnagel, "The Structure of Cleaned and Polished (100) GaAs Surfaces," Int. J. Electron., 41, 185-8 (1976).

44. F. P. Fehlner and N. F. Mott, "Low-temperature and Anodic Oxidation of Metals and Semiconductors. Comments," Oxid. Metals, 4, 75-8 (1972).

45. G. Weimann and W. Schlapp, "Anodic Oxidation of Gallium Arsenide," Thin Solid Films, 38, 15-7 (1976).

46. B. M. Arora and M. G. Bidnurkar, "Anodic Oxidation of Gallium Arsenide," Solid State Electronics, 19, 657-8 (1976).

47. D. Law and C. A. Lee, "A New Aqueous Solution for the Anodic Oxidation of Gallium Arsenide," J. Electrochem. Soc., 123, 768-9 (1976).

48. S. Szpak, "Electro-oxidation of Gallium Arsenide. I. Initial Phase of Film Formation in Tartaric Acid-Water-Propylene Glycol Electrolyte," J. Electrochem. Soc., 124, 107-12 (1977).

49. D. J. Coleman, Jr., D. W. Shaw and R. D. Dobrott, "On the Mechanism of Gallium Arsenide Anodization," J. Electrochem. Soc., 124, 239-41 (1977).

50. C. S. Guenthner, P. V. S. Rao, S. Thomas and W. Paulson, "On the Anodic Oxidation of GaAsP," Electrochem, Soc., Fall Meeting, 5-10 October 1975, Dallas, Texas.

51. O. A. Weinreich, "Oxide Films Grown on GaAs in an Oxygen Plasma," J. Appl. Phys., 37, 2924 (1966).

52. J. R. Ligenza, "Silicon Oxidation in an Oxygen Plasma Excited by Micro-waves," J. Appl. Phys., 36, 2703 (1965).

53. T. Sugano and Y. Mori, "Oxidation of Gallium Arsenide Phosphide ($GaAs_{1-x}P_x$) Surface by Oxygen Plasma and Properties of Oxide Film," J. Electrochem. Soc., 121, 113-8 (1974).

54. T. Oda and T. Sugano, "Studies on Surface Plasma-oxidized Films of III-V Compound Semiconductors by Auger Electron Spectroscopy," Ann. Rep. Eng. Res., Inst. Fac. Eng., Univ. Tokyo, 33, 153-9 (1974).

55. R. P. H. Chang and A. K. Sinha, "Plasma Oxidation of Gallium Arsenide," Appl. Phys. Lett., 29, 56-8 (1976).

56. R. P. H. Chang, C. C. Chang and T. T. Sheng, "Plasma Oxidation of Aluminum Film on Gallium Arsenide--A Study by Auger Spectroscopy and Transmission Electron Microscopy," Appl. Phys. Lett., 30, 657-9 (1977).

57. R. L. Kauffman, L. C. Feldman, J. M. Poate and R. P. H. Chang, "Analysis of Plasma-grown GaAs Oxide Films," Appl. Phys. Lett., 30, 319-21 (1977).

58. F. Lukes, "Oxidation of Silicon and Gallium Arsenide in Air at Room Temperature," Surf. Sci., 30, 91-100 (1972).

59. K. Loeschke and G. Kuehn, "Oxidation of Gallium Arsenide Single Crystal Faces in Air," Krist. Tech., 10, K45-8 (1975).

60. R. S. Lorenz, "Preparation and Characteristics of the GaAs-Deposited SiO_2 Interface," Ph.D. Thesis, Ohio State (1970). Available Univ. Microfilms Order No. 70-26,322.

61. Y. Sato and M. Ikeda, "Surface Passivation of Gallium Arsenide," Rev. Elec. Commun. Lab. (Japan), 18, 618-23 (1970).

62. W. Kern and J. P. White, "Interface Properties of Chemically Vapor Deposited Silica Films on Gallium Arsenide," RCA Rev., 31, 771-85 (1970).

63. R. H. Weissman, "The Electrical Characteristics of Insulator-Gallium Arsenide Interfaces," Ph.D. Thesis, Stanford Univ. (1971). Available Univ. Microfilms Order No. 71-19776.

64. T. Ito and Y. Sakai, "The GaAs Inversion-type MIS Transistors," Solid State Elect., 17, 751-9 (1974).

65. N. A. Semushkina, V. M. Marakhonov and R. P. Seisyan, "Nature of Carrier Depletion Layers on the Surface of Gallium Arsenide in MIS Systems," Sov. Phys.-Semicond., 10, 292-6 (1976).

66. G. D. Stareev, M. Piskorski and Z. Majewski, "Au-GaAs Schottky Barrier Diodes for X-Band Application," Electron. Technol. (Poland), 8, 77-85 (1975).

67. L. Messick, "A GaAs/Si$_x$O$_y$N$_z$ MIS FET," J. Appl. Phys., 47, 5474-5 (1976).

68. T. Sugano, H. Sakai and Y. Mori, "Deposition of Insulating Film on GaAs by R.F. Glow Discharge (MIS Structures)," Ann. Rep. Eng. Res., Inst. Fac. Eng., Univ. Tokyo, 30, 205-10 (1971).

69. E. R. Ward, "The Electrical Properties of the Silicon Nitride-Gallium Arsenide Interface," Ph.D. Thesis, Purdue (1971). Available Univ. Microfilms Order No. 71-2707.

70. J. A. Cooper, Jr., E. R. Ward and R. J. Schwartz, "Surface States and Insulator Traps at the Si$_3$N$_4$-GaAs Interface," Solid State Elect., 15, 1219-27 (1972).

71. H. Seki, S. Ohosaka, M. Kanda, Y. Kawasaki, H. Yamazaki and M. Fujimoto, "Passivation of Gallium Arsenide with Silicon Nitride," Rev. Elec. Commun. Lab. (Japan), 20, 810-6 (1972).

72. R. Singh and H. L. Hartnagel, "Reduction in Surface Charge Density by New GaAs Passivation Method," J. Phys. D., 8, L42-3 (1975).

73. W. W. Siekanowicz, H. Huan, D. Hoffmann, S. Jolly and Y. C. Chiang, "Aluminum Oxide Passivation of Electron-beam Semiconductor Silicon and Gallium Arsenide Diodes," U.S. NTIS, Gov't. Rep Announce., 74, (1974).

74. O. Wada, S. Yanagisawa and H. Takanashi, "The Effect of Heat Treatment on Al-GaAs Schottky Barriers," Jap. J. Appl. Phys., 12, 1814-5 (1973).

75. B. Feuerbacher, B. Fitton, "Photoemission Spectroscopy," Electron Spectroscopy for Surface Analysis: Topics in Current Physics, Vol. 4, ed. by H. Ibach (New York, Springer-Verlag, 1977).

76. B. Feuerbacher, R. F. Willis, J. Phys. C: Solid State Phys., 9, 169 (1976).

77. J. Bardeen, Phys. Rev., 71, 717 (1947).

78. F. G. Allen and G. W. Gobeli, Phys. Rev., 137, 150 (1962).

79. G. Chiarotti, S. Nannarone, R. Pastore, P. Chiaradia, Phys. Rev. B, 4, 3398 (1971).

80. D. E. Eastman and W. D. Grobman, Phys. Rev. Lett., 28, 1378 (1972).

81. L. F. Wagner and W. E. Spicer, Phys. Rev. Lett., 28, 1381 (1972).

82. F. G. Allen and G. W. Gobeli, J. Appl. Phys., 35, 597 (1964).

83. M. Erbudak and T. E. Fischer, Phys. Rev. Lett., 29, 732 (1972).

84. J. E. Rowe and J. C. Phillips, Phys. Rev. Lett., 32, 1315 (1974).

85. T. Murotani, K. Fujiwara and M. Nishijima, <u>Jap. J. Appl. Phys., Suppl. 2</u>, <u>2</u>, 409 (1974).

86. J. E. Rowe, <u>Phys. Lett.</u>, <u>46A</u>, 400 (1974).

87. W. E. Spicer in <u>Vacuum Ultraviolet Radiation Physics</u>, E. E. Koch, R. Haensel and C. Kunz, eds., Pergamon Vieweg, Hamburg (1974).

88. L. F. Wagner and W. E. Spicer, <u>Phys. Rev. B</u>, <u>9</u>, 1512 (1974).

89. J. E. Rowe and H. Ibach, <u>Phys. Rev. Lett.</u>, <u>32</u>, 421 (1974).

90. J. E. Rowe and J. C. Phillips, <u>Phys. Rev. Lett.</u>, <u>32</u>, 1315 (1974).

91. J. E. Rowe, H. Ibach and H. Froitzheim, <u>Surf. Sci.</u>, <u>48</u>, 44 (1975).

92. E. O. Kane, <u>Phys. Rev.</u>, <u>146</u>, 558 (1966).

93. R. O. Jones, <u>J. Phys. C: Solid St. Phys.</u>, <u>5</u>, 1615 (1972).

94. F. Yndurain and M. Elices, <u>Surf. Sci.</u>, <u>29</u>, 540 (1972).

95. V. Bortolani, C. Calandra and M. J. Kelly, <u>J. Phys. C: Solid St. Phys.</u>, <u>6</u>, L239 (1973).

96. J. A. Appelbaum and D. R. Hamann, <u>Phys. Rev. Lett.</u>, <u>31</u>, 106 (1973).

97. J. A. Appelbaum and D. R. Hamann, <u>Phys. Rev. Lett.</u>, <u>32</u>, 225 (1974).

98. J. A. Appelbaum and D. R. Hamann, <u>Surf. Sci.</u>, <u>68</u>, 167 (1977).

99. K. C. Pandey and J. C. Phillips, <u>Phys. Rev. Lett.</u>, <u>32</u>, 1433 (1974).

100. I. P. Batra and S. Ciraci, <u>Phys. Rev. Lett.</u>, <u>34</u>, 1337 (1975).

101. S. Ciraci and I. P. Batra, <u>Solid St. Commun.</u>, <u>16</u>, 1375 (1975).

102. M. Schlüter, J. R. Chelikowsky, S. G. Louie and M. L. Cohen, <u>Phys. Rev. Lett.</u>, <u>34</u>, 1385 (1975).

103. A. Selloni and E. Tosatti, <u>Solid St. Commun.</u>, <u>17</u>, 387 (1975).

104. J. E. Rowe, M. M. Traum and N. V. Smith, <u>Phys. Rev. Lett.</u>, <u>33</u>, 1333 (1974).

105. E. W. Plummer, "Photoemission and Field Emission Spectroscopy in <u>Inter-actions on Metal Surfaces: Topics in Applied Physics</u>," Vol. 4, ed. by R. Gomer, Springer-Verlag, 1975.

106. C. Kunz and W. Gudat, <u>Phys. Rev. Lett.</u>, <u>29</u>, 169 (1972).

107. J. L. Freeouf and D. E. Eastman, <u>CRC Crit. Rev. Solid State Sci.</u>, <u>5</u>, 245 (1975) and references therein.

108. W. Gudat, D. E. Eastman and J. L. Freeouf, J. Vac. Sci. Tech., 13, 250 (1976).

109. A. Koma and R. Ludeke, Phys. Rev. Lett., 35, 107 (1975).

110. R. S. Bauer, R. Z. Bachrach, S. A. Flodstrom and J. C. McMenamin, J. Vac. Sci. Tech., 14, 378 (1976).

111. W. E. Spicer in Photoemission Spectroscopy and the Electronic Structure of Amorphous Materials, J. Stuke and W. Brenig, eds., Taylor and Francis Ltd., London, p. 499 (1974).

112. W. E. Spicer, CRC Crit. Rev. Solid St. Sci., 6, 317 (1976).

113. J. A. Appelbaum and D. R. Hamann, Phys. Rev. Lett., 34, 806 (1975).

114. K. C. Pandey, T. Sakurai and H. D. Hagstrum, Phys. Rev. Lett., 35, 1728 (1975).

115. P. K. Larsen, N. V. Smith, M. Shlüter, H. H. Farrell, K. M. Ho and M. L. Cohen, Phys. Rev., B17, 2612 (1978).

116. J. van Laar and J. J. Scheer, Surf. Sci., 8, 342 (1967).

117. J. H. Dinan, L. K. Galbraith and T. E. Fischer, Surf. Sci., 26, 587 (1971).

118. D. E. Eastman and W. D. Grobman, Phys. Rev. Lett., 28, 1378 (1972).

119. D. E. Eastman and J. L. Freeouf, Phys. Rev. Lett., 33, 1601 (1974).

120. A. Huijser, J. Van Laar and T. L. van Rooy, Surf. Sci., 62, 472 (1977).

121. P. E. Gregory, W. E. Spicer, S. Ciraci and W. A. Harrison, Appl. Phys. Lett., 25, 511 (1974).

122. P. E. Gregory and W. E. Spicer, Phys. Rev. B, 12, 2370 (1975).

123. I. Lindau, P. Pianetta, C. M. Garner, P. W. Chye, P. E. Gregory and W. E. Spicer, Surf. Sci., 63, 45 (1977).

124. A. Huijser and J. van Laar, Surf. Sci., 52, 202 (1975).

125. R. Ludeke and L. Esaki, Phys. Rev. Lett., 33, 653 (1974).

126. D. E. Eastman and J. L. Freeouf, Phys. Rev. Lett., 34, 1624 (1975).

127. J. L. Freeouf and D. E. Eastman, CRC Crit. Rev. Solid State Sci., 5, 245 (1975).

128. G. J. Lapeyre and J. Anderson, Phys. Rev. Lett., 35, 117 (1975).

129. P. E. Gregory and W. E. Spicer, Surf. Sci., 54, 229 (1976).

130. W. E. Spicer and P. E. Gregory, CRC Crit. Rev. Solid State Sci., 5, 231 (1975).

131. J. D. Joannopoulos and M. L. Cohen, Phys. Rev. B, 10, 5075 (1974).

132. N. Garcia, Solid State Commun., 17, 397 (1974).

133. C. Calandra and G. Santoro, J. Phys. C: Solid State Phys., 8, L.86 (1975).

134. J. R. Chelikowski and M. L. Cohen, Phys. Rev. B, 13, 826 (1976).

135. P. E. Gregory, P. Chye, P. Pianetta, J. Lindau, and W. E. Spicer, Bull. Am. Phys. Soc., 21, 319 (1976).

136. W. E. Spicer, J. Lindau, P. E. Gregory, C. M. Garner, P. Pianetta and P. W. Chye, J. Vac. Sci. Tech., 13, 780 (1976).

137. W. Gudat, D. E. Eastman and J. L. Freeouf, J. Vac. Sci. Tech., 13, 250 (1976).

138. K. C. Pandey, J. L. Freeouf and D. E. Eastman, J. Vac. Sci. Tech., 14, 904 (1977).

139. P. W. Chye, I. A. Babalola, T. Sukegawa and W. E. Spicer, Phys. Rev. Lett., 35, 1602 (1975).

140. P. Pianetta, I. Lindau, P. E. Gregory, C. M. Garner and W. E. Spicer, Surf. Sci., 72, 298 (1978).

141. I. Lindau, P. Pianetta, W. E. Spicer, P. E. Gregory, C. M. Garner and P. W. Chye, J. Elec. Spec. and Rel. Phen., 13, 155 (1978)

142. P. Pianetta, I. Lindau, C. M. Garner and W. E. Spicer, Phys. Rev. Lett., 37, 1166 (1976).

143. R. Dorn, H. Lüth and G. J. Russell, Phys. Rev. B, 10, 5049 (1974).

144. P. Pianetta, I. Lindau, C. Garner and W. E. Spicer, Phys. Rev. Lett., 35, 1356 (1975).

145. P. Pianetta, Ph.D. Thesis (Stanford University, 1976).

146. J. Bardeen, Phys. Rev., 71, 717 (1947).

147. C. A. Mead and W. G. Spitzer, Phys. Rev., 134, A713 (1964).

148. C. A. Mead, Solid State Electron., 9, 1023 (1966).

149. V. Heine, Phys. Rev., 138, A1689 (1965).

150. A. J. Bennett and C. B. Duke, Phys. Rev., 160, 541 (1967); 162, 578 (1967).

151. J. C. Inkson, J. Phys. Chem., 5, 2599 (1972); 6, 1350 (1973).

152. F. Yndurain, J. Phys. Chem., 4, 2849 (1971).

153. F. Flores, E. Louis and F. Yndurain, J. Phys. Chem., 6, L465 (1973).

154. J. C. Phillips, Phys. Rev. B, 1, 593 (1970); J. Vac. Sci. Tech., 11, 947 (1974).

155. E. J. Mele and J. D. Joannopoulos, Phys. Rev. B, 17, 1528 (1978).

156. W. E. Spicer, P. E. Gregory, P. W. Chye, I. A. Babalola and T. Sukegawa, Appl. Phys. Lett., 27, 617 (1975).

157. W. E. Spicer, P. W. Chye, P. E. Gregory, T. Sukegawa and I. A. Babalola, J. Vac. Sci. Tech., 13, 233 (1976).

158. J. Froitzheim, "Electron Energy Loss Spectroscopy" in Electron Spectroscopy for Surface Analysis, Topics in Current Physics, Vol. 4, ed. by H. Ibach, Springer-Verlag (1977).

159. J. Froitzheim and I. Ibach, Z. Phys., 269, 17 (1974).

160. H. Froitzheim, I. Ibach and D. L. Mills, Phys. Rev. B, 11, 4980 (1975).

161. F. Meyer, Phys. Rev. B, 9, 3622 (1974).

162. G. Chiarotti, S. Nannarone, R. Pastore and P. Chiaradia, Phys. Rev. B, 4, 3398 (1971).

163. H. Ibach and J. E. Rowe, Phys. Rev. B, 9, 1951 (1974).

164. R. Ludeke and L. Esaki, Phys. Rev. Lett., 33, 653 (1974).

165. R. Ludeke and A. Koma, Phys. Rev. Lett., 34, 817 (1975).

166. R. Ludeke and A. Koma, Phys. Rev. Lett., 34, 1170 (1975).

167. R. Ludeke and A. Koma, Phys. Rev. B, 13, 739 (1976).

168. R. Ludeke and A. Koma, Crit. Rev. Solid State Sci., 5, 259 (1975).

169. A. Koma and R. Ludeke, Surf. Sci., 55, 735 (1976).

170. J. E. Rowe, H. Ibach and H. Froitzheim, Surf. Sci., 48, 44 (1975).

171. J. E. Rowe, Solid State Comm., 15, 1505 (1974).

172. H. Froitzheim and H. Ibach, Surf. Sci., 47, 713 (1975).

173. I. Lindau, P. Pianetta, C. M. Garner, P. W. Chye, P. E. Gregory, and W. E. Spicer, Surf. Sci., 63, 45 (1977).

174. R. Ludeke, Solid State Commun., 21, 815 (1977).

175. R. Ludeke and A. Koma, J. Vac. Sci. Tech., 13, 241 (1975).

176. A. van Oostrom, J. Vac. Sci. Tech., 13, 224 (1976).

177. A. Y. Cho and J. R. Arthur, Prog. in Solid State Chem., 10, 157 (1975).

178. R. Ludeke, Phys. Rev. B, 16, 5598 (1977).

179. P. Pianetta, I. Lindau, C. M. Garner and W. E. Spicer, Phy. Rev. B, 16, 5600 (1977).

180. G. J. Lapeyre and J. Anderson, Phys. Rev. Lett., 35, 117 (1975).

181. W. E. Spicer, I. Lindau, P. E. Gregory, C. M. Garner, P. Pianetta and P. W. Chye, J. Vac. Sci. Tech., 13, 780 (1976).

182. W. Gudat and D. E. Eastman, J. Vac. Sci. Tech., 13, 831 (1976).

183. E. J. Mele and J. D. Joannopoulos, Phys. Rev. Lett., 40, 341 (1978).

184. R. Ludeke and L. Esaki, Surf. Sci., 47, 132 (1975).

185. N. N. Sirota in Physics of III-V Compounds, Vol. 4, ed. by R. K. Willardson and A. C. Beer (Academic Press, New York, 1968) p. 45.

186. J. E. Rowe, J. Vac. Sci. Tech., 13, 798 (1976).

187. W. Gudat, D. E. Eastman and J. L. Freeouf, J. Vac. Sci. Tech., 13, 250 (1976).

188. J. M. Borrego, R. J. Gutmann and S. Ashok, Solid State Elect., 20, 125 (1977).

189. J. B. Pendry, Low Energy Electron Diffraction (Academic Press, New York, 1974)..

190. A. U. MacRae and G. W. Gobeli, J. Appl. Phys., 35, 1629 (1964).

191. C. B. Duke, A. R. Lubinsky, B. W. Lee and P. Mark, J. Vac. Sci. Tech., 13, 761 (1976) and references therein.

192. J. E. Rowe, S. B. Christman and G. Margaritando, Phys. Rev. Lett., 35, 1471 (1975).

193. A. R. Lubinsky, C. B. Duke, B. W. Lee and P. Mark, Phys. Rev. Lett., 36, 1058 (1976).

194. C. B. Duke, Adv. Chem. Phys., 27, 1 (1974).

195. C. B. Duke, N. O. Lipari and U. Landman, Phys. Rev. B, 8, 2454 (1973).

196. J. B. Pendry, Phys. Rev. Lett., 27, 856 (1971).

197. K. C. Pandey, J. L. Freeouf and D. E. Eastman, J. Vac. Sci. Tech., 14, 904 (1977).

198. I. Lindau, P. Pianetta, C. M. Garner, P. W. Chye, P. E. Gregory, and W. E. Spicer, Surf. Sci., 63, 45 (1977).

199. S. Y. Tong, A. R. Lubinsky, B. J. Mrstik and M. A. van Hove, Phys. Rev. B, 17, 3303 (1978).

200. S. Y. Tong and M. A. van Hove, Phys. Rev. B, 16, 1459 (1977).

201. J. R. Chelikowsky, S. G. Louie and M. L. Cohen, Phys. Rev., 14, 4724 (1976).

202. I. Lindau, P. Pianetta, W. E. Spicer, P. E. Gregory, C. M. Garner and P. W. Chye, J. Elect. Spec. and Rel. Phen., 13, 155 (1978).

203. P. W. Anderson, Concepts in Solids (W. A. Benjamin, Inc., NY, 1964) Chapter 2.

204. J. C. Slater, Quantum Theory of Matter (McGraw-Hill, NY, 1968) Chaps. 16-18.

205. N. Rosen, Phys. Rev., 38, 2099 (1931).

206. P. C. Hariharan and J. A. Pople, Mol. Phys., 27, 209 (1974).

207. W. A. Goddard III, Phys. Rev., 157, 81 (1967).

208. C. C. J. Roothaan, Rev. Mod. Phys., 32, 179 (1960).

209. S. F. Boys, Proc. Roy. Soc. London, Ser. A., 200, 542 (1950).

210. J. A. Pople in Applications of Electronic Structure Theory; Modern Theoretical Chemistry, Vol. 4, Edited by H. F. Schaefer (Plenum Press, NY, 1977) Chapter 1 and references therein.

211. W. J. Henre, R. F. Stewart and J. A. Pople, J. Chem. Phys, 51, 2657 (1969).

212. T. H. Dunning and P. J. Hay in Methods of Electronic Structure Theory, Modern Theoretical Chemistry, Vol. 3, Edited by H. F. Schaefer, (Plenum Press, NY, 1977) Chapter 1 and references therein.

213. R. C. Raffenetti, J. Chem. Phys., 58, 4452 (1973).

214. S. Huzinaga, J. Chem. Phys., 66, 4245 (1977).

215. A. B. Kunz, M. P. Guse and R. J. Blint, J. Phys. B., 8, L358 (1975)

216. C. F. Melius, J. W. Moskowitz, A. P. Mortola and M. B. Baillie, Surf. Sci., 59, 279 (1976).

217. R. H. Paulson and T. N. Rhodin, Surf. Sci., 55, 61 (1976).

218. A. C. Wahl and G. Das, Adv. Quantum Chem., 5, 261 (1970).

219. W. J. Hunt, P. J. Hay and W. A. Goddard III, J. Chem.Phys., 57, 738 (1972).

220. D. L. Wilhite and R. N. Euwema, J. Chem. Phys., 61, 375 (1974).

221. L. R. Kahn, P. Baybutt and D. G. Truhlar, J. Chem. Phys., 65, 3826 (1976).

222. C. F. Melius, B.D. Olafson and W. A. Goodard III, Chem. Phys. Lett., 28, 4 (1974).

223. R. N. Euwema and L. R. Kahn, J. Chem. Phys., 66, 306 (1977).

224. V. Bonifacic and S. Huzinaga, J. Chem. Phys., 60, 2779 (1974); 62, 1507, 1509 (1975).

225. B. Cartling, B. Roos and U. Wahlgren, Chem. Phys. Lett., 21, 380 (1973).

226. I. P. Batra and S. Ciraci, Phys., Rev. Lett., 34, 1337 (1975).

227. M. Nishida, Surf. Sci., 72, 589 (1978).

228. R. P. Messmer and G. D. Watkin, Phys. Rev. Lett., 25, 656 (1970).

229. F. P. Larkins, J. Phys. C., 4, 3065, 3077 (1971).

230. T. P. Batra and P. S. Bagus, Solid State Commun., 16, 1097 (1975).

231. J. R. Chelikowsky, S. G. Louie and M. L. Cohen, Phys. Rev., B14, 4724 (1976).

232. E. J. Mele and J. D. Joannopoulos, Surf. Sci., 66, 38 (1977).

233. G. T. Surratt and A. B. Kunz, Phys. Rev. Lett., 40, 347 (1978).

234. F. W. Bobrowitz and W. A. Goddard III., in Chapter 4 of Reference 212.

235. K. Hermann and P. S. Bagus, Phys. Rev., B17, 4082 (1978).

236. C. W. Bauschlicher, Jr., P. S. Bagus and H. F. Schaefer III, IBM J. Res. Develop., 22, 213 (1978).

237. S. Huzinaga, private communication.

238. G. H. Wannier, Phys. Rev., 52, 191 (1937).

239. J. Frenkel, Phys. Rev., 17, 17 (1931).

240. J. Koutecký and M. Tomášek, J. Phys. Chem. Solids, 14, 241 (1960).

241. W. Kohn, Phys. Rev., 115, 809 (1959).

242. J. des Cloizeau, Phys. Rev. 129, 554 (1963); 135, A685, A698 (1964).

243. W. Kohn, Phys. Rev., B7, 4388 (1973).

244. W. Kohn and J. R. Onffroy, Phys. Rev. B8, 2485 (1973).

245. J. J. Rehr and W. Kohn, Phys. Rev., B9, 1981 (1974).

246. J . G. Gay and J. R. Smith, Phys. Rev. B9, 4151 (1974).

247. J. G. Gay, J. R. Smith and F. J. Arlinghaus, Phys. Rev. Lett, 38, 561 (1977).

248. J. J. Rehr and W. Kohn, Phys. Rev., B10, 448 (1974).

249. J. R. Smith and J. G. Gay, Phys. Rev. Lett., 32, 774 (1974).

250. J. G. Gay and J. R. Smith, Phys. Rev., B11, 4906 (1975).

251. J . D. Levine, Phys. Rev., 171, 701 (1968).

252. S. G. Davison and J. D. Levine, Solid State Physics, 25, 1 (1970).

253. J. C. Slater, Symmetry and Energy Bands in Crystals (Dover, New York, 1972), Chapter 6.

254. J. R. Smith in Interactions on Metal Surfaces: Topics in Applied Physics, Vol. 4, Ed., by R. Gomer (Springer-Verlag, New York, 1975).

255. Cheng-Chih Pei and W. Kohn, Interface Energies, Final Report, 31 October 1976-1 Nov. 1977, Contract No. N00014-76-C-0050, Nov. 1977.

256. J. C. Phillips, Phys. Rev., 112, 685 (1958).
J. C. Phillips and L. Kleinman, Phys. Rev., 116, 287, 880 (1959); 118, 1153 (1960).

257. B. J. Austin, V. Heine and L. J. Sham, Phys. Rev., 127, 276 (1962).

258. M. L. Cohen and T. K. Bergstresser, Phys. Rev., 141, 789 (1966).

259. M. L. Cohen and J. C. Phillips, Phys. Rev., 139, A912 (1965).

260. W. A. Harrison, Pseudopotentials in the Theory of Metals (Benjamin, New York, 1966).

261. V. Heine, M. L. Cohen and D. Weaire, Solid State Physics, Vol. 24, (Academic Press, New York, 1970).

262. M. Schlüter, J. R. Chelikowsky, S. G. Louie and M. L. Cohen, Phys. Rev. Lett., 34, 1385 (1975); Phys. Rev., B12, 4200, 5575 (1975).

263. S. G. Louie and M. L. Cohen, Phys. Rev. Lett, 35, 866 (1975); Phys. Rev., B13, 2461 (1976).

264. S. G. Louie, J. R. Chelikowsky and M. L. Cohen, J. Vac. Sci. Tech., 13, 790 (1976).

265. J. A. Appelbaum and D. R. Hamann, Phys. Rev. Lett., 31, 106 (1973); 32, 225 (1974); Phys. Rev., B8, 1777 (1973).

266. K. C. Pandey and J. C. Phillips, Phys. Rev. Lett, 32, 1433 (1974).

267. J. R. Chelikowsky and M. L. Cohen, Phys. Rev., B13, 826 (1976).

268. J. K. Chelikowsky, S. G. Louie and M. L. Cohen, Solid State Commum, 20, 641 (1976).

269. P. E. Gregory and W. E. Spicer, Phys. Rev., B13, 725 (1976).

270. D. E. Eastman and J. L. Freeouf, Phys. Rev. Lett., 33, 1601; 34, 1624 (1975).

271. E. J. Mele and J. D. Joannopoulos, Phys. Rev., B17, 1528 (1978).

272. E. J. Mele and J. D. Joannopoulos, Phys. Rev., B17, 1816 (1978).

273. E. E. Caruthers and P. J. Lin-Chung, Phys. Rev., B17, 2705 (1978).

APPENDIX

APPENDIX A

GaAs WET CHEMICAL CLEANING PROCEDURE

1. Deionized water rinse

2. Blow dry - 30 P.S.I. N_2

3. Methanol rinse

4. Vapor degrease in trichloroethylene - 2 minutes

5. Methanol rinse

6. Deionized water rinse

7. Blow dry - 30 P.S.I. N_2

8. "Piranha" bath (1 part deionized water) - 60 seconds
   (1 part H_2O_2)
   (5 part H_2SO_4)

9. Hot deionized water immersion

10. Deionized water rinse - 1 minute

11. Blow dry - 30 P.S.I. N_2

12. Bromine etch (1 part bromine) - 60 seconds
    (75 parts methanol)

13. Methanol rinse - 60 seconds

14. Deionized water rinse

15. Blow dry - 30 P.S.I. N_2